universität wien

MASTERARBEIT / MASTER'S THESIS

Titel der Masterarbeit / Title of the Master's Thesis

„Current and Historical Soot Particle Concentrations in the Vienna Urban Aerosol“

verfasst von / submitted by

Eva Sommer, BSc

angestrebter akademischer Grad / in partial fulfilment of the requirements for the degree of

Master of Science (MSc)

Wien, 2020 / Vienna, 2020

Studienkennzahl lt. Studienblatt / degree programme code as it appears on the student record sheet:	A 066 876
Studienrichtung lt. Studienblatt / degree programme as it appears on the student record sheet:	Physik UG2002
Betreut von / Supervisor:	Mag. Anna Wonaschütz, PhD

Acknowledgements

First and foremost I want to thank my supervisor Anna Wonaschütz for her immeasurable support and her inexhaustible patience. I know that she did not provide her guidance due to some professional obligation but because of her enthusiasm for the subject and her dedication to teaching and supporting prospective scientists. She was always kind and supportive in our numerous conversations and she has truly inspired me in many ways.

I also want to thank Regina Hitzenberger for supplying the data underlying this thesis and for providing her expertise and her time in various personal communications. Furthermore, I want to thank Theresa Haller for providing the filter samples and Judith Kasper for helping with the sample analysis. I also want to thank Harald Schuh for his help and support with various technical challenges.

I want to thank my partner Elias Leutgeb, who has not only supported me throughout the most frustrating times but has given me the courage to trust in my abilities. Through his admirable curiosity and enthusiasm he has given me a sense for the beauty in learning, without which this thesis would have never been finished.

I want to thank my friends, especially Lukas Schumi and Judith Painsi, for making my student years so wonderfully unforgettable.

I want to thank my grandmother Maria Sommer for encouraging me to be inquisitive throughout my whole life.

I want to thank my mother Gerda Sommer. Without her unconditional love and support and her perpetual encouragement, none of this would have been possible.

Zusammenfassung

Licht absorbierende kohlenstoffhaltige Aerosole werden im Allgemeinen nach ihren Absorptionseigenschaften unterschieden, wobei Kohlenstoffpartikel, die Licht aller Wellenlängen gleich stark absorbieren schwarzer Kohlenstoff (BC für Black Carbon) und solche, die vorwiegend Licht kürzerer Wellenlängen absorbieren brauner Kohlenstoff (BrC für Brown Carbon) genannt werden. Vor allem im urbanen Bereich können diese beiden Arten von lichtabsorbierenden Teilchen unterschiedlichen Quellen zugeordnet werden: BC wird vor allem durch unvollständige Verbrennungsprozesse fossiler Brennstoffe, wie sie z.B. beim Betreiben eines Dieselfahrzeugs vorkommen, emittiert, während BrC zusammen mit BC bei der Verbrennung von Biomasse, die im urbanen Bereich z.B. für private Heizsysteme verwendet wird, entsteht.

In dieser Arbeit werden die zeitliche Veränderung und saisonale Trends von BC und BrC Konzentrationen in den vergangenen Jahrzehnten in der Wiener Luft abgeschätzt. Tägliche Filterproben von 2014 bis 2016 wurden mit einer optischen Messmethode auf BC- und BrC-Konzentrationen untersucht. Es wurde nachgewiesen, dass die saisonale Schwankung des BrC-Anteils in PM2.5 weit ausgeprägter ist als die des BC-Anteils. Dies ist wahrscheinlich auf die Nutzung von Biomasse als Heizbrennstoff zurückzuführen. Es konnte gezeigt werden, dass die Konzentration von BrC an Tagen, die so kühl waren, dass Wohnräume beheizt werden mussten, im Mittel höher war, als an Tagen an denen keine Heizung notwendig war. Für BC wurde kein solcher Zusammenhang beobachtet.

Zusätzlich zu dem Zeitraum von 2014 bis 2016 wurden Daten von BC-Konzentrationen zwischen 1985 und 2001 aus drei weiteren (teilweise publizierten) Studien desselben Messstandorts untersucht. Dabei zeigte sich in einer vorsichtigen Schätzung, dass die saisonalen Mittelwerte der BC-Konzentrationen seit 1985 im Winter um ca. 88% und im Sommer um ca. 70% gesunken sind. Diese Ergebnisse stehen in gutem Einklang mit aktuellen Studien, die von rückläufigen BC-Konzentrationen während der letzten Jahrzehnte in westlichen Städten berichten.

Weiters konnte gezeigt werden, dass die saisonalen Trends der BC-Konzentrationen über den untersuchten Zeitraum deutlich abflachen, was wahrscheinlich die vermehrte Nutzung von saubereren, also weniger BC-emittierenden, Heizmethoden widerspiegelt. Der Unterschied der BC-Konzentrationen zwischen Winter- und Sommermittelwerten betrug in den Mitt-1980ern noch 75%, sank auf 57% in den frühen 2000ern und erreichte seinen niedrigsten Wert von ca. 40% Mitte der 2010er Jahre.

Abstract

The light absorbing fraction of carbonaceous aerosols is divided into particles absorbing light equally at all wavelengths (black carbon, BC) and particles which predominantly absorb light at shorter wavelengths (brown carbon, BrC). Especially in an urban environment, these carbonaceous aerosol species can be attributed to different sources: BC tends to be produced via fossil fuel combustion, like it is used to operate diesel vehicles, while BrC mainly originates from biomass burning, which, in an urban environment, is mainly used for domestic space heating.

This study makes a first order estimate of the change of BC and BrC concentrations in the urban area of Vienna over several decades as well as their seasonal behaviour. Daily filter samples from 2014 to 2016 were analysed for BC and BrC concentrations using an optical measurement method. The seasonal variation of the fraction of BrC in PM2.5 was found to be more prevalent than that of BC. This is likely due to the seasonality of biomass burning as a method for domestic space heating. It could be demonstrated that the mean concentration of BrC is higher on days when space heating is necessary, while for BC no such relationship was observable.

In addition to the period between 2014 and 2016, BC concentrations from three other (partly published) studies, conducted at the same sampling site since the 1980s, were evaluated. In a first estimate, it was found that the seasonal mean BC concentrations decreased by about 88% in winter and by about 70% in summer months since 1985. These results are in good agreement with recent literature reporting remarkable decreases in BC concentrations during the past decades in urban areas of the Western hemisphere.

Furthermore, it could be shown that the seasonal variation of BC concentrations flattened during the investigated time periods, which likely reflects a change from coal or oil to cleaner (less BC emitting) methods for domestic space heating. While the difference between winter and summer averages was as high as 75% in the mid-1980s, it was 57% in the early 2000s and declined to 40% in the mid-2010s.

Contents

1 Introduction

1.1 Aerosol Science

An aerosol is defined as a suspension of solid or liquid particles in a gaseous medium (Hinds, 2011). Naturally occurring aerosol, which surrounds us every day, ranges from mineral dust and sea salt particles to volcanic ashes and tiny water droplets suspended in air. The main sources of natural aerosols are deserts, the world seas, volcanoes, wildfires and the biosphere. Another important aerosol source is human civilization, emitting, among many other particulates, lagre amounts of soot particles and other carbonaceous aerosols via combustion processes used in industry, transportation or space heating. A fraction of these carbonaceous particles is light absorbing (black carbon, BC, absorbing at all visible wavelengths and brown carbon, BrC, wavelength dependent absorption), which makes them play an important role in various phenomena including cloud formation and cloud lifetimes. Through these influences, they are a cause for vast uncertainties when estimating the influence of aerosols on climate change.

There are not many reports on in-situ measurements investigating BC long term trends to be found in literature. This might be due to the fact that, to the knowledge of the author, BC-monitoring is not required in most European or North-American countries by climate or environmental policies. They usually impose upper concentration limits for mass concentrations of particulate matter (PM2.5 and PM10, see Appendix A for definitions) but not for BC specifically (Kuklinska et al., 2015). Furthermore, the clear definition of BC has been a matter of debate within the scientific community (see Section 1.4) and there is no universally agreed on standard measurement method for BC (Adler et al., 2019; Petzold et al., 2013). Even less data exists on BrC. This is especially due to the sometimes unclear terminology and the relative lack of specific measurement techniques for BrC. To the knowledge of the author, there is not a single scientific study specifically dedicated to BrC long term trends.

The present thesis focuses on measurements of carbonaceous particles in urban aerosol. The contents of BC (and BrC) in the Viennese urban air have been monitored in different campaigns during the last few decades and both their seasonal and long term change in concentrations are reported. To accomplish this goal, several studies conducted previously at the Physics Department at the University of Vienna are evaluated in addition to the analysis of more recent samples of ambient aerosol conducted by the author.

The following chapter gives a brief introduction into important concepts and most commonly used terms in aerosol science, always with a focus on carbonaceous aerosols. A list of technical terms and abbreviations used in this thesis can be found in Appendix A.

1.2 General Properties of Aerosols

Since aerosol science covers a wide range of solid or liquid particles in gaseous suspensions, it is necessary to introduce certain classification concepts.
Any solid particle or droplet in a stable suspension in a gaseous medium can be described as an aerosol particle. Ambient aerosol particles range from tiny clusters of just a few molecules to pollen grain and whole plant fragments suspended in air. Therefore, aerosol particles range from just a couple of nanometers to several hundred micrometers in diameter. Due to the fact that their sizes cover a range of several orders of magnitude, both measuring and theoretically describing ambient aerosols proves to be quite challenging.

An aerosol size distribution shows the number concentration of particles as a function of particle size. Depending on the instrument, with which the distribution was measured, often ranges of sizes are given instead of discrete values. To account for the fact that aerosol size distributions usually cover several orders of magnitude, logarithmic scales are used. A detailed discussion of size distributions of urban aerosols can be found in Chapter 1.3.4.

Suspensions of chemically identical particles are called "homogeneous" aerosols. "Monodisperse" aerosols consist only of equally sized particles, while "polydisperse" aerosols are composed of particles of different sizes and shapes. Atmospheric aerosols are always polydisperse and not homogeneous.

Another distinction can be made between internally and externally mixed aerosols. Externally mixed aerosols consist of groups of different particles, with each group containing only one pure chemical component. Internally mixed aerosols consist of particles, which themselves contain various chemical components. A fully internal mixture describes an aerosol that contains only identically internally mixed particles (Riemer and West, 2013).

1.3 Atmospheric Aerosols

Aerosols are studied in various ways, ranging for example from laboratory generated particulates used in experiments or medical applications to dust particles naturally occurring both indoors and outdoors all around the world. One important field of aerosol science is the study of particles contained in ambient outdoor air. In the present study, the ambient aerosol in the city of Vienna is investigated. The annual mean particle number concentration in the city of Vienna was found to be as high as 8 000 particles per cm^3 (Borsós et al., 2012). The following section narrows down the discussion of aerosols in general, to the analysis of light absorbing atmospheric aerosols.

1.3.1 Sources of Atmospheric Aerosols

There are many different ways aerosol particles can be emitted to or created in the atmosphere. Since describing all of them would go well beyond the scope of this work, the following section will focus on the main mechanisms of light absorbing carbonaceous aerosol production. In general, two main production mechanisms can be distinguished. When particles are directly emitted into the atmosphere, the process is called primary production. The term secondary production stands for processes where particles are produced within the atmosphere via gas-to-particle conversion.
The main primary particles in the atmosphere are mineral dust, sea salt, biogenic aerosols like pollen, and BC-containing soot particles, while ammonium nitrate, ammonium sulphate and many carbonaceous compunds are produced via secondary processes (Boucher et al., 2013). Although BC only makes up a relatively small fraction of an ambient atmospheric particle number or mass concentration, it is a very important climate agent and is therefore often listed as an important atmospheric aerosol component in literature.
Globally relevant sources for primary particles are deserts emitting mineral dust (Shi et al., 2019), blowing snow (Huang and Jaeglé, 2017) and ocean waves emitting sea salt particles. Primary carbonaceous aerosols are mainly emitted by volcano eruptions (Beresnev and Vasiljeva, 2018), fossil fuel combustion, biomass burning and vegetation (Gelencsér et al., 2007)
Another important kind of aerosol source is secondary production. This term sums up various mechanisms which can either form aerosol particles out of a gas phase ("nucleation"), or enlarge preexisting particles by condensation of a gas. This is also called gas-to-particle conversion. There are two nucleation mechanisms that can be distinguished: homogeneous nucleation and heterogenous nucleation. In homogeneous nucleation, condensation takes place solely on clusters of vapour molecules, therefore the

vapour must be highly supersaturated. Heterogenous nucleation occurs when vapour condenses on condensation nuclei (e.g. small dust particles) and therefore requires far lower levels of supersaturation (Hinds, 2012). Carbonaceous aerosols that are formed via secondary processes from vapours (volatile organic compounds, VOCs) are called secondary organic aerosol (SOA) particles. Various chemical reactions of VOCs reduce their volatility and they finally form aerosol particles via condensation or nucleation (Seinfeld and Pandis, 2006). Some of these secondary carbonaceous aerosol products have light absorbing properties that depend on the wavelength of the incident light. Therefore, these processes can be a significant source of brown carbon (BrC) (Xie et al., 2019).

BC particles are mainly emitted as primary aerosol particles via combustion processes. They have both anthropogenic and natural sources including diesel engines, industrial coal, residential solid fuel and field or forest fires (Bond et al., 2013). The contribution of each of these sources varies strongly depending on the considered region. BrC particles can have both primary and secondary sources. They are emitted primarily by biomass and biofuel burning (Liu et al., 2013) but can also be formed via secondary processes (Xie et al., 2019) involved in the evaporation of droplets containing dissolved organics (Nguyen et al., 2012).

1.3.2 Removal of Atmospheric Aerosols

There are several processes by which aerosol particles can be removed from the atmosphere. The number concentration (i.e. the number of particles per volume) of an aerosol is often reduced by coagulation of particles: Aerosol particles collide and stick together and therefore reduce the number concentration while the average particle size increases. These collisions take place either due to Brownian motion (thermal coagulation) or due to motion induced by external forces (kinematic coagulation) (Hinds, 2012).
Furthermore, small particles are often removed by impaction or serve as nucleation sites for cloud droplets, while larger particles are more often swept out by falling rain or snow or are removed from the air via gravitational settling. Smaller particles have a mean lifetime in the troposphere of a few days. Larger particles with a diameter above 20 µm stay in the atmosphere for no longer than a few hours (Hinds, 2012).

1.3.3 Urban Aerosol

Urban aerosols contain a mixture of particles from various origins. Therefore, they are a mix of many kinds of chemical compounds and sizes. Urban aerosol typically consists of chemical compounds like sulfates, nitrates, various kinds of organic carbon (Jimenez et al., 2009) and a comparatively small amount of BC. The total aerosol concentration as well as the chemical composition of urban aerosols strongly varies with both, the location of the city (e.g. Northern vs. Southern Europe) and the location of the measurement station within the urban area (e.g. urban background vs. kerbside) (Van Dingenen et al., 2004).

Since light absorbing carbonaceous aerosol (often referred to as black carbon (BC) and brown carbon (BrC), see Section 1.4) is mainly produced by combustion processes, it makes up an important fraction of the total aerosol concentration within a city, where there is a high population density, a lot of traffic and industry. Putaud et al. (2004) found that light absorbing carbonaceous aerosol in an annual average makes up about 10% of PM10 (see Appendix A for definitions) at a Viennese kerbside and about 2.5% of PM10 at an urban background site in Zurich. However, concentrations of urban aerosols (and thereby also that of BC and BrC) can vary significantly with the changing seasons. Hitzenberger and Tohno (2001) found that in 1999, the fraction of BC in the total urban background aerosol mass concentration in Vienna was 8.8% in summer and 10.7% in winter months. Meotrological conditions like temperature inversion scenarios prohibit the vertical layers of air masses from mixing, thereby aerosol particles accumulate in the lower layers, causing increased aerosol concentrations (Gramsch et al., 2014). These scenarios are relatively common in the Viennese basin and most frequently occur during the winter months (Hiebl and Schöner, 2018). Another possible reason for the seasonality of light absorbing carbonaceous aerosol concentrations is that it has an additional, season-dependent source: domestic space heating. Since BC mainly originates from incomplete combustion processes (see Section 1.4) (Bond et al., 2013), the usage of coal or oil for space heating contributes strongly to the higher BC fractions in winter months (Hitzenberger, 1993b; Kirchstetter et al., 2017). Furthermore, since BrC is largely produced by biomass burning, the combustion of wood and other organic material strongly contributes to BrC concentrations (Wonaschütz et al., 2009). As can be seen in Figure 1, throughout the last decades, the usage of coal and oil combustion for domestic space heating has declined significantly, while biomass burning and district heating increased (Statistik Austria, 2018). One of the main goals of this thesis is to determine if this

change in space heating sources can be found to have an effect on the light absorbing carbonaceous aerosol fraction of the urban area of Vienna.

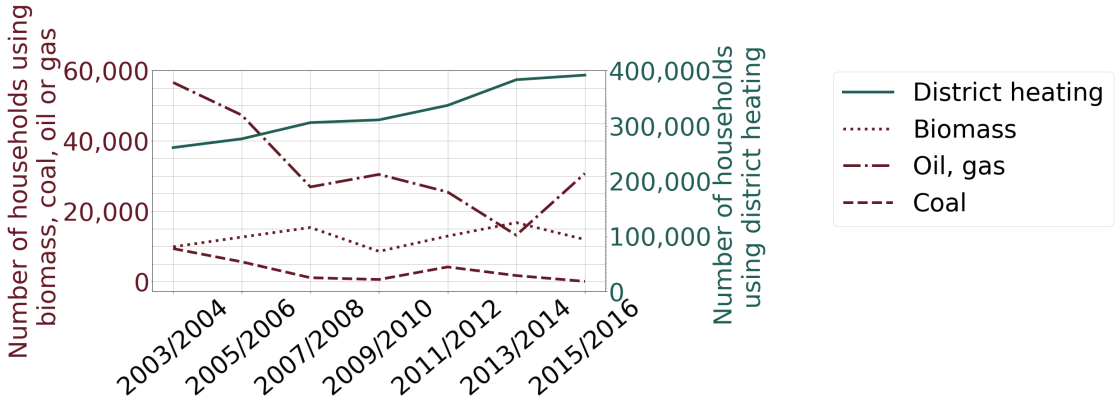

Figure 1: Usage of different sources for domestic space heating in Vienna over time (Statistik Austria, 2018)

1.3.4 Size Distributions of Urban Aerosols

Within an urban aerosol's size distribution, one can usually distinguish three separate modes: they are called the nucleation, the accumulation and the coarse mode. Figure 2 shows a typical size distribution of an urban aerosol. The three size modes are indicated by dashed lines (Hinds, 2012).

The nucleation mode is the smallest of particle size modes. Particles in this mode are usually smaller than 0.01 µm. Those particles are mainly results of recent nucleation events (gas-to-particle conversion) (Hinds, 2012) or they are directly emitted into the atmosphere via combustion processes (e.g. in diesel exhaust) (Filippo and Maricq, 2008). Due to their small size, they contribute very little to the total mass of all particles, however, they account for most of the particle number concentration. Particles in this size mode have rather short lifetimes (often less than a couple of minutes) (Finlayson-Pitts and Pitts, 1986). In most cases they quickly coagulate with larger particles and sometimes they grow out of their size range via condensation (Kulmala et al., 2004; Mohr et al., 2019).
The next larger particle size mode is called accumulation mode. These particles usually account for the major fraction of an ambient aerosol's surface area concentration and for one to two thirds of an ambient aerosol's total mass. Particles in this size range

have the longest mean lifetime (Finlayson-Pitts and Pitts, 1986). Since they are in the size range of the wavelength of visible light, they can cause severe visibility effects (e.g. haze). BC and BrC particles are usually in the size range of nucleation or accumulation mode particles (Bond et al., 2013).

The largest aerosol size mode is called coarse mode. Particles in this mode are usually larger than 1 µm. While making up the lowest number concentration, coarse mode particles account for about two thirds of an aerosol's total mass (Hinds, 2012). Their sources are often natural (wind blown dust or sand, large sea salt particles or pollen), although they can have anthropogenic sources as well, like dust from agriculture or surface mining. They are usually removed from the atmosphere quite rapidly due to gravitational settling, impact on surfaces or washout. Therefore, they have rather short lifetimes of no more than a few hours.

The size distribution of BC-containing particles is determined by the size of the BC particles at their emission and by coagulation either with larger particles or with other BC particles. Depending on the way they were produced, most BC particles are either in nucleation or accumulation mode. Particles produced by combustion at higher temperatures tend to be smaller than those produced by less efficient combustion processes (Bond et al., 2013, Chapter 3.7). Furthermore, BC particles originating from urban fossil fuel burning tend to be in a much smaller size regime than BC particles produced by biomass burning (Schwarz et al., 2008). Light absorbing organic carbon, or brown carbon (BrC) particles, tend to be larger than black carbon particles. They are largely produced via incomplete combustion processes and biomass burning and their aerodynamic mean diameter was found to be 0.5 µm, which puts them into the size regime of the accumulation mode (Liu et al., 2013).

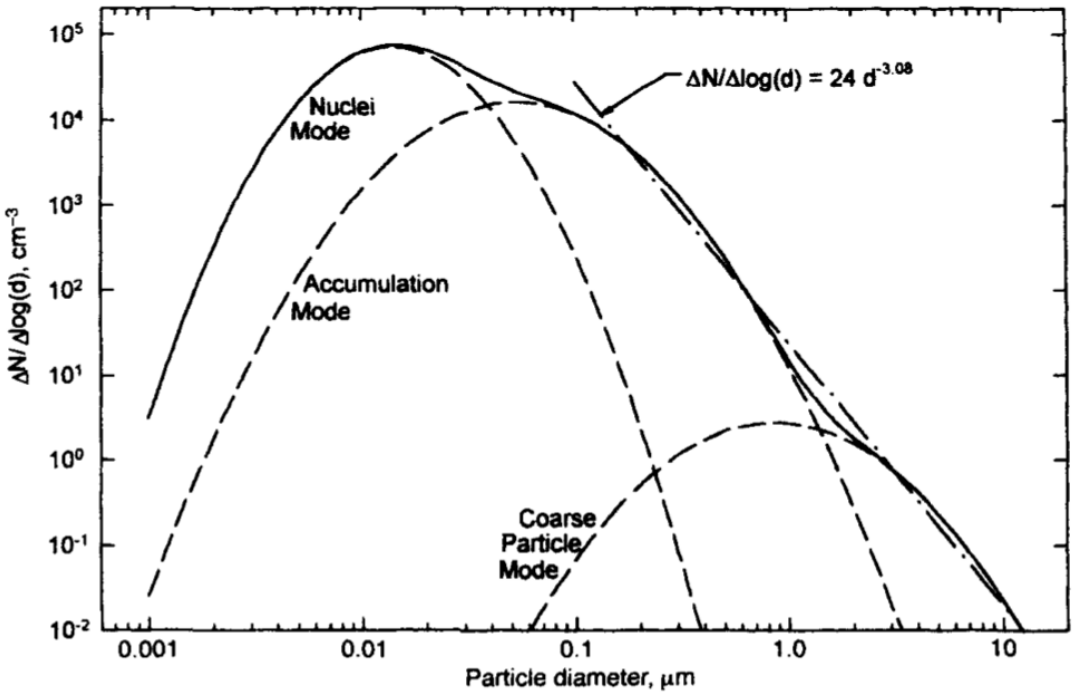

Figure 2: Typical urban aerosol size distribution (from Hinds (2012) Chapter 14.2)

1.4 Light Absorbing Carbonaceous Aerosols - BC, BrC and EC

Aerosols containing a significant amount of carbon are called carbonaceous aerosols. The term carbonaceous fraction of an aerosol refers to the fraction of particulates within an aerosol that contains carbonaceous compounds (i.e. chemical compounds containing carbon). A part of this carbonaceous fraction has light absorbing properties. The present thesis sets its focus on the light absorbing carbonaceous fraction of urban aerosol, therefore, when referring to "light absorbing carbonaceous aerosol", the light absorbing part of the carbonaceous fraction of urban aerosol is implied. The following section discusses this fraction in more detail.

Carbonaceous aerosol compounds make up a large fraction of the global fine aerosol (i.e. particles with a diameter $d < 2$ µm) and have various sources. Distinguishing this carbonaceous fraction any further is not an easy task. In the present thesis, two major distinctions are made: classification according to their optical and to their chemical properties (see Figure 3).
Figure 3 shows both the thermochemical (left column) and the optical (right column)

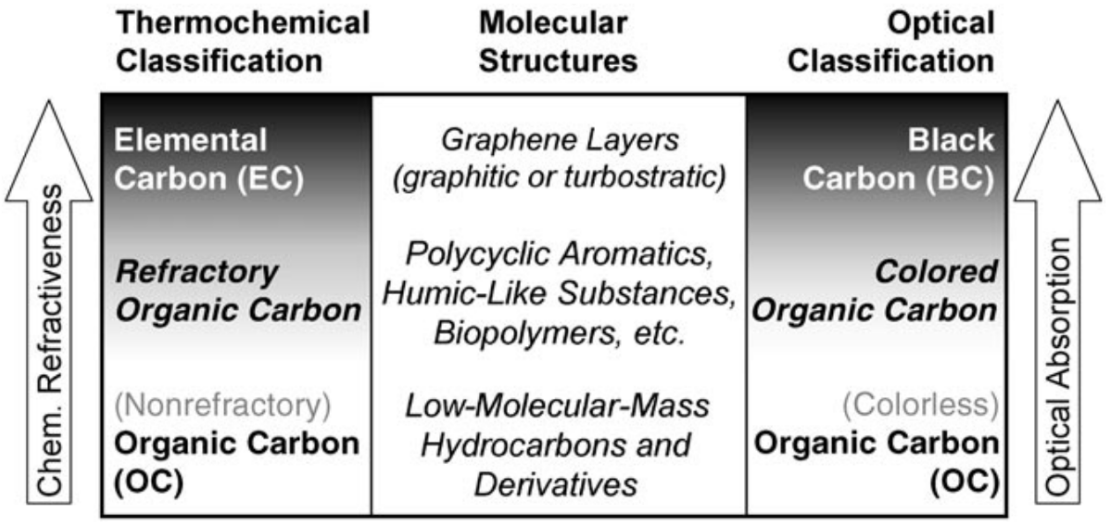

Figure 3: Classification of carbonaceous aerosol by both chemical and optical properties from Pöschl (2005). 'Colored Organic Carbon' is roughly equivalent to the term 'BrC' in this thesis (see also Appendix A)

classifications of carbonaceous aerosols. Pöschl (2005) makes a differentiation by chemical composition distinguishing organic and non-organic carbons. Light absorbing organic carbonaceous aerosols originate from wood or biofuel burning, as well as secondary aerosol formation processes (Xie et al., 2019) and have various chemical structures. Non-organic light absorbing carbonaceous particles are of a mainly graphite-like structure, which makes them very resistant to heat. They mostly originate from incomplete combustion processes like they occur in diesel engines (Raza et al., 2018). A large part of this thesis will be dedicated to this strongly light absorbing carbonaceous fraction. In literature it is often referred to as black carbon (BC) or elemental carbon (EC). These two terms are often used synonymously, even though they actually mean something inherently different. EC usually refers to inorganic carbonaceous particulates, that oxidise in combustion analysis only in an oxygenated atmosphere above a certain temperature threshold. BC is most commonly defined as the fraction of inorganic carbonaceous aerosol that absorbs light at all visible wavelengths and therefore appears to be black. The fraction of carbonaceous aerosol that absorbs light depending on its wavelength is called coloured organic carbon in Figure 3. These types of carbonaceous structures absorb short wavelengths more strongly than long ones and therefore appear brownish, rather than black. This kind of aerosol is called brown carbon (BrC) (Andreae and Gelencsér, 2006). In contrast to BC and EC, BrC is usually organic and has various

origins like humic-like substances or bioaerosols (Andreae and Gelencsér, 2006). BrC can have both primary or secondary sources. Primary sources of BrC are biomass burning or incomplete combustion of hydrocarbons. Its secondary sources can be various chemical formation processes, which are most frequent in the urban environments with high anthropogenic emissions (Liu et al., 2013).
The classifications made in Figure 3 are mainly of experimental origin. Depending on whether a chemical or an optical analysis method is used, concentrations of either EC and OC (left column) or BC and OC (right column) are reported.
It is still an ongoing controversy within the scientific community about how to correctly distinguish different types of carbonaceous aerosols, especially since there seems to be a fluent transition from black (or elemental) to brown carbon (Adler et al., 2019; Andreae and Gelencsér, 2006; Petzold et al., 2013). In the present thesis, mainly the suggestions from Petzold et al. (2013) will be used and when referring to EC, BC and BrC the following definitions are adhered to:

- EC: inorganic carbonaceous aerosol that is thermally stable in an inert atmosphere up to very high temperatures (about 3 700°C) and only oxidises at temperatures above 340°C (Petzold et al., 2013).
- BC: inorganic carbonaceous aerosol that absorbs light at all wavelengths in the visible spectrum
- BrC: carbonaceous aerosol particulates that absorb light depending on its wavelength.

1.4.1 Structure of Light Absorbing Carbonaceous Aerosols

The exact chemical structure of EC particles can vary considerably with their source of emission (Jiang et al., 2011). EC emitted from a diesel bus, for example, has been found to consist of spherical particles of about 50 nm made of an aggregate of a fullerene $C_{36}(OH_2)$ (Jiang et al., 2011). In Figure 4, an image of such EC particles, recorded with an electron dispersive x-ray spectroscope (EDX) is displayed. It clearly shows agglomerates of smooth spherical EC particles with a mean diameter of about 50 nm. However, the exact chemical structure of EC (or BC) particles depends on various factors like the combustion temperature and the fuels involved and is therefore highly heterogenous (Bond et al., 2013; Pósfai and Buseck, 2010; Raza et al., 2018).

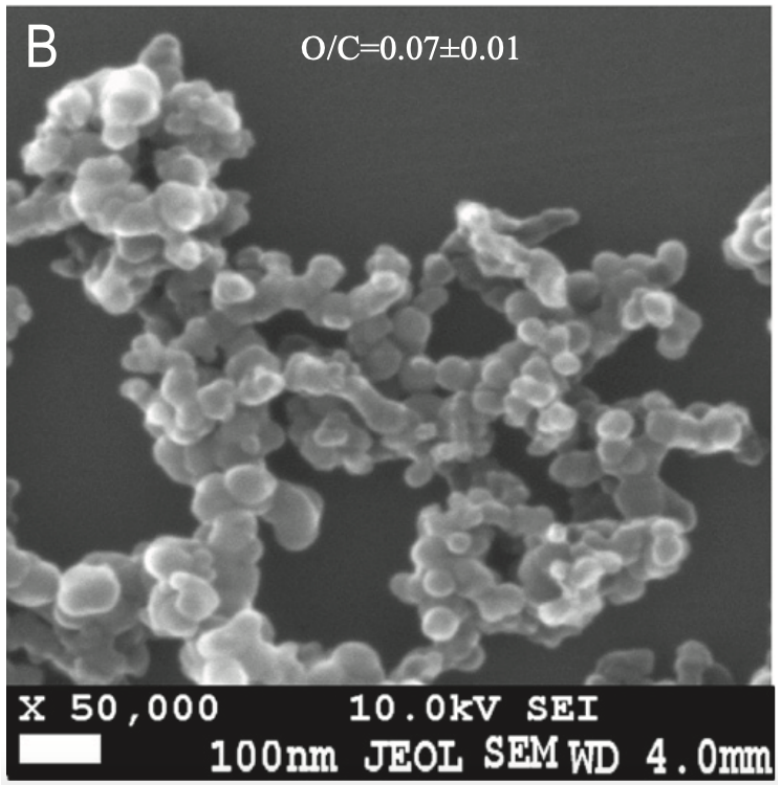

Figure 4: EDX-image of EC particles emitted by a diesel bus from Jiang et al. (2011)

OC particles can have a great variety of chemical structures. The 'brown' fraction of light absorbing carbonaceous particulates is part of this class of aerosol particles. What is referred to as 'brown carbon' in the present thesis can therefore have an immense variety of origins and chemical structures. However, some chemical compounds, such as nitrophenols, supramolecular aggregates and complexes of organic molecules with transition metals, have been identified as possible contributors to the light absorbing properties of BrC (Laskin et al., 2015).

In an urban environment, one of the most important sources for EC particles is fossil fuel combustion. There are many different chemical mechanisms that can lead to the formation of these particles (Bond et al., 2013). In the following paragraphs, one possibility of how EC particles can form in a combustion process is described.

One of the most important mechanisms leading to particle formation by combustion is thermal pyrolysis. In this process, the fuel molecules are broken up into hydrogen (H),

hydroxide (OH), methyl (CH_3) and various kinds of organic compounds (Raza et al., 2018). These compounds can then form so-called soot precursors. The precursors are polycyclic aromatic hydrocarbons (PAH) and serve as the origin of EC particles. In Figure 5, a possible scheme for the formation of such PAHs is shown.
After their formation, the PAHs can collide to form clusters and eventually nucleate to form EC particles (Raza et al., 2018). They can then undergo further chemical reactions with acetylene (C_2H_2) and build larger particles via coagulation. An illustration of the whole particle formation process in fossil fuel combustion is shown in Figure 6. PAHs serve as precursors for the nucleation of EC, which grows into primary particles via coagulation and surface growth (illustrated by the three uppermost circles in Figure 6). In the last step, these primary particles grow into larger agglomerates via agglomeration (last circle in Figure 6). An EDX-image of such agglomerates is shown in Figure 4.
EC particles produced in this manner tend to be very small and are mainly to be found within a size range smaller than 200 nm (Bond et al., 2013; Raza et al., 2018).

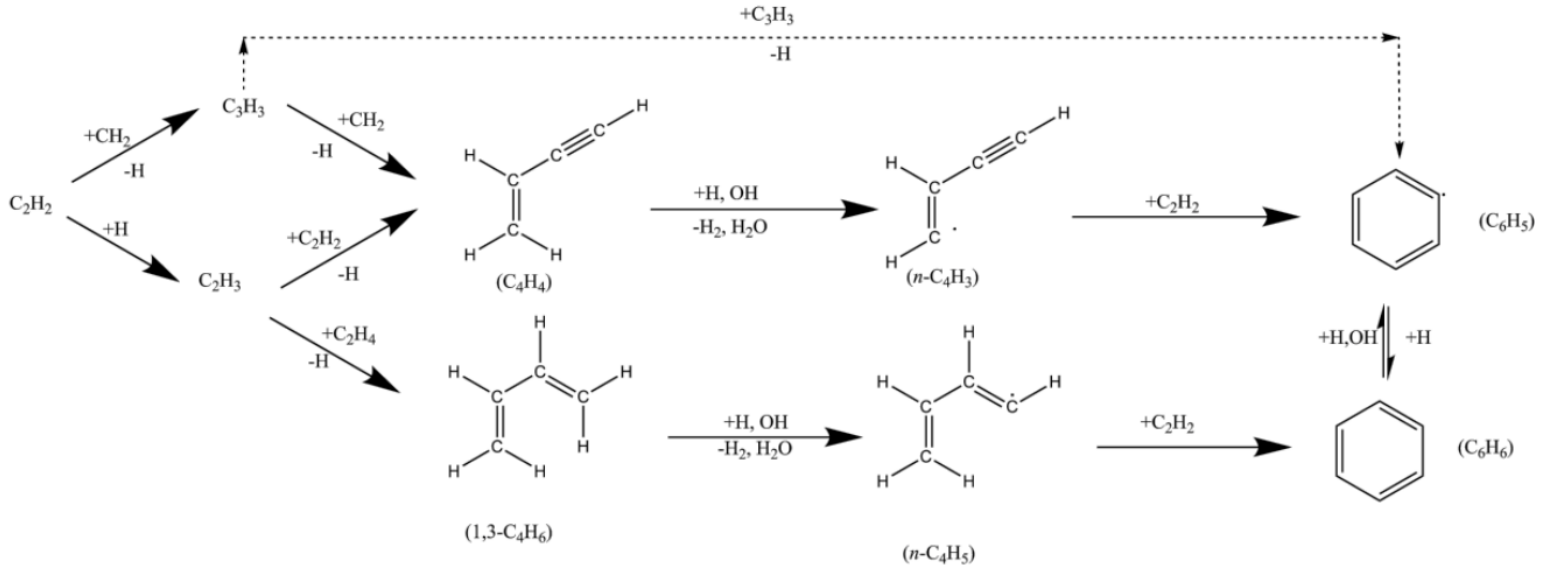

Figure 5: Possible pathway for the formation of polycyclic aromatic hydrocarbons, which can act as origin for EC particles in fossil fuel combustion processes from Raza et al. (2018)

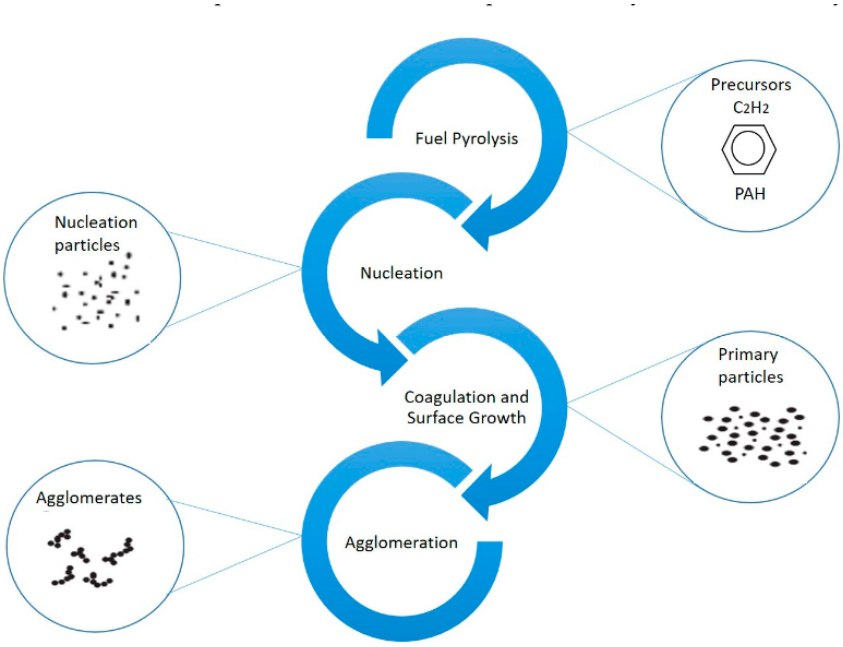

Figure 6: Illustration of the processes underlying EC particle formation via fossil fuel combustion from Raza et al. (2018)

1.5 Environmental Impacts of Atmospheric Aerosols

Aerosols can have a large impact on our everyday lives, both on a global and a very personal scale. They can serve as cloud condensation nuclei, absorb or scatter solar radiation and penetrate deep into our lungs. This section provides an overview of the various impacts aerosols can have on both our climate and our health, always with a focus on light absorbing carbonaceous aerosols.

1.5.1 Global Climate Impacts of Aerosols

The earth is constantly exposed to solar radiation, which is partly reflected directly by the atmosphere, clouds or snow and partly absorbed inside the atmosphere and on the planet's surface. The sun emits ultraviolet, visible and a small amount of near infrared light. This combination is sometimes referred to as shortwave radiation. The planet itself emits some of the absorbed radiation as longwave radiation, which is either transmitted through the atmosphere or reflected back to the surface. Depending on their properties, aerosols in the atmosphere can have both warming and cooling effects (Seinfeld and Pandis, 2006).

The Earth's albedo determines the portion of incoming light that is being reflected back to space. It strongly depends on the surface of the planet (e.g. it is very high in polar regions due to large amounts of snow and ice and comparatively low at equatorial regions). Its global average value is usually taken to be about 30% of the total incoming radiation (Loeb et al., 2009). The earth's albedo is an important factor contributing to its mean temperature. Aerosols can have a severe impact on a planet's ability to scatter and absorb light, and thereby contribute significantly to changes in its mean temperature. Such changes imposed on the Earth's radiation balance are called radiative forcing (Seinfeld and Pandis, 2006).

Figure 7, shows a bar chart depicting various agents of radiative forcing. The vertical axis shows the agents, while on the horizontal axis the magnitude of the forcing is displayed. Blue bars pointing to the left indicate negative forcing (cooling effects), while red bars to the right indicate positive forcing (warming effects) (Myhre et al., 2013).
It is clearly visible that, while most types of aerosols have a cooling effect on the planet, black carbon is the only component in the box "Aerosols and Precursors" that clearly shows a warming effect (Myhre et al., 2013). In addition to its contributions to aerosol-radiation interactions (see below), the deposition of BC on snow reduces the snow sur-

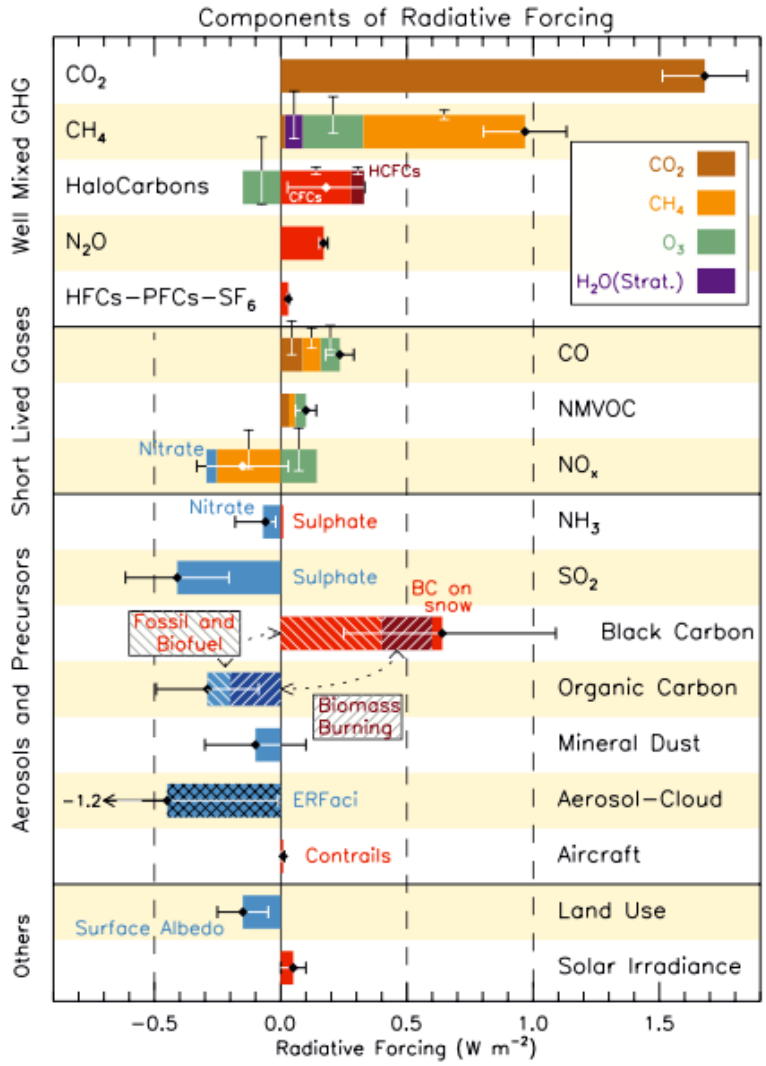

Figure 7: Bar Chart depicting the various agents of radiative forcing. From (Myhre et al., 2013, Chapter 8.5).

face's ability to reflect sunlight and thereby contributes further to global warming. Aerosol concentrations show a large spatial variation across the planet. Therefore, they cause a different amount of heating and cooling in different regions, which can have a severe impact on the local wheather conditions (Boucher et al., 2013).
There are four distinct ways aerosols can affect the global climate (Boucher et al., 2013). Figure 8 shows an illustration of these effects. The effects can be divided into two seperate kinds of interactions: aerosol radiation interactions (ari) and aerosol cloud

interactions (aci) (Boucher et al., 2013). The following paragraphs give a brief description of these effects.

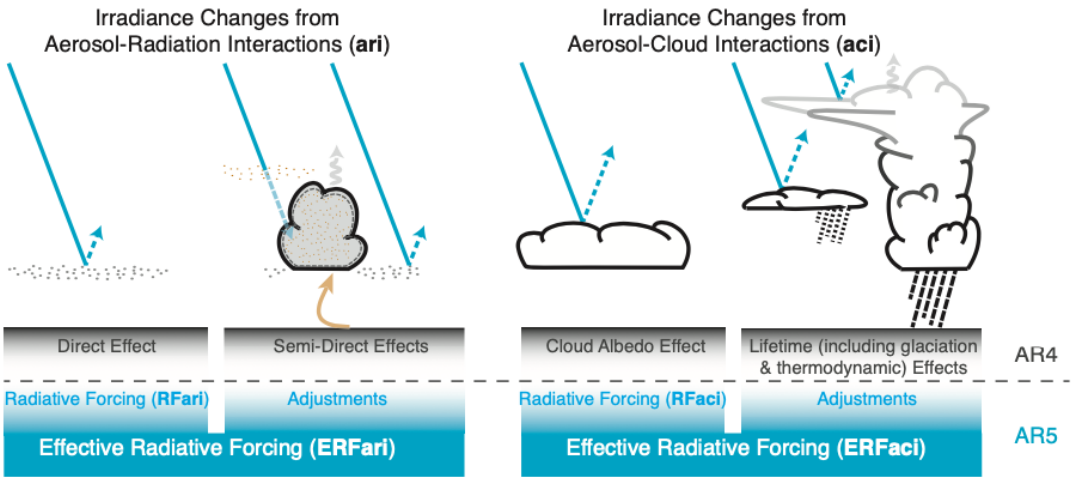

Figure 8: A schematic illustration of the different types of effects aerosols have on the global climate from Boucher et al. (2013, Chapter 7.1).

Aerosol-radiation interactions There are two kinds of aerosol-radiation interactions: direct effects and semi-direct effects. Direct effects occur when the aerosol particles in the atmosphere directly scatter solar radiation back to space (non-absorbing aerosol particles) or when they absorb solar radiation and thereby contribute to warming the atmosphere (BC and BrC). BC contributes about 72% to the global absorption of radiation by aerosols of anthropogenic origin (Feng et al., 2013). This effect is included in the left-most image in Figure 8. Furthermore, it was shown that, due to its light absorption properties, BrC could contribute significantly to global aerosol warming effects. Feng et al. (2013) showed that strongly absorbing BrC accounts for up to 19% of the solar light absorption of anthropogenic aerosols.
Furthermore, aged BC particles are known to act as cloud condensation nuclei. A cloud droplet containing a light absorbing BC particle can have a significantly decreased lifetime, since the particle tends to warm the droplet and contribute to its dissipation (Boucher et al., 2013, Chapter 7.3). This semi-direct effect is included in the second image in Figure 8.

Aerosol-cloud interactions Higher aerosol concentrations and more specifically, higher concentrations of cloud condensation nuclei (CCN), lead to an increased number of small

droplets within a cloud, on which light is scattered more effectively, making the cloud "brighter". This is called the Twomey effect (Twomey, 1977) and it is illustrated in the third image in Figure 8. More but smaller droplets in a cloud can inhibit precipitation formation and thereby severely increase its lifetime. This phenomenon, called Albrecht effect (Albrecht, 1989), contributes to the overall cooling effect of aerosols (Boucher et al., 2013, Chapter 7.5) and is shown in the fourth image in Figure 8. Apart from that, it is known that some kinds of aerosols (BC among others), can cause clouds to rain out prematurely, thereby significantly reducing the clouds' lifetime. The physical and chemical mechanisms underlying these effects are not yet fully understood, which makes it difficult to assess the magnitude of these effects in climate models (Boucher et al., 2013).

1.5.2 Impacts on Human Health

Aerosols have a significant impact on human health. Figure 9 shows a schematic of the human respiratory system with its different areas indicated by the colours blue, green and red. On the right hand side of Figure 9, the regional particle deposition as a function of particle diameter is given. One can clearly see that in the uppermost region, consisting of nasal airway and throat, both very small and very large particles are deposited rather effectively with a minimum particle deposition at diameters around 0.1 µm. Furthermore, as it is indicated by the red line, particles with very small diameters (around 20 nm) are penetrating deep into the alveolar regions with a regional deposition of about 50% (Oberdörster et al., 2005). Particles within the ultrafine size regime are known to pass through the air-blood barrier when they are inhaled (Kreyling et al., 2006).

While such phenomena have inspired the development of many new technologies greatly improving medical drug delivery (Hickey and Mansour, 2019), strong increases in ambient aerosol concentrations have been linked to strong increases in mortality rates (e.g. Dockery et al., 1993). Both long and short time exposure have been linked to various kinds of diseases. Long term exposure to high concentrations of particulate matter can have severe effects on the lung development of children (Gauderman et al., 2004) and additionally, a clear association between high PM concentrations and hospital admissions for cardiovascular diseases has been shown (e.g. Chen et al., 2019). One of the most infamous examples for air pollution causing increased mortality rates is the London fog event from 1952, which caused approximately 12,000 premature deaths (Bell and Davis,

2001). On a global level, up to 9 million deaths have been attributed to exposure to particulate matter in the year 2015 (Burnett et al., 2018).

Besides the risk imposed by high concentrations of particulate matter in general, exposure to elevated BC concentrations has been shown to be especially dangerous (Peng et al., 2009). In a report from 2012, the World Health Organisation states that BC poses a greater threat to human health than any other component found in urban ambient aerosol (Janssen et al., 2012). Diesel exhaust, which is the main contributor to BC concentrations in urban aerosols (Bond et al., 2013), has been classified as carcinogenic by the International Agency for Research on Cancer (IARC Working Group on the Evaluation of Carcinogenic Risks to Humans, 2014)

In light of these facts, it becomes even more important to monitor and understand the behaviour of these kinds of aerosols. Especially since they are largely of anthropogenic origin, one might even say, we have a responsibility to do so.

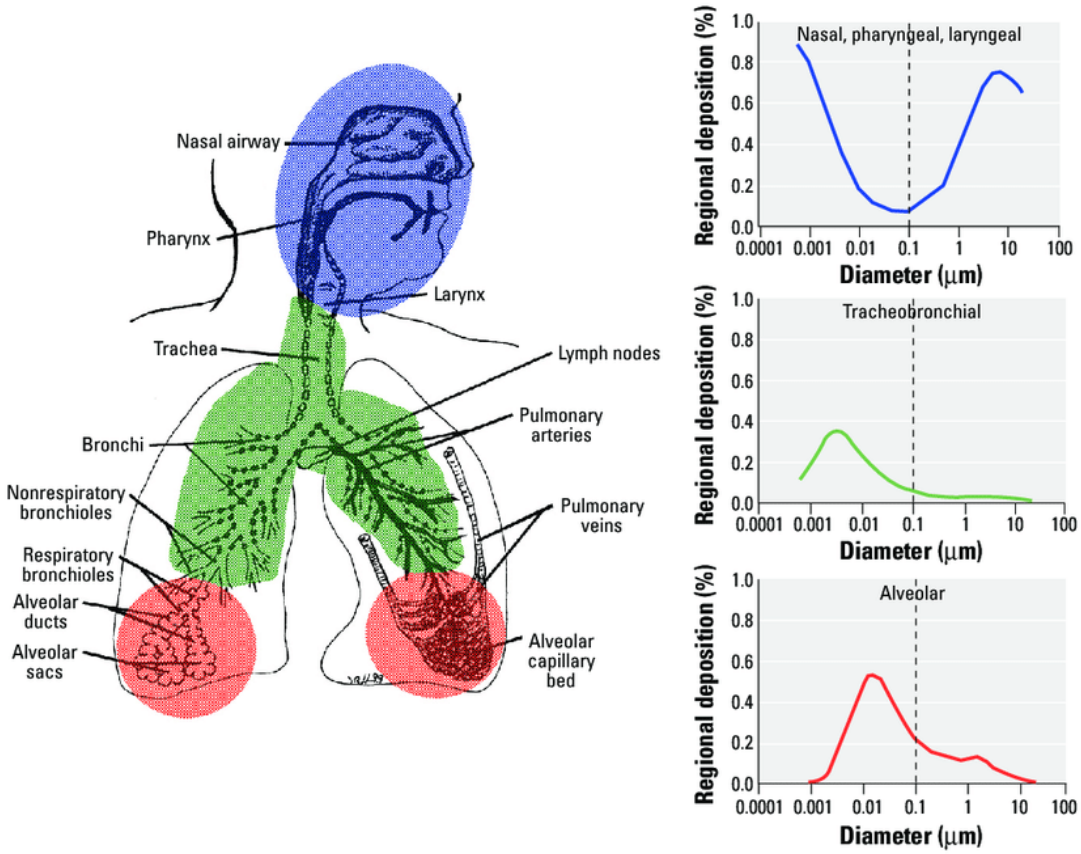

Figure 9: A schematic illustration of the deposition of aerosol particles in different areas of the human resporatory system depending on particle size from Oberdörster et al. (2005)

1.6 Typical Aerosol Concentrations and Their Regulation in the Urban Environment

Concentrations of ambient aerosols can vary quite significantly in different areas around the world, depending on settlement density, industrial development and various environmental factors like vegetation, climate volcanic activity and the presence of an ocean. Aerosol mass concentrations are often measured as PM10 or PM2.5 (particulate matter with a diameter smaller than 10 µm or 5 µm respectively). When there is no upper limit on particle size, the concentration of the total suspended particulate matter (TSP) is given.

Massey et al. (2012) report an average annual value of approximately 150 µg/m^3 of PM2.5 at a roadside measurement station in urban northern India. For comparison, the

annual mean concentration of PM2.5 in the urban area of Tucson, Arizona, was found to be about 5.3 µg/m^3 in the year 2016 (Pima County Department of Environmental Quality, 2017), which makes a difference of almost a factor of 30. Furthermore, aerosol concentrations, especially in urban areas, have varied greatly over time. In February 1979 Berner and Luerzer (1980) measured a daily mean concentration of TSP at 20 m altitude in the urban area of Vienna of 175 µg/m^3. On February 15th 2020 the Austrian environmental agency (Umweltbundesamt) reports a daily average value of PM10 in the same district of approximately 12 µg/m^3 (Österreichisches Umweltbundesamt, 2020b). However, mainly due to insufficient ground based monitoring, in many parts of the planet, the actual ambient aerosol concentration is still not known (Martin et al., 2019) and has to be estimated via computer modelling rather than by actual measurements.
Due to the known health risks and for reasons of general environmental protection, many governments have set target concentration limits of PM in the ambient air. These threshold values vary quite strongly around the world. In Austria, as well as the European Union, the annual mean threshold for PM2.5 is 25 µg/m^3 (European Commission, 2019; Österreichisches Umweltbundesamt, 2020a). The USA and the Republic of India have set an annual mean PM2.5 limit of 15 µg/m^3 (United States Environmental Protection Agency, 2016) and 40 µg/m^3 (Chowdhury et al., 2019) respectively. The World Health Organization warns about the severe health effects of particulates in the ambient air and proposes an annual mean threshold of PM2.5 of 10 µg/m^3 (World Health Organization, Occupational and Environmental Health Team, 2006). Usually, such regulations only exist for daily and annual values of PM10 or PM2.5, but not for specific chemical fractions of the PM such as BC, even though thresholds for these types of aerosols have been strongly recommended by numerous scientists not only for health but also for climate effects (Cavazos-Guerra et al., 2017; Hansen et al., 2000; Kholod and Evans, 2016; Kopp and Mauzerall, 2010; Peng et al., 2016; Yamineva and Liu, 2019). Furthermore, it is often argued that specifying a threshold only for mass concentrations of PM10 or PM2.5 might be not as effective as it is thought to be (Paasonen et al., 2013). When measuring mass concentrations, small particles are basically not taken into account, since their mass is usually exceeded by larger particles by several orders of magnitude. Even large number concentrations of very small particles might not be detected by measuring a mass concentration. These ultrafine particles, however, are much more dangerous to human health than larger particulates (Li et al., 2016).

1.7 Long Term Investigations of Black Carbon

The present thesis focuses on measurements of concentrations of black carbon (BC) in the urban atmosphere in Vienna over the past few decades. Measuring BC specifically has become of interest to the scientific community in the early 1980s. The earliest data used in this thesis were obtained as early as 1985 by Hitzenberger (1993b), who also state that the source of these particles is largely anthropogenic fuel combustion. Since the early times of BC measurements, concentrations are expected to have changed quite significantly. Especially in Western countries, the awareness for environmental protection and health risks due to air pollution has increased fundamentally and with it, the usage of coal and oil for space heating in private households has declined steadily throughout the last decades (Statistik Austria, 2018). Furthermore, better filter systems for vehicle exhaust pipes and industrial exhausts have been developed, with the aim to specifically reduce soot (or BC) emissions. On a global scale however, no such decline in BC concentrations is expected. With the economic growth of large parts of Asia and increased industrial activities in developing countries, global BC emissions might in fact be on the rise.

Using computational modelling and emission inventories, global BC emissions were reported to have increased by 10 to 20% throughout the past decades (Amann et al., 2013; Klimont et al., 2017; Myhre et al., 2017). However, BC emission trends vary strongly depending on the location. While annual mean BC concentrations have significantly increased in developing countries, especially in Asia and India (Lu et al., 2011), they have been reduced by almost one third in Europe (Amann et al., 2013; Kupiainen and Klimont, 2007).
The following section gives an overview of the existing literature on in-situ measurements of the long term development of BC concentrations through the past decades. To provide context with the investigations conducted in the present thesis, this section sets its focus on Western urban areas.

Kutzner et al. (2018) evaluated data from 213 stations spread across Germany using a variety of different measurement methods. They divided the methods used at these stations into two groups: 'evolved carbon measurements' and 'optical detection' measuring EC and BC respectively. Most of the measurement stations detecting EC used a thermo-optical method similar to the one described in Section 3.2.3. The optical detection methods group used either an aethalometer (Hansen et al., 1984) or a Multi Angle

Absorption Photometer (MAAP) (see Section 3.1.1). In this study, Kutzner et al. (2018) found a decreasing trend for BC between -0.07 µg m^{-3} y^{-1} and -0.02 µg m^{-3} y^{-1} for urban background sites over a time period from 2005 to 2014. Furthermore, they found the greatest decrease in annual mean BC concentrations at sites with heavy traffic. They argue that this is due to traffic restriction measures and improved end of pipe technology such as diesel particulate filters. Overall, they observed that the decreasing trends are more significant, the higher the mean BC value was at a measurement station in 2005 (Kutzner et al., 2018).

Kirchstetter et al. (2017) investigated BC concentrations in urban areas in the United States from 1965 to 2000. They estimated BC concentrations from an early air pollution metric called Coefficient of Haze (COH) (Hemeon et al., 1953) and correlated results from this method with the more modern aethalometer measurements (Hansen et al., 1984). Like the aethalometer, the COH monitor collects the aerosol on filter paper and measures the decreasing light transmission as the concentration of light absorbing particles on the filter increases (Hansen et al., 1984; Hemeon et al., 1953). Compared to the COH monitor, the aethalometer shows an increased accuracy in BC measurements due to a more adequate light source and the implementation of quartz fibre filters instead of simple filter paper (Kirchstetter et al., 2017). It was shown that annual BC concentrations declined significantly between the 1960s and the year 2000 (Kirchstetter et al., 2017). They report decreases in annual averages from 13 µg m^{-3} to 2 µg m^{-3} in New Jersey and from 4 µg m^{-3} to 1 µg m^{-3} in California. They argue that the main reason for this is that California used predominantly clean burning natural gas as main energy source throughout the whole time period, while in New Jersey residual and distilled fuel oils were used until 1974 (Kirchstetter et al., 2017). Besides the large reductions in annual BC mean concentrations, also an overall flattening in the seasonal cycles of BC values was found. BC reductions took place predominantly in winter, which reflects the transition to cleaner fuels used for space heating (Kirchstetter et al., 2017).

Font and Fuller (2016) examined several atmospheric chemical compounds, like NO_2, as well as PM and BC from 2005 to 2014 at 65 monitoring sites in London. However, their study did not focus on BC concentration trends, since most of the monitoring sites they used only measured gas phase pollutants. A general downward trend of NO_2 concentrations was found. Like in most other studies presented here, an aethalometer was used for BC monitoring. While they did state that they found decreasing trends of BC and PM concentrations in roadside measurement stations, they argue that their number

of measurement sites was too small to draw definitive conclusions (Font and Fuller, 2016).

From September 2012 to December 2017 Mbengue et al. (2020) monitored the light absorbing carbonaceous aerosol fraction (referred to as equivalent black carbon, EBC) in a rural background area in the Czech Republic. In their study they used a multi wavelength aethalometer to distinguish between EBC originating from fossil fuel and from biomass burning, which can be assumed to be very similar to the distinction of BC and BrC (see Section 1.4) made in the present study. They found a strong seasonal variation in EBC concentrations originating from biomass burning and a less prevalent one for EBC with a fossil fuel burning source (Mbengue et al., 2020).

Overall, these studies report that BC concentrations in western urban areas have decreased over the past decades. Based on these reports, the present thesis aims to investigate if such a decreasing trend is also present in the city of Vienna. With this in mind, BC data from several publications (Hitzenberger et al., 1996b; Hitzenberger, 1993b) as well as unpublished data were compared to recent (2014 - 2016) BC measurements. Another hypothesis underlying the present thesis is that the increased usage of biomass burning as a source for space heating in Vienna (see Figure 1 in Section 1.3.3) might be observable in the seasonal variations of brown carbon (BrC), similar to what was shown for a rural area in the Czech Republic by Mbengue et al. (2020). To assess this hypothesis, the seasonality of the fractions of BC and BrC in PM2.5 concentrations is evaluated.

2 Theoretical Background

The following chapter provides a brief overview of the theoretical background underlying the measurement techniques used in the course of this thesis. To this end, the optical properties of carbonaceous aerosols are explained and some background information on aerosol filter measurements is given.

2.1 Light Absorption and Scattering Properties of Aerosol Particles

The main part of this thesis is dedicated to measurements of light absorbing carbonaceous aerosols. In the following section, a brief theoretical background to the description of absorption and scattering of light by aerosol particles is given.

Figure 10 shows the various mechanisms by which an incoming light beam with wavelength λ_0 can interact with an aerosol particle. The measurement methods used in the present thesis measure the relative attenuation of incoming light at a certain wavelength. In some processes depicted in Figure 10, the incoming radiation is absorbed by the particle and reemitted at a different wavelength. The radiation is reemitted via Raman scattering, fluorescence or thermal emission. Due to the changed wavelength, the radiation is lost to the detection systems used in this thesis. Therefore, only the elastic scattering processes (reflection, refraction diffraction) and absorption are relevant for the measurement methods used in the present thesis. The following section provides a brief theoretical description of these elastic scattering processes.

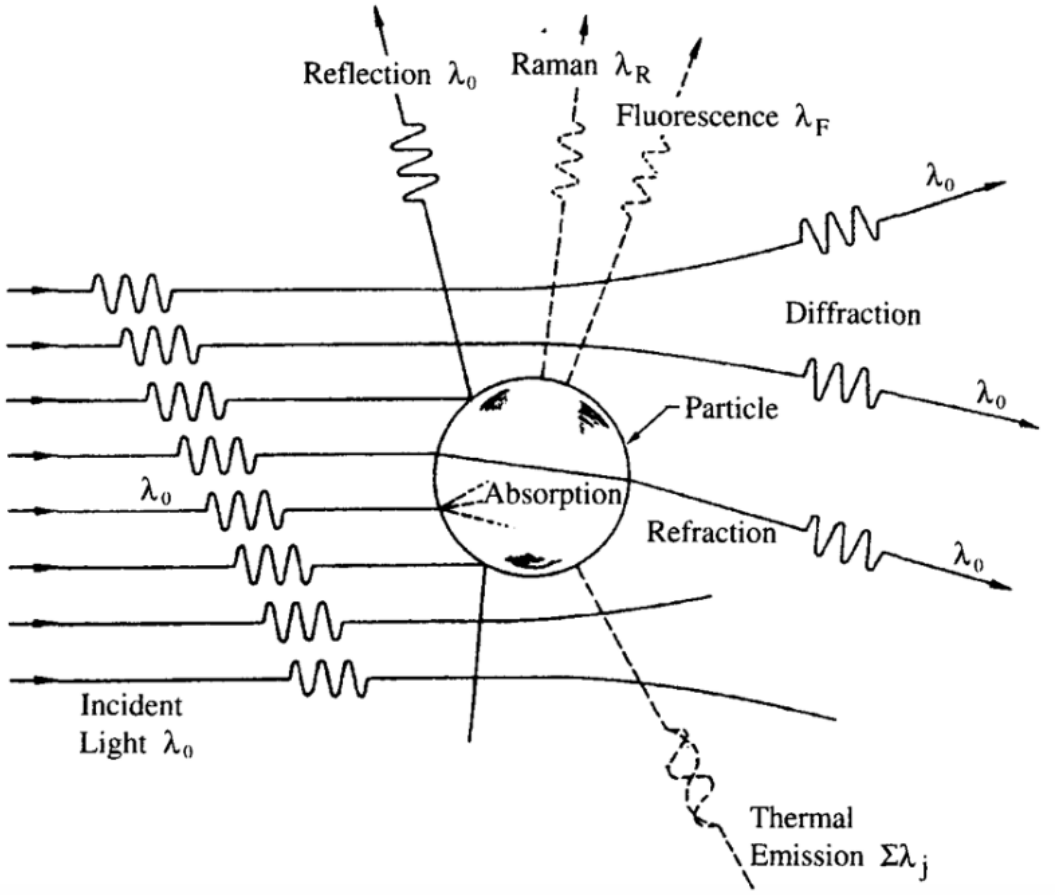

Figure 10: Interaction mechanisms of light with an aerosol particle from Seinfeld and Pandis (2006)

2.1.1 Scattering and Extinction Efficiency of a Single Particle

A particle's extinction efficiency Q_e is a relative value describing how much more intensity of an incoming light beam is removed by the particle rather than by simply blocking an area of the same size as the particle's cross section (Hinds, 2012).

$$Q_e = \frac{\textit{radiant power scattered and absorbed by a particle}}{\textit{radiant power geometrically incident on the particle}} \tag{1}$$

Since both the scattering efficiency Q_s and the absorption efficiency Q_a contribute to the light extinction caused by an aerosol particle, Q_e can be written as

$$Q_e = Q_s + Q_a \tag{2}$$

Another important quantity related to the scattering properties of a single aerosol particle is the single-scattering albedo ω, which is defined as follows:

$$\omega = \frac{Q_s}{Q_e} \tag{3}$$

The most important parameters to describe scattering and absorption of light by a particle are the particle diameter D_p, the wavelength of the incoming light λ and the particle's complex refractive index m.
The index of refraction m for a specific non-absorbing substance is defined as the ratio of the speed of light in vacuum v_c and the speed of light within the considered material v_p:

$$m = \frac{v_c}{v_p} \tag{4}$$

For absorbing materials it is represented by a complex number $m = m' + iam'$, where m' is the real refractive index and the value a is related to the absorption coefficient A of the material:

$$A = \frac{4\pi a}{\lambda} \tag{5}$$

The relation between the particle diameter D_p and the wavelength of the incoming light is usually expressed by the size parameter α:

$$\alpha = \frac{\pi D_p}{\lambda} \tag{6}$$

Using the size parameter α, light scattering on a single particle can be divided into three separate regimes, each requiring its own theoretical description:

$\alpha << 1$: Rayleigh scatteiring

$\alpha \approx 1$: Mie scattering

$\alpha >> 1$: Geometric scattering

In all of these regimes, the intensity of the scattered light is highly dependent on the scattering angle Θ, which is the angle of the scattered beam with respect to the incident light beam. This angle-dependency of the scattered light is illustrated in Figures 11 and 12.

The intensity of the light scattered by a particle depending on the scattering angle Θ is given by the phase function $P(\Theta)$. This phase function can be interpreted as a probability

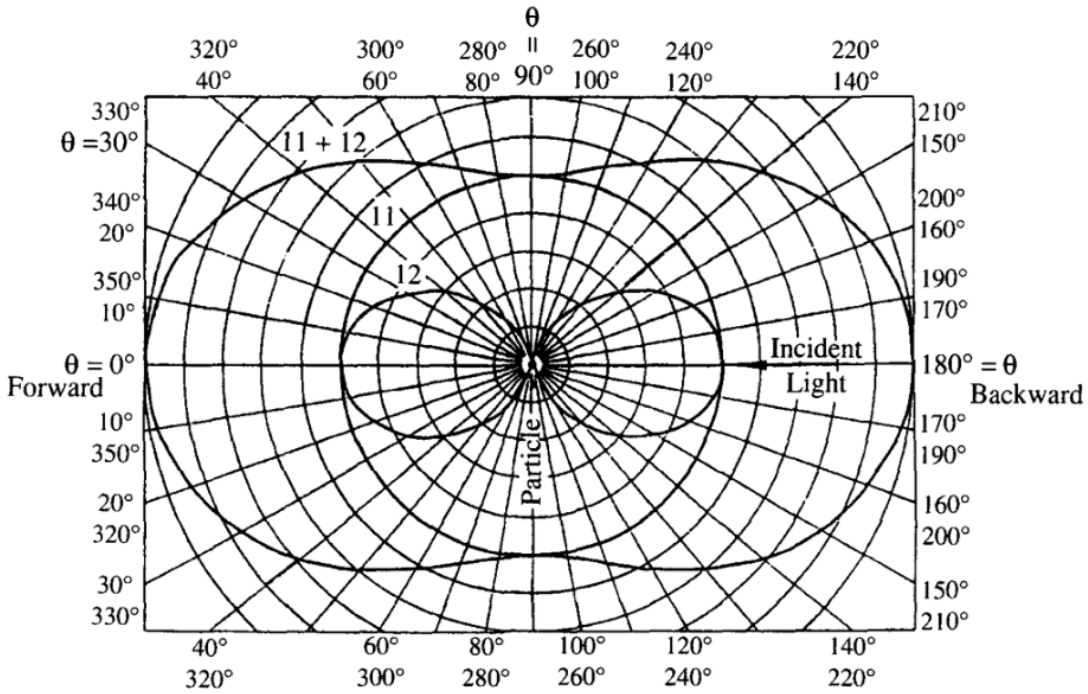

Figure 11: Pattern of the light intensity scattered on a single particle in the Reyleigh regime from Seinfeld and Pandis (2006). The resulting phase function is given by the line denoted as 11+12.

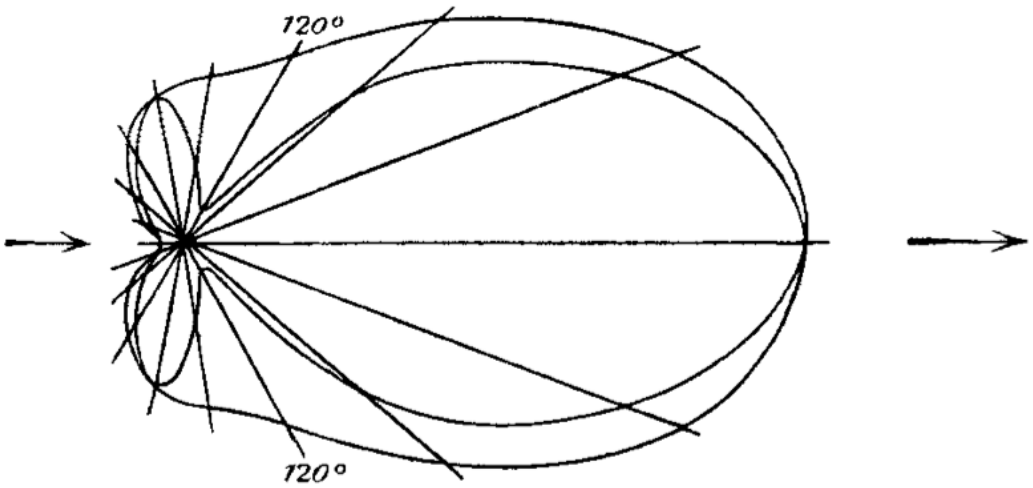

Figure 12: Polar plot of light scattering on a particle in the Mie regime from Mie (1908)

density function that describes the probability for a single photon to be scattered by the particle at an angle Θ.

$$P(\Theta) = \frac{F(\Theta, \alpha, m)}{\int_0^\pi F(\Theta, \alpha, m) sin\Theta \, d\Theta} \tag{7}$$

with $F(\Theta, \alpha, m)$ being the light intensity scattered at an angle Θ with a size parameter α on a particle with refractive index m.

For light scattered on a particle in the Rayleigh regime, the phase function $P(\Theta)$ takes the following form:

$$P(\Theta) \propto \frac{\lambda^2}{8\pi^2} \left(\frac{\pi D_p}{\lambda} \right)^6 \left| \frac{m^2 - 1}{m^2 + 2} \right| (1 + cos^2\Theta) \tag{8}$$

Figure 11 shows the phase function of light scattering on a single particle in the Rayleigh regime ($D_p << \lambda$). The incident light beam coming from the right hits an aerosol particle in the center of the plot and the resulting phase function is given by the line denoted as 11+12. It is a product of the lines 11 and 12, which refer to the circularly symmetric and the Θ-dependent part of Equation 8 respectively. One can see that the intensity of the scattered light is symmetric in the forward and backward direction. However, the scattering intensity is highly wavelength dependent and decreases as wavelengths increase with a factor proportional to the fourth power of λ (Seinfeld and Pandis, 2006).

Figure 12 shows the intensity of light scattered on a particle with a diameter of 180 nm in the Mie regime ($D_p \approx \lambda$). The direction of the incident light is indicated by the arrow on the left. A strong angular dependance of the intensity of the scattered light can be observed. The pattern of the scattered intensity becomes more and more complicated as the size parameter α increases, but also when an imaginary component is added to the refractive index m (i.e. when the particle is light absorbing). The scattering and absorption characteristics for any spherical particle as a function of wavelength can be calculated with a rather complex formalism called Mie Theory (Mie, 1908). For large size parameters α, Mie Theory converges to the limit of geometrical optics.

BC was well as BrC particles are usually smaller than 500 nm (Bond et al., 2013; Liu et al., 2013), which, when analysed with visible light, places them in the Mie, or, for very small particles, in the Rayleigh regime.

2.1.2 Extinction Efficiency of Polydisperse Aerosols

When a certain volume of an aerosol is illuminated by a light source with intensity I_0, the aerosol particles absorb and scatter some of the incoming light. A detector placed behind the aerosol will therefore measure a smaller intensity I of the light beam. This process is called extinction and can be described by Lambert-Beer's law:

$$\frac{I}{I_0} = e^{-\sigma_e L} \tag{9}$$

where σ_e [m^{-1}] is the extinction coefficient of the aerosol. It describes the fraction of intensity lost per unit path length and is expressed in units (length^{-1}). The path length the light takes through the aerosol is denoted by L in units (m).

The extinction coefficient of a monodisperse aerosol with N particles per unit volume is related to the extinction efficiency given in Equation 1 via the following relation:

$$\sigma_e = N A_p Q_e = N \frac{\pi D_p^2 Q_e}{4} \tag{10}$$

with A_p being the cross Section area and D_p being the diameter of the particles.
Light extinction is in fact a result of both scattering and absorption effects. The aforementioned quantities can be written as

$$\sigma_e = \sigma_s + \sigma_a \tag{11}$$

with the subscripts e, s and a denoting extinction, scattering and absorption respectively. In a case where only absorption effects are considered and scattering effects can be neglected, the following relations hold:

$$\frac{I}{I_0} = e^{-\sigma_a L} \tag{12}$$

$$\sigma_a = N A_p Q_a = N \frac{\pi D_p^2 Q_a}{4} \tag{13}$$

The aerosol studied in this thesis is highly polydisperse (i.e. containing particles of various shapes and sizes). The extinction coefficient of a polydisperse aerosol with a given number size distribution $n(D_p)$ can be calculated via integration over all particle diameters D_p.

$$\sigma_e = \int_0^{D_p^{max}} \frac{\pi D_p^2}{4} Q_e(m, \alpha) n(D_p) dD_p \tag{14}$$

Here, $Q_e(m, \alpha)$ denotes the extinction efficiency as a function of the refractive index m and the size parameter α (Equation 6).
Several measurement methods used in the present thesis effectively measure the light intensity absorbed by an externally mixed aerosol, sometimes at various wavelengths. The measurement systems are usually calibrated with a well known standard allowing to measure mass concentrations of particulates with certain absorption properties.
In the present thesis a distinction is made between black (no wavelength dependency of the absorption coefficient) and brown (weaker absorption of larger wavelengths) carbon. Measuring relative absorption of samples at different wavelengths makes it possible to distinguish these two aerosol species.

2.2 Filter Characteristics

Filtration is one of the most common methods to effectively sample aerosol particles. For the present thesis, all of the samples were taken using filter methods. The principle idea is to let a known volume of air pass through a filter, which collects the particles suspended in the air. Given a known flow rate and sampling time, a concentration of the quantity the filter is analysed for, can be calculated. The types of filters most commonly used for scientific sampling are fibrous and porous filters. The following section is dedicated to the principle mechanisms underlying the function of these filter types. If not labelled otherwise, all the information in the following section is taken from (Hinds, 2012).

2.2.1 Filter Collection Efficiency and Deposition Mechanisms

The collection efficiency of a filter is defined as follows:

$$E = \frac{N_{in} - N_{out}}{N_{in}} \quad or \quad E_m = \frac{C_{in} - C_{out}}{C_{in}} \tag{15}$$

E is called the filter's count efficiency, with N_{in} and N_{out} being the number of particles entering and exiting the filter respectively. Since the present thesis focuses on mass concentrations rather than number concentrations of aerosols, the mass efficiency E_m is more important here, with C_{in} and C_{out} being the incoming and outgoing mass concentration respectively.
The decrease of the mass concentration across the filter can be expressed as $dC = -c_e$,

where c_e is the fraction of the mass concentration remaining in the filter. This relation can be written as:

$$dC = -c_e = -C\gamma\, dt \tag{16}$$

where γ is a constant factor, which depends on the particle diameter, the velocity of the air at the face of the filter (i.e. the face velocity U_0), the filter's solidity (i.e. the fraction of fibre volume in total volume) and its fibre size. dt is an increment of the filter thickness t. Through integration over the whole filter thickness one obtains:

$$\int_{C_{in}}^{C_{out}} \frac{dC}{C} = \int_0^t -\gamma\, dt \tag{17}$$

$$ln(\frac{C_{out}}{C_{in}}) = -\gamma\, t \tag{18}$$

The fraction of entering particles that also exit the filter is called particle penetration $P = \frac{C_{out}}{C_{in}}$, which gives:

$$P = e^{-\gamma\, t} \tag{19}$$

Therefore, the particle penetration decreases exponentially with filter thickness. These calculations, however, only hold for the simplified case of a monodisperse aerosol, since the value of γ strongly depends on the particle diameter.
Therefore, also the collection efficiency of a fibrous filter is dependent on the particle size and, in the case of a measurement of ambient air, on the aerosol size distribution. Additionally, the collection efficiency of a filter strongly depends on the aerosol filter's face velocity U_0 (see Figure 13). Usually fibrous filters have a minimum sampling efficiency at a particle size between 0.05 and 0.5 µm (see Figure 13). This means, that particles both smaller and larger than this specific size are collected more efficiently. In general, a filter's mass efficiency is higher than its count efficiency (Hinds, 2012).
In Figure 13, the collection efficiency of a certain fibrous filter is displayed as a function of the particle size and for two different face velocities, $U_0 = 1$ cm/s and $U_0 = 10$ cm/s. As indicated by Figure 13, there are different mechanisms responsible for the collection of particles of different sizes.

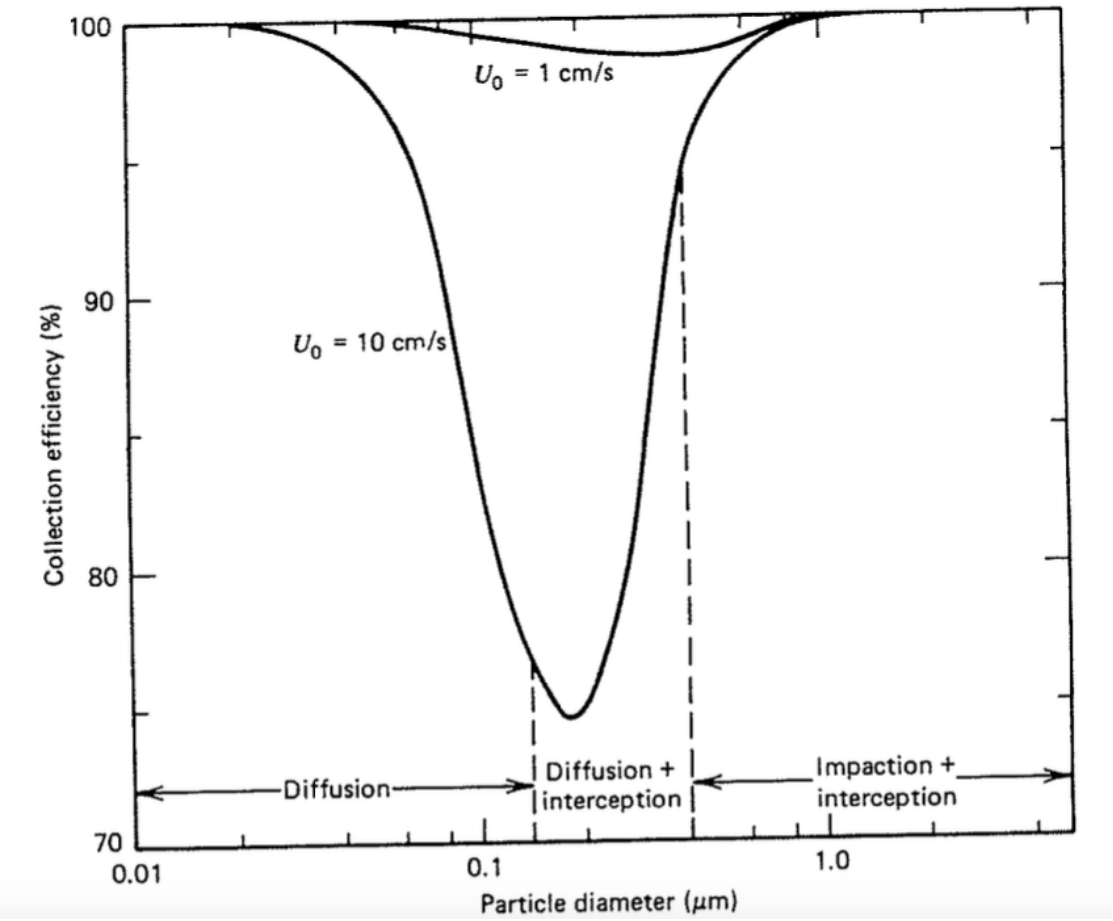

Figure 13: Filter efficiency versus particle size for two different face velocities from Hinds (2012)

In general, there are five different deposition mechanisms that cause particles to be deposited on a filter:

1. Interception
2. Inertial impaction
3. Diffusion
4. Gravitational settling
5. Electrostatic interaction

The particle size ranges where mechanisms 1 to 3 are effective are displayed in Figure 13. A particle intercepts when it follows a gas streamline, which comes closer than one

particle radius to the fibre surface. Inertial impaction occurs when the gas streamline bends around a fibre, but the particle impacts on the fibre because of its inertia. Both these mechanisms are most relevant for larger particles (> 0.4 µm). Smaller particles ($<$ 0.1 µm) tend to diffuse onto filter fibres due to their Brownian motion. Most black carbon (BC) particles, which are the main subject of this thesis, have diameters ranging from 90 to 600 nm (Bond et al., 2013). Therefore, all three of these mechanisms (interception, inertial impaction and diffusion) can be responsible for the collection of BC particles on a filter.

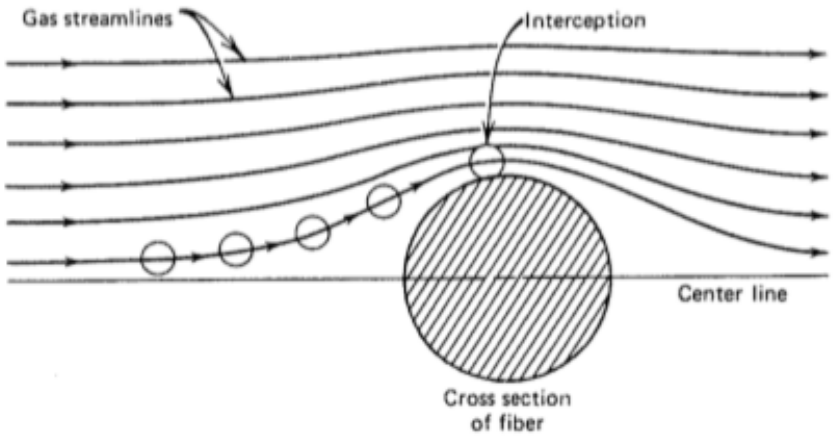

Figure 14: Filter fibre collection by interception from Hinds (2012)

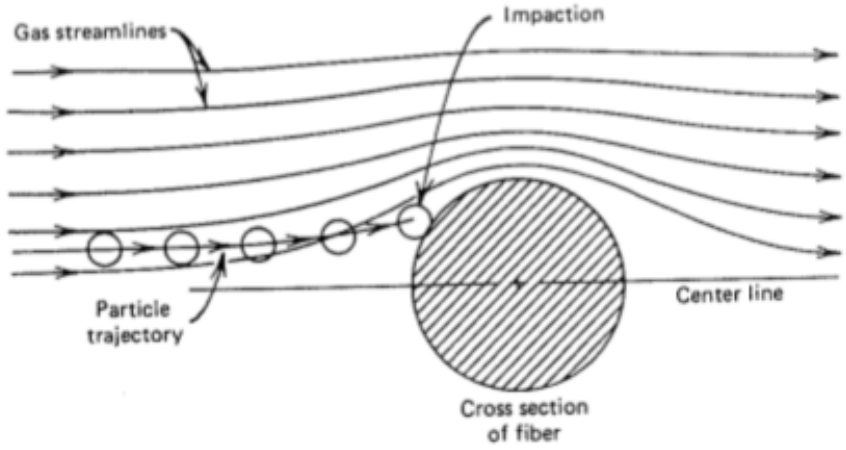

Figure 15: Filter fibre collection by impaction from Hinds (2012)

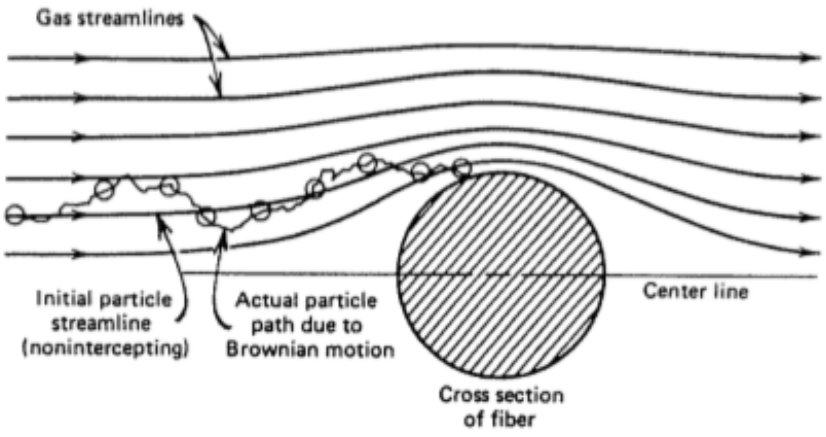

Figure 16: Filter fibre collection by diffusion from Hinds (2012)

Figures 14 to 16 show graphic illustrations of these mechanisms. Both gravitational settling and electrostatic attraction effects are not relevant for the sampling methods used in the course of this thesis and will not be taken into account any further. For the purposes of the present thesis it can be assumed, that the aerosol's face velocity is too high for gravitational settling to occur and that neither the sampled particles nor the filters, on which the samples were collected were electrically charged.

2.2.2 Common Filter Types

Some of the most commonly used filter types are polycarbonate (Nuclepore or Isopore) filters and fibre filters. Figure 17 shows a scanning electron microscope photograph of a glass fibre filter. Another important example for fibrous filters are quartz fibre filters, as they were used for ambient aerosol sampling for this thesis (see Section 3.1.1). Fibrous filters are largely 'empty', having porosities (i.e. percentarge of "empty" volume in the whole volume of a filter) ranging from 70 to 99% (Hinds, 2012).

The mechanism underlying fibrous filtration cannot be understood as the filter acting like a microscopic sieve, collecting all the particles larger than its pore size. In fact, the aerosol particles are collected in the filter when they intercept, impact or diffuse onto the surface of the fibres. For each layer of fibres there is a certain probability for a particle of a given size to attach to the fibre and thereby be removed from the air. Therefore, a fibrous filter's collection efficiency increases with its thickness (see also Equation 19).

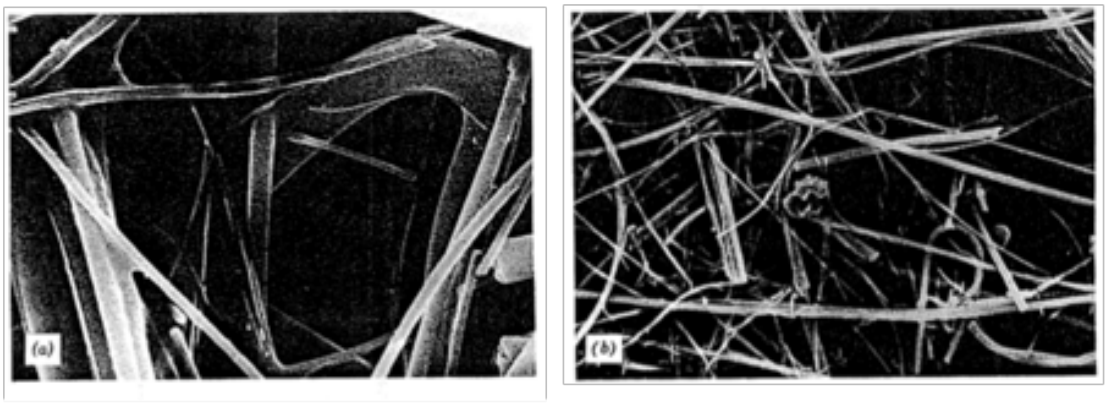

Figure 17: Scanning electron microscope photograph of a high-efficiency glass fibre filter. Magnification of (a) 4150x and (b) 800x. (Hinds, 2012)

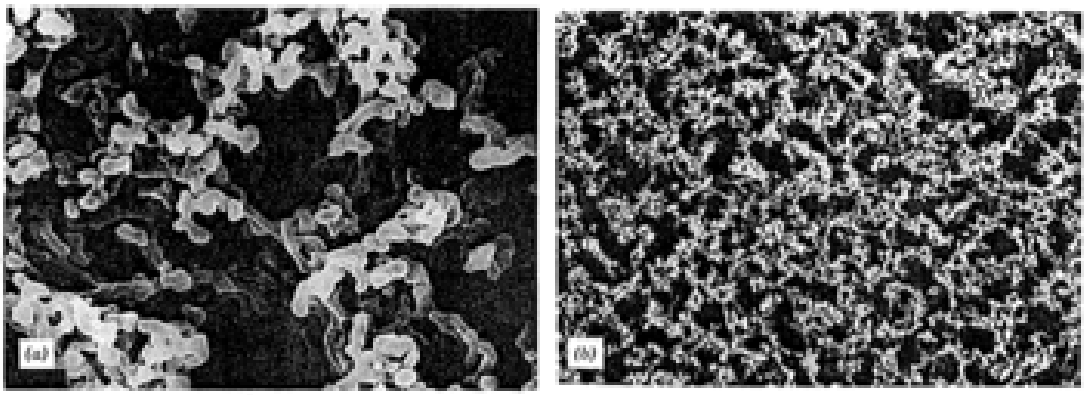

Figure 18: Scanning electron microscope photograph of a cellulose ester porous membrane filter with a pore size of 0.8 µm. Magnification of (a) 4150x and (b) 800x. (Hinds, 2012)

In Figure 18, a photograph of a porous membrane filter is displayed. They usually are less porous than membrane filters (around 50 to 90%) (Hinds, 2012).
Figure 19 shows a capillary pore membrane filter (i.e. a Nuclepore filter) as it was used in some of the studies underlying this thesis (Hitzenberger, 1993a,b) (see Section 3.2.1). Nuclepore filters consist of a polycarbonate filter that has cylindrical holes with a uniform diameter (Hinds, 2012). It is important to note that their collection efficiency of very small particles (i.e. smaller than the uniform pore size) is lower than that of porous membrane filters.

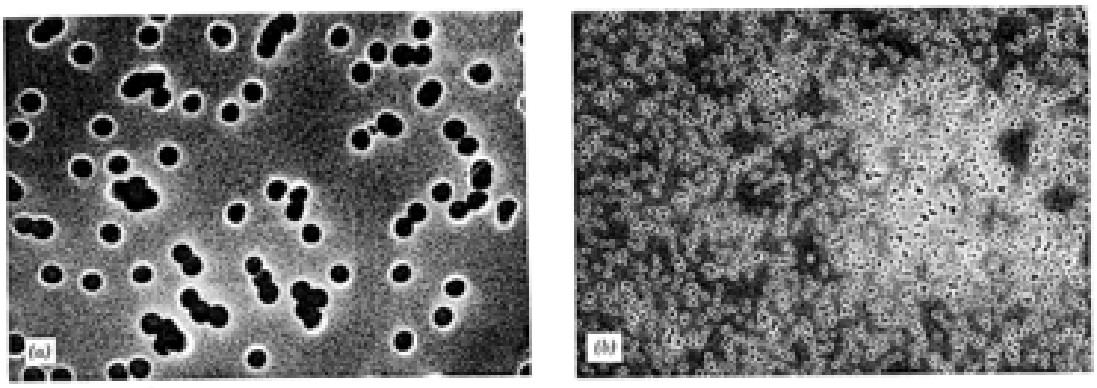

Figure 19: Scanning electron microscope photograph of a capillary pore membrane filter with a pore size of 0.8 µm. Magnification of (a) 4150x and (b) 800x. (Hinds, 2012)

It has been shown that porous membrane filters can effectively be viewed as fibrous filters having the same thickness and solidity and an effective fibre diameter slightly less than the pore size (Rubow, 1982). Therefore, all definitions and explanations given for fibrous filters are also applicable to the case of porous filters.

3 Methods

The aim of the present thesis was the investigation of both seasonal and long term trends of BC concentrations in the urban aerosol of Vienna. For this purpose, filter samples that were collected by Theresa Haller were analysed by the author for BC concentrations. Additionally, data from several publications as well as unpublished data that were provided by Regina Hitzenberger were examined. This section provides an overview of the various data sources, timeframes and measurement methods used in this thesis.

3.1 Sampling Site and Summary of Sampling Periods

All the data used in this study originate from filter samples collected at the same measurement site: the Physics Department at the University of Vienna. From January 1985 to December 1986 and from February 2014 to October 2016 the samples were taken at the roof top laboratory. The laboratory is situated close to the Vienna city centre at a height of approximately 30 m above the street level. The sampling inlets were faced towards the courtyard. Due to the height and the positioning of the inlets, the sampled aerosol is well mixed and can be viewed as urban background aerosol (Hitzenberger, 1993b). For the time from October 1994 to May 1995 and from January 2001 to December 2002, the sampling site was a balcony underneath the lab facing the same courtyard. It is assumed that the air masses reaching the balcony are overall the same as those measured on the roof top lab.

In 1985 and 1986, filter samples were taken and analysed with the Integrating Plate Photometer (see Section 3.2.1) by Regina Hitzenberger. The results of this study were published by Hitzenberger (1993b).

The filter samples from the time periods 1994 to 1995 and 2001 to 2002 were taken by Regina Hitzenberger as well, who conducted the analysis for BC using the Integrating Sphere Method (see Section 3.2.2). Parts of the data gathered in 1994 and 1995 are already published by Hitzenberger et al. (1996b) while the study conducted in 2001 and 2002 was never published.

From 2014 to 2016, filter samples were taken by Theresa Haller. They were sampled using a Leckel Filter Sampler (see Section 3.1.1) and stored in a freezer immediately after sampling. In 2018/19, in the course of this thesis, they were analysed by the author for BC concentrations using the Integrating Sphere Method. Furthermore, a selection of samples from the time period between 2014 and 2016 was analysed for EC using a Sunset Analyser (see Section 3.2.3) by Judith Kasper and the author of this thesis. Additionally,

BC concentrations were monitored by Anna Wonsachütz and Harald Schuh using a Multi Angle Absorption Photometer (see Section 3.1.1) during the same timeframe.
An overview of the various measurement periods can be found in Table 2 in Section 3.4. Figure 27 in Section 3.3 shows a timeline of all the data used in this thesis. For a detailed description of the sampling time periods, see Section 3.3.

3.1.1 Filter Sampling Methods

From 1985 to 1986, almost daily filter samples were taken on Nuclepore filters with pore sizes of 0.2 µm (Hitzenberger, 1993b). These filters were put into downward-facing filter holders with a 10 mm opening. No additional inlet was used, so there is no specified upper cutoff concerning the size of the sampled aerosol particles. Due to the downwards positioning of the filter holders, extremely large particles could not reach the filters due to their gravitational settling velocity (Regina Hitzenberger, personal communication). It was shown that only about 2.6% of the total mass of BC particles exceed a diameter of 2 µm (Hitzenberger et al., 2006b). Due to the smallness of the fraction of large particles, it is not relevant for the resulting BC concentrations whether particles with diameter larger than 2 µm are sampled or cut off, which makes the absence of an additional impactor inlet rather irrelevant.
As outlined by Hitzenberger (1993b), the filters were weighed using a Mettler ME 30 microbalance, in order to determine the total aerosol mass concentration. The absorption coefficient σ_a of the aerosol was measured with an Integrating Plate Photometer (see Section 3.2.1) at a nominal wavelength of 550 nm. Additionally, the specific absorption coefficient $B_{a,ae}$ of the aerosol was calculated following Equation 22 in Section 3.4.1. In order to get an estimate of the BC content of the aerosol, the mass concentration of BC was calculated using a $B_{a,BC}$-value of 8 m^2/g for BC (for further details, see Section 3.4.1). However, later studies showed that assuming a $B_{a,BC}$-value of 8 m^2/g was a clear overestimation of $B_{a,BC}$, resulting in an underestimation of BC concentrations, and that choosing $B_{a,BC}$ to be 6 m^2/g is more appropriate (Hitzenberger et al., 1996b). Additionally, Hitzenberger (1993b) argues that, since $B_{a,BC}$ strongly depends on the aerosol's size distribution and can only be estimated for a specific local area, the BC values reported in this study can only be treated as a first order estimate.

From October 1994 to May 1995, almost daily filter samples were taken. Some of the data was published by Hitzenberger et al. (1996b); the raw data of the whole campaign was made available for the present thesis by Regina Hitzenberger. Otherwise, the sam-

pling method was the same as in 1985 and 1986 (Hitzenberger, 1993b). Isopore filters with a 0.2 µm pore size were used in a downwards facing filter holder.
In 1994, two filters were taken most days: one day-time and one night-time filter with filter changing times in the morning and in the evening. In the calculations conducted in the course of this thesis, only the day-time filters were used, since all other samples (except for those from 2014 to 2016, which were 24-hour filters), were taken during day-time. The BC content of these filters was measured using an Integrating Sphere (Hitzenberger et al., 1996a). It is important to note that this was before the Integrating Sphere Method was extended by Wonaschütz et al. (2009) to measure both BC and BrC (see Section 3.2.2).

From January 2001 to December 2002 almost daily filter samples were taken by Regina Hitzenberger on a balcony underneath the roof top lab. Also, in this study the sampling procedure was the same as in 1994 and in 1985. Sampling times were about three to four hours a day centered around noon. Ambient aerosol was collected on Isopore filters which were analysed for BC concentrations using the original version of the Integrating Sphere Method (see Section 3.2.2) by Regina Hitzenberger.

The samples from 2014 to 2016 were taken on quartz fibre filters by Theresa Haller and analyzed for BC using the extended Integrating Sphere method by the author of this thesis. A Leckel Filter Sampler was used, which was situated at the same roof top lab where the other studies were conducted. The transition to quartz fibre instead of polycarbonate filters (which were used in all previous measurements) has been found to keep results still reasonably comparable (Reisinger et al., 2008). Furthermore, in 2014 - 2016, an impactor inlet was used, removing all particles with diameters larger than 2.5 µm. Due to the sampling location and the downwards facing inlets, it can be assumed that no significant amount of particles larger than 2.5 µm were sampled in the previous studies either. Furthermore, this change in sample inlets can also be assumed to have negligible effects on the measured BC and BrC concentrations, since both of these aerosol fractions originate from combustion processes and usually have diameters much smaller than 2.5 µm (Bond et al., 2013).

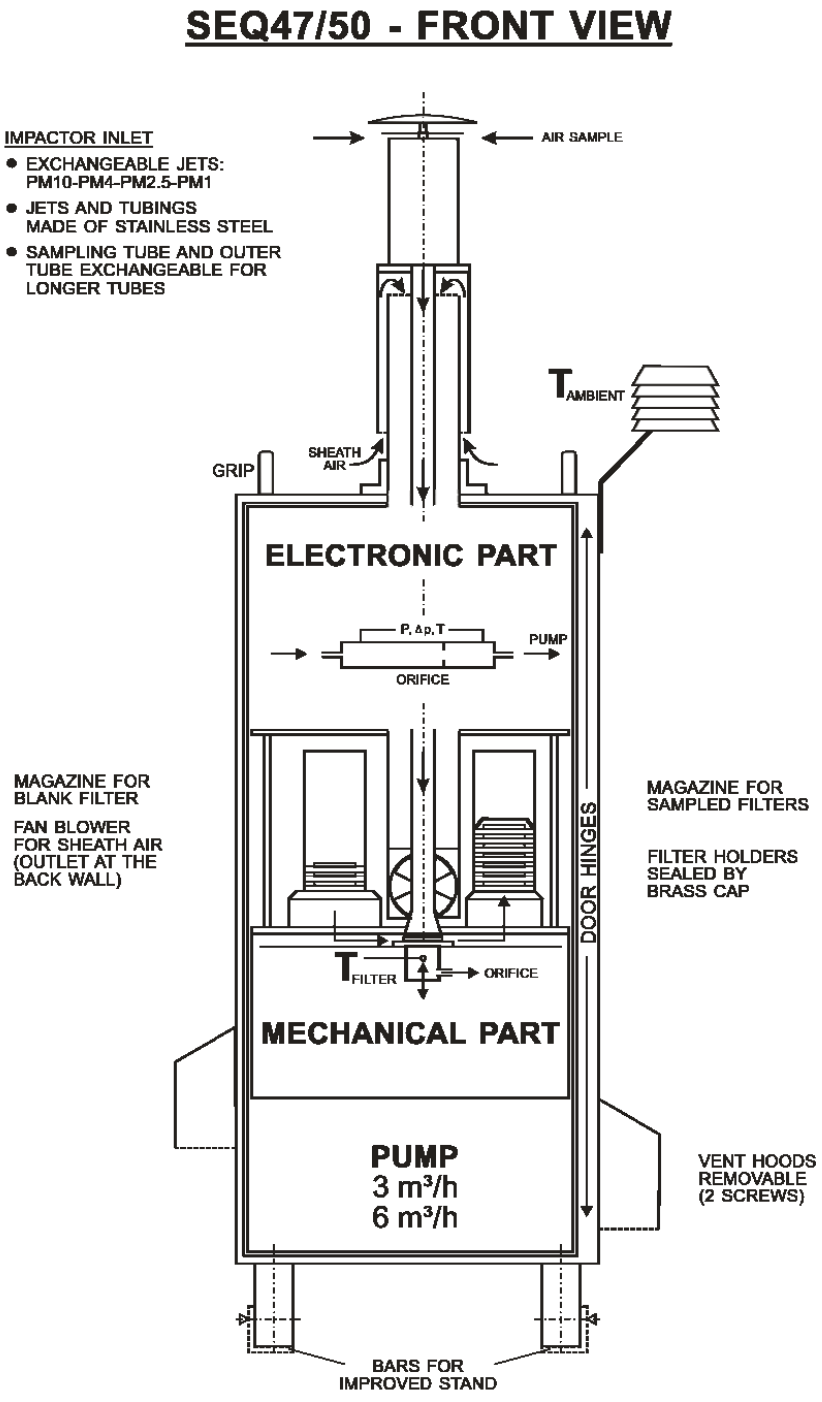

Figure 20: Schematic of the Leckel Filter Sampler Model SEQ 47/50 from Sven Leckel Ingenieurbüro GmbH (2008)

The filter samples from the time period 2014 - 2016 taken by Theresa Haller were acquired using a Leckel Filter Sampler Model SEQ 47/50.
The filter sampler pulls ambient air through the sample head using a rotary vane vacuum pump. The aerosol passes through an impactor-inlet, removing all particles with diameters larger than 2.5 µm. The impactor inlet forces the incoming aerosol stream around sharp turns, thereby larger particles cannot follow the stream due to their inertia and are removed from the incoming aerosol. The volumetric flow rate is monitored between the filter and the vacuum pump with a measuring orifice. The sampler automatically changes filters at a set time and can hold up to 17 filters at once (Sven Leckel Ingenieurbüro GmbH, 2008). Figure 20 shows a schematic illustration of the instrument's setup.

In the study conducted from 2014 to 2016, the volumetric flow rate was set to a target value of 2.3 m^3/h and the sampling time was 23 h, resulting in a total volume of sampled air of roughly 53 m^3 per filter. The filter change was set to be around noon, leaving one hour each day where the sampling was paused. For the calculations of EC, BC and BrC concentrations, the actual flow rates, monitored and reported by the Leckel Filter Sampler's firmware were used (see Section 3.4.2).

Sampling and Analysis with the Multi Angle Absorption Photometer (MAAP)

In addition to the filter samples collected from 2014 to 2016, a Multi Angle Absorption Photometer (MAAP) was operated to provide another source for BC measurement values. The MAAP is a filter based instrument for monitoring BC concentrations (Petzold and Schönlinner, 2004). This instrument not only collects ambient aerosol particles, but also performs optical measurements and a complete numerical analysis of the measured data returning values of BC mass concentrations in real time. An aerosol is collected on a filter tape and a light source illuminates the sample at a given wavelength with a known intensity. Similar to the Aethalometer (Hansen et al., 1984), the intensity of the light transmitted through a filter is measured to determine the absorption coefficient of the sample. In contrast to previous techniques used for measuring BC at the time the instrument was developed, the MAAP also measures the intensity of the light scattered by the aerosol particles at different angles. The following section describes its measurement principle. If not indicated otherwise, all the information is taken from Petzold and Schönlinner (2004).

The main objective of the MAAP is measuring BC concentrations while taking aerosol particle scattering effects into account. For this purpose, the aerosol is collected on a fibre filter tape and is illuminated with a collimated light source. The transmitted light intensity as well as the intensity of the reflected light are measured simultaneously while the filter spot is being loaded with aerosol particles. The sample aerosol is continuously collected on the same spot of the filter tape until the transmitted light intensity falls below a threshold value and the filter spot is regarded as loaded to its maximum capacity. Then, the instrument mechanically moves the filter tape forward exposing a fresh, unloaded spot of filter tape, on which the collection and measurement of BC is continued.

In contrast to membrane filters, aerosol particles collected in a fibre filter, are collected not only on the filter surface, but penetrate the filter and are deposited inside the diffusely scattering filter matrix. For their analysis, Petzold and Schönlinner (2004) use a radiative transfer model dividing the filter into two layers: 1) The layer facing the sampling inlet, where the aerosol particles are deposited, which consists of both particles and filter fibre, is called aerosol-filter layer. 2) The rest of the filter, which makes up most of the filters' thickness, the particle-free filter matrix. Figure 21 shows a schematic illustration of this two layer system. The collimated incident radiation interacts with the aerosol-filter layer and the light scattered from it further interacts with the particle-free filter matrix. Direct interactions of the incident light with the particle-free filter matrix are not taken into account, since they are not influenced by the loading of the aerosol-filter layer. The measurable values are a) the transmitted and forward scattered radiation and b) the backward scattered radiation. The radiation passing through the aerosol-filter layer is mostly diffuse with a small fraction remaining collimated. The back scattered radiation can be regarded as solely diffuse radiation (Petzold and Schönlinner, 2004). To calculate the radiation properties of this system, a radiative transfer approximation is performed. Intensities are always regarded in relation to those measured with a blank filter, for which the same filter, before loading it with an aerosol sample, is used. The important values that can be measured are therefore the fraction of radiation passing through $P/P^{(0)}$ and the radiation scattered back $B/B^{(0)}$ by the whole filter system (i.e. both layers) in relation to the blank filter (Petzold and Schönlinner, 2004). These values are calculated using a simplified adding method (Hänel, 1987). Furthermore, the scattering properties of the particle-filter layer alone are calculated using a two stream approximation (Petzold and Schönlinner, 2004).

Petzold and Schönlinner (2004) measured the angular dependance of the scattered ra-

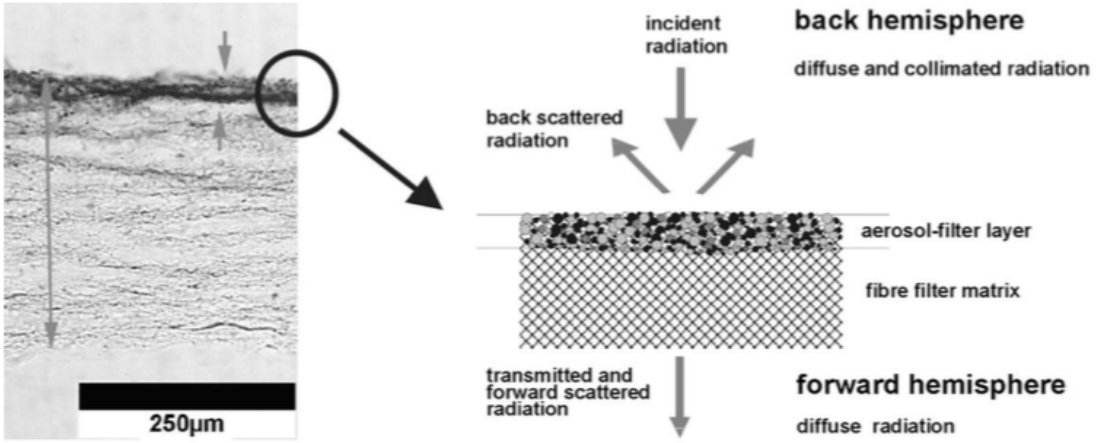

Figure 21: Image and schematic illustration of the two filter layers used in the radiative transfer model to calculate the BC concentrations from Petzold and Schönlinner (2004)

diation for a lab generated test aerosol consisting of different ratios of absorbing (BC) and scattering (NaCl) fractions. They then fitted the observed angular distribution with a linear combination of the Lambertian cosine law and a Gaussian-type distribution. Thereby they found that the back scattered radiation was completely diffuse for a purely scattering aerosol while it was completely Gaussian when the aerosol consisted only of absorbing components. In order to determine the absorbing fraction of an aerosol, a second detector in the backwards hemisphere was necessary. Further investigation by Petzold and Schönlinner (2004) showed that the largest difference between diffuse and Gaussian scattering can be found when the two detectors in the backwards hemisphere are positioned at the angles $\Theta_1 = 130°$ and $\Theta_2 = 165°$ (Petzold and Schönlinner, 2004). Figure 22 shows an illustration of the positioning of the optical detectors.
Using the setup described above, the absorption coefficient of the aerosol deposited on the fibre filter can be measured. The BC mass concentration is calculated by the instrument automatically via the relationship given in Equation 22 (see Section 3.4.1) using a preset value of $B_a(BC) = 9.1$ - $10.7\ m^2/g$ (Petzold and Schönlinner, 2004). All the calculations are performed automatically by the instrument, which, with the settings used for the present thesis, returns a data point of BC mass concentration every six minutes. Using the internal data network developed by Wolfgang Ludwig for the research group for Aerosol Physics and Environmental Physics at the University of Vienna, the data was automatically saved on a server.

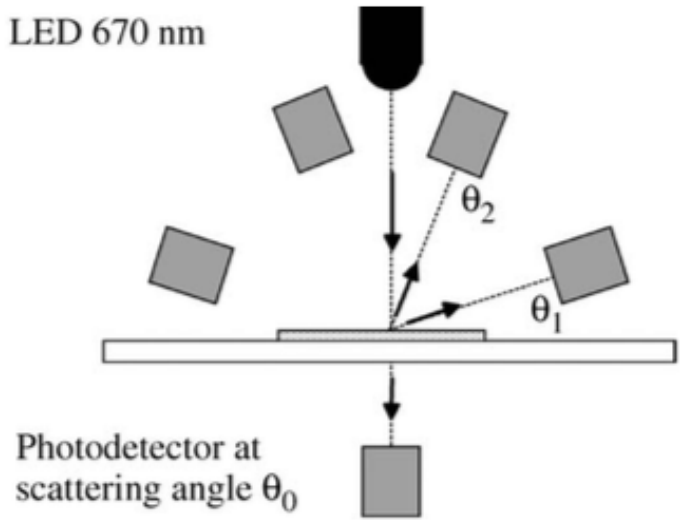

Figure 22: Schematic illustration of the positioning of the optical detectors from Petzold and Schönlinner (2004). $\Theta_0 = 0°$, $\Theta_1 = 130°$, $\Theta_2 = 165°$

In the present thesis, a model 5012 MAAP (Thermo Fisher Scientific) was used. The instrument was situated at the University on Vienna roof top laboratory, where most of the filter samples used in this thesis were taken (see Sections 3.1.1). It was continuously measuring during most of the time period from 2014 to 2016 and was maintained by Anna Wonaschütz and Harald Schuh during this time.

3.2 Sample Analysis Methods

As will be described in Section 3.3, different kinds of measurement methods were used to acquire the BC and BrC data from filter samples from different sampling periods. This section provides a detailed description of the various methods used to acquire both BC and BrC data used in the course of this thesis.

3.2.1 Integrating Plate Photometer

The Integrating Plate Photometer (IP) is an instrument used to measure the absorption coefficient of an atmospheric aerosol. The method was first developed in 1973 by Lin et al. (1973). A slightly modified version by Habenreich (1983) is relevant for the present work, since it was used to measure the absorption coefficient of the Viennese urban air in the time period from 1985 to 1986 (Hitzenberger, 1993b). The data acquired for this

study was used in the present thesis to calculate the corresponding BC concentrations (see Section 3.4 and Table 2 in Section 3.4).

The principal idea of the Integrating Plate method is to measure the absorption coefficient of an aerosol collected on a filter in relation to a filter blank. The sample filter is illuminated by a well known light source and the intensity of the light passing through the filter is measured with a photodetector. With I being the intensity measured with a loaded sample filter, I_0 being the one measured with a blank filter and L referring to the length of the sampled air column, applying Lambert-Beer's law (Equation 20) allows to calculate the absorption coefficient $\sigma_{a,ae}$.

$$\frac{I}{I_0} = e^{-\sigma_{a,ae} * L} \tag{20}$$

$$\sigma_{a,ae} = -\frac{A}{V}\, ln \frac{I}{I_0} \tag{21}$$

where A is the area of the sample filter, and V refers to the sample volume.
Fig 23 shows a schematic illustration of the experimental setup. In order to integrate the light scattered by the aerosol particles, an opal glass plate is inserted between the sample filter and the detector (Habenreich, 1983). To maximise the transmitted light for filter samples with non-absorbing particles, the sample filters are positioned in such a way, that the loaded side faces away from the light source, towards the detector. Additionally, an interference filter with a nominal wavelength of 550 nm is placed in front of the sample filters to select a specific wavelength (Hitzenberger, 1993a).
However, this method suffers from several inaccuracies and is no longer in use. One of its major downsides is that is does not account for back-scattering on particles very well. Light scattered into directions outside the opening angle of the detector is lost to the detection apparatus, which can lead to a severe over estimation of absorption coefficients. This problem is addressed much more accurately in other, more modern methods used in the present thesis like the MAAP (Section 3.1.1) and the Integrating Sphere method (Section 3.2.2).

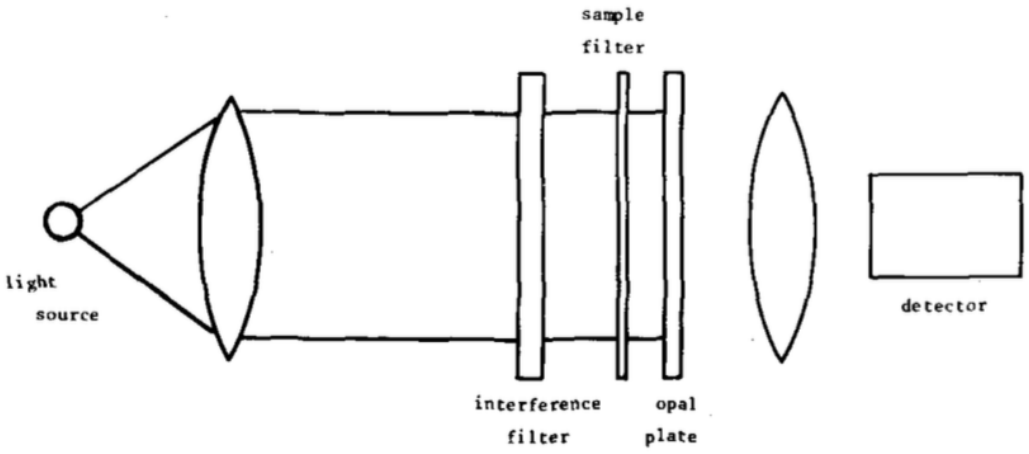

Figure 23: Setup of the Integrating Plate Photometer (Hitzenberger, 1993a)

3.2.2 Integrating Sphere

The Integrating Sphere method was originally developed by Heintzenberg (1982) to measure BC concentrations in aerosol samples. The method was then developed further by Hitzenberger et al. (1996a), Hitzenberger and Tohno (2001) and again by Wonaschütz et al. (2009).
The Integrating Sphere method is used to determine the content of black carbon (later extended also for brown carbon (Wonaschütz et al., 2009)) in a sample containing an externally or internally mixed aerosol. A schematic representation of the experimental setup can be found in Figure 25. The Integrating Sphere (Labsphere Inc.) is internally coated with a material that reflects incoming light almost perfectly diffusely ("Spectraflect", Labsphere Inc.). It is furthermore equipped with 1) a sample port, through which a sample holder (coated with opaque white) can be inserted placing the sample into the center of the sphere, 2) a port through which the inside of the sphere can be illuminated with a light source and 3) a small outlet at the bottom of the sphere at the end of which a photodiode detects the outgoing radiation (see also Figure 25).

The measurement principle is as follows:
1) A small section (usually a circular punch) of a loaded filter is immersed in a liquid solution in a transparent plastic vial to dissolve soluble coatings on the BC particles. The influence of insoluble coatings that might remain on the BC particles is negligible, since they have refractive indices very similar to that of the liquid solution (Hitzenberger

and Tohno, 2001). The vial is inserted into the sphere via the sample port.
2) Light from a halogen lamp passes through a diffusor, one out of three interference filters (selecting a wavelength of 450, 550 or 650 nm) and another diffusor before entering the Integrating Sphere.
3) Inside the sphere, the incoming radiation is either scattered by various sample contents, or absorbed by the light absorbing carbonaceous material on the filter sample. The scattered radiation is again diffusely reflected by the walls inside the sphere and either reabsorbed by the sample, or scattered again. The amount of radiation exiting the sphere is measured by the photodetector.
The Integrating Sphere prevents overestimations of the BC content on the sample that might occur in other absorption-based measurement methods due to backscattering. All the scattered radiation is reflected diffusely by the inside walls and is reabsorbed by the sample or measured by the detector. Therefore, possible losses due to light scattering are prevented and the overall light attenuation by the sample is measured.
The steps described above are repeated with an empty vial after every other sample. Thereby, the overall light attenuation by the filter sample can be measured in relation to an empty vial. Measuring the empty vial after every other sample makes it possible to account for possible fluctuations of incoming light intensity caused by the light source. The actual amount of BC in a sample is determined via instrument calibration with a well known BC standard. The integrating sphere was calibrated with graded suspensions of Carbon Black (Elftex 124, Cabot Corporation) for BC and graded solutions of humic acid sodium salt (Acros Organics, no. 68131-04-4) for BrC (Wonaschütz et al., 2009). In the course of the present thesis, filter samples from the mid 2010s were analysed for BC and BrC using this extended version of the Integrating Sphere method with the calibration curves given in Figure 24.
While the measurement principle has remained the same, over the years this instrument has been in use, different filter materials, sample preparation procedures and solutions have been used. From 1994 to 2001 Isopore polycarbonate filters were dissolved in chloroform following the procedure given by Hitzenberger et al. (1996a). From 2006 onwards, since the instrument was extended for detection of BrC, glass fibre filters were used for sampling and placed in a mixture of 50% acetone and 50% of a 80:20 water/isopropanol mixture (Wonaschütz et al., 2009). A comprehensive study on the different measurement techniques (polycarbonate filters in chloroform vs. quartz fibre filters in acetone and water/isopropanol) was conducted by Reisinger et al. (2008), who found that the techniques were overall well comparable.

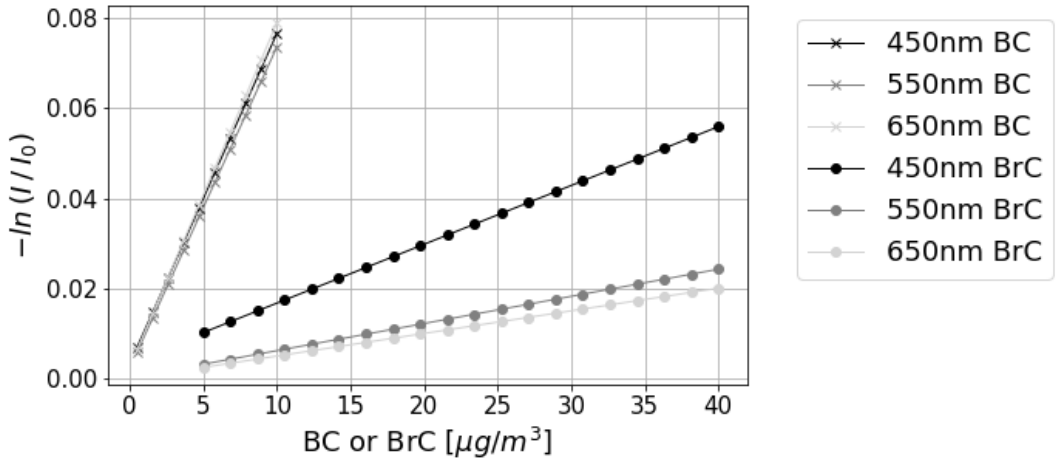

Figure 24: Calibration curves of the Integrating Sphere (Wonaschütz et al., 2009) as they were used in the analysis of the recent filter samples conducted by the author. Mass of BC or BrC in µg/m^3 vs light attenuation (logarithm of intensity after passing through sphere (I) over incident intensity (I_0))

The calculation of masses of BC and BrC in the sample is conducted using the calibration curves, which can be found in Figure 24. The different shades indicate the three different wavelengths. It can be easily observed, that the signal for BrC (lines marked with full circles) varies greatly with the wavelengths, while the curves obtained for the three different wavelengths are almost identical for the BC signal (lines marked with x).

The following iterative procedure developed by Wonaschütz et al. (2009) is used to determine the BC and BrC masses on the filter samples: First, the absorption signal of light at a wavelength of 650 nm is determined. Since BrC is known to be a very weak absorber of longer wavelength light, this signal is solely assigned to BC. From the calibration curve for BC at 650 nm (light gray curve with markers 'x' in Figure 24), the corresponding BC concentration is calculated. Then, the expected signal for 450 nm light for this BC concentration is calculated from the calibration curve for BC at 450 nm. This signal is then subtracted from the measured signal at 450 nm. This difference is assumed to be the signal coming from BrC and a first guess BrC concentration is calculated from the calibration curve for BrC at 450 nm. Then, the expected contribution of this amount of BrC to the signal at 650 nm is calculated and subtracted from the measured signal. A new value for BC is then calculated from the calibration curve using the 'new' signal at

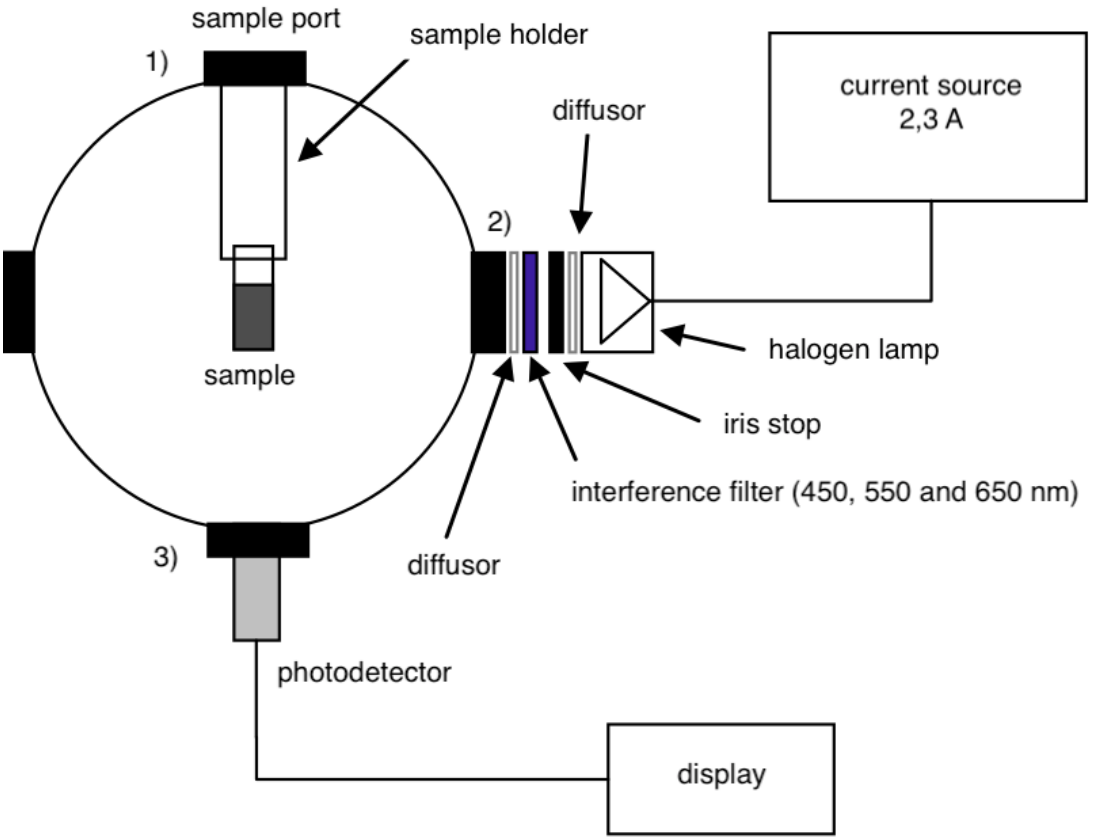

Figure 25: Setup of the Integrating Sphere (Wonaschütz et al., 2009, modified)

650 nm. This procedure is then repeated four times, which is when it was usually found to converge (Wonaschütz et al., 2009).

In the author's experimental work for the dataset spanning the period from February 2014 to October 2016 the method was applied as follows:
Small circular punches with a diameter of 10 mm were punched out of the loaded filter areas and put into translucent plastic vials. A 4 ml solution consisting of 2 ml of Acetone and 2 ml of an Isopropanol (20 %) - water (80 %) mixture was added to the filter punches. Usually, 22 samples were analysed in one run. Additionally, two vials containing only 4 ml of solution but no filter punches were prepared. They are used as a reference, to take possible absorption effects of the solution itself into account. These 24 vials were put into an ultrasonic bath for 10 min. Furthermore, before measuring the first batch of samples each day, a waiting time of approximately 30 minutes had to be kept after

switching on the Integrating Sphere components, in order to let the light signal of the halogen lamp stabilise.
Using a slider with the three interference filters, one of the three wavelengths was chosen and the absorption signal of all 24 samples was analysed as described above. Every two samples were followed by a blank reference to account for possible instabilities in the light source. After all 24 samples were measured, this procedure was repeated for the other two wavelengths.
A Microsoft Excel template, created by Regina Hitzenberger and Robert Wagner, was used to perform the iterations determining BC and BrC concentrations.

3.2.3 Sunset Analyzer

The Sunset Analyzer (Sunset Laboratory Inc.) is a thermo-optical measurement device that aims at determining the ratio of EC to OC in an aerosol filter sample. In the following chapter its measurement principle is explained briefly. Afterwards, some problems that occurred during the actual measurement as well as their corrections are described. An instruction for a standard operating procedure that was developed thereafter can be found in Appendix B.

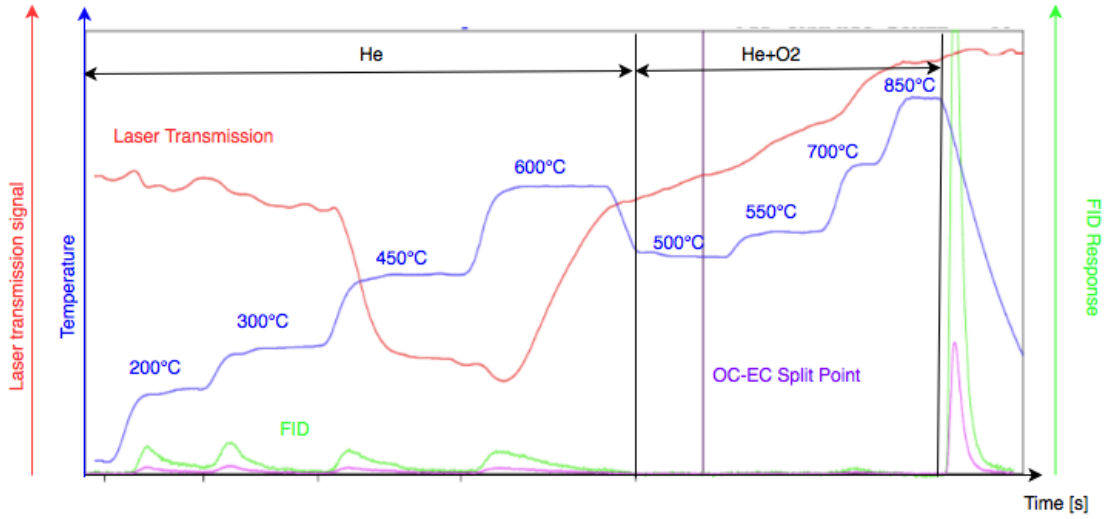

Figure 26: Thermogram resulting from an EC/OC measurement conducted with the Sunset Analyzer

Measurement principle The Sunset Analyzer's operation principle is based on stepwise heating of the sample in order to vaporize and oxidize the carbonaceous fraction

of the collected aerosol. The EUSAAR2 protocol (Cavalli et al., 2010) determining the magnitude and duration of the temperature steps was applied in all filter measurements. The analyzer basically consists of the following parts: a sample oven, an oxidizer oven and a flame ionization detector. There are two separate measurement cycles in order to detect OC and EC respectively. Figure 26 shows a typical thermogram that was recorded during a measurement.

For the detection of OC, a filter punch is placed on the sample holder which is inserted into the sample oven. Within the sample oven, the temperature is increased stepwise to 600°C in a helium atmosphere (as indicated by the blue curve in Figure 26). The helium prevents the carbonaceous molecules from oxidizing and ensures that only volatile organic carbon vaporizes. The organic compounds, now in the gas phase, are then moved into the oxidizing oven, where they are oxidized with a catalyzer via the following reaction: $C_XH_X \xrightarrow{O_2,Cat,\Delta} CO_2 + H_2O$. However, CO_2 can not be detected by the flame ionization detector, therefore it has to be transformed into methane: $CO_2 + 4\,H_2 \xrightarrow{-\,2\,H_2O,500\,C} CH_4$, which is detectable by the flame ionisation detector. The signal of the flame ionization detector is indicated by the green curve in Figure 26.

EC is detected the following way: Since EC is not volatile, after the vaporization of OC in a helium atmosphere, all of the EC still remains on the filter. In the next step, a mixture of helium and oxygen is introduced into the sample oven and the temperature is again increased stepwise from 500°C to 850°C. In the course of this, the EC oxidizes and no further catalytic oxidation is needed. After the transformation of the resulting CO_2 to methane, as described above, it can be detected by the flame ionization detector.

During these processes, the optical reflection and transmission of the sample are measured using a laser and two optical detectors (the laser transmission signal is depicted by the red curve in Figure 26). This is necessary, because in reality, not all of the OC is vaporized at high temperatures in a helium atmosphere. Through pyrolytic effects, some of the OC is transformed into pyrolytic carbon. This pyrolytic carbon is a strong light absorber and shows no volatility, so would it be detected as EC in the helium oxygen atmosphere. To prevent this overestimation of EC, the actual split point (purple line in Figure 26) of when the FID signal corresponds to OC or EC is set at the point of time when the reflection (or transmission) signal reaches the value it had when the sample was first inserted into the oven.

Experimental Implementation For calibration and in order to ensure a stable measurement operation, sucrose standards containing a well known amount of carbon, are analysed. A stable working condition of the Sunset Analyzer is ensured by the measurement of at least one sucrose standard in the beginning of each day the instrument is used. For a detailed description of the experimental implementation of the Sunset Analyzer, see Appendix B.

During the analysis, which was conducted by Judith Kasper and the author of this thesis, strong fluctuations (in the range of $\pm 25\%$) in the measured values of the sucrose standards were observed. After a closer inspection, streaks/contaminations in the solution were discovered. In order to determine the source of these contaminations and to find out whether they are the cause of the fluctuations, the following possible effects were tested for and eventually ruled out:

1. Faulty preparation practice
    - Fresh sucrose provided by the department of chemistry was used
    - Fresh solutions were prepared strictly according to the instructions given in an extension of the Sunset manual
    - Fresh sucrose standards produced by the department of chemistry were used
    - A different kind of standard (phthalic acid) was used instead of sucrose. In contrast to the sucrose solution, this standard was far better reproducible.
2. Contamination of the ultrapure water
    - Solutions were prepared once with ultrapure water provided by the department of chemistry and in all the following cases with ultrapure water provided by the working group of Bernadett Weinzierl
3. Improper cleaning and storing
    - The cleaning procedure, which used to include cleaning with isopropanol was changed to using the laboratory dishwasher and only ultrapure water, leaving out isopropanol entirely.
    - The stock solution was stored in the refrigerator to inhibit possible bacterial growth.

- Several blank filter measurements were conducted, also resulting in overestimated carbon concentrations.

Finally, the methanator, which is one of the key parts of the instrument, transforming the CO_2 formed during the heating of the sample into methane, which is detectable by the FID, was replaced. It turned out, that the problems that occurred during sucrose measurements were most likely caused by the old methanator ceasing to work properly. Evidently, it had been exposed to ambient air quite frequently while still at a high temperature, which has caused it to produce only a very weak signal, which was of the same order of magnitude as the background noise (see Appendix B for further information). The strong fluctuations occurred, because the instrument basically averaged over the background noise. Replacing the methanator and avoiding exposure to air when still at high temperatures finally solved the problem.

3.3 Data Availability and Repositories

As already described in Section 1, the aim of the present thesis was to examine both seasonal and long term trends and variations of the BC mass concentration in the urban aerosol of Vienna. For this purpose, several sources of data, both published and unpublished, were used. Figure 27 provides an overview of the various kinds of data and the timeframes for which they were available. The horizontal axis shows a timeline and the different data types are displayed on the vertical axis. Different colours and patterns indicate different types of data.

The most important data for the present thesis were acquired by the analysis of filter samples for BC. For this data-group, four distinct measurement periods can be distinguished: the mid-1980s, the mid-1990s, the early 2000s and the mid-2010s. They are shown in more detail in Table 2. As already outlined in Chapter 3.1, the data from the timeframes of the mid-1980s (Jan. 1985 to Dec. 1996), the mid-1990s (Oct. 1994 to May 1995) and the early 2000s (Jan. 2001 to Dec. 2002) was provided by Regina Hitzenberger, who performed both the filter sampling and the analysis. In the mid-2010s (Feb. 2014 to Oct. 2016), filters were sampled by Theresa Haller. These filters were analysed for BC by the author of this thesis. The data coverage (i.e. the fraction of days for which filter samples were available in the total number of days within the investigated timeframe) for each of these sampling periods is shown in Table 1. Unfortunately, the coverage is unknown for the timeframe in the mid-1980s. The best data coverage could be achieved in the mid-2010s (78%) and in the mid-1990s (73%), while in the early 2000s

Time Period	Data Coverage
Jan. 1985 - Dec. 1986	Unknown
15.10.1994 - 15.05.1995	73%
03.01.2001 - 26.12.2002	55%
15.02.2014 - 02.10.2016	78%

Table 1: Data coverage of all investigated timeframes

only 55% of all days are covered. However, in these three timeframes, the days on which no BC measurements were conducted, are spread very evenly throughout the months, usually originating from single missing days and not from missing consecutive weeks. Therefore, the data coverage is assumed to be sufficient for the purposes of the present thesis.

In Figure 27, the black bars show BC data obtained with different instruments at different times. The black and brown bar indicates the most recent measurement period, where the filters were analysed for both black and brown carbon. The red bar represents the timeframe for which also EC was measured. Since analyzing filters with the Sunset Analyzer proved to be rather time consuming, every six$^{\text{th}}$ day's filter was chosen for analysis. Thereby the total workload was severely reduced and systematic errors that might have occurred when always measuring the same day of the week were avoided. Hourly data on PM10 and PM2.5 concentrations were provided by the Austrian Environmental Agency (Österreichisches Umweltbundesamt) as indicated by the dotted orange bar in Figure 27. The data was obtained at the measurement station "AKH", situated about 1 km linear distance from the measurement site of this thesis. The orange bar with a wave pattern represents hourly temperature data, which was provided by the Austrian Central Agency of Meteorology (Zentralanstalt für Meteorologie, ZAMG). It was measured at the Central Institute for Meteorology and Geodynamics, Hohe Warte 38, 1190 Wien, which is about 3 km linear distance away from the site were the filters used in this thesis were taken. Both PM and temperature data were available for the whole measurement period in the mid-2010s.

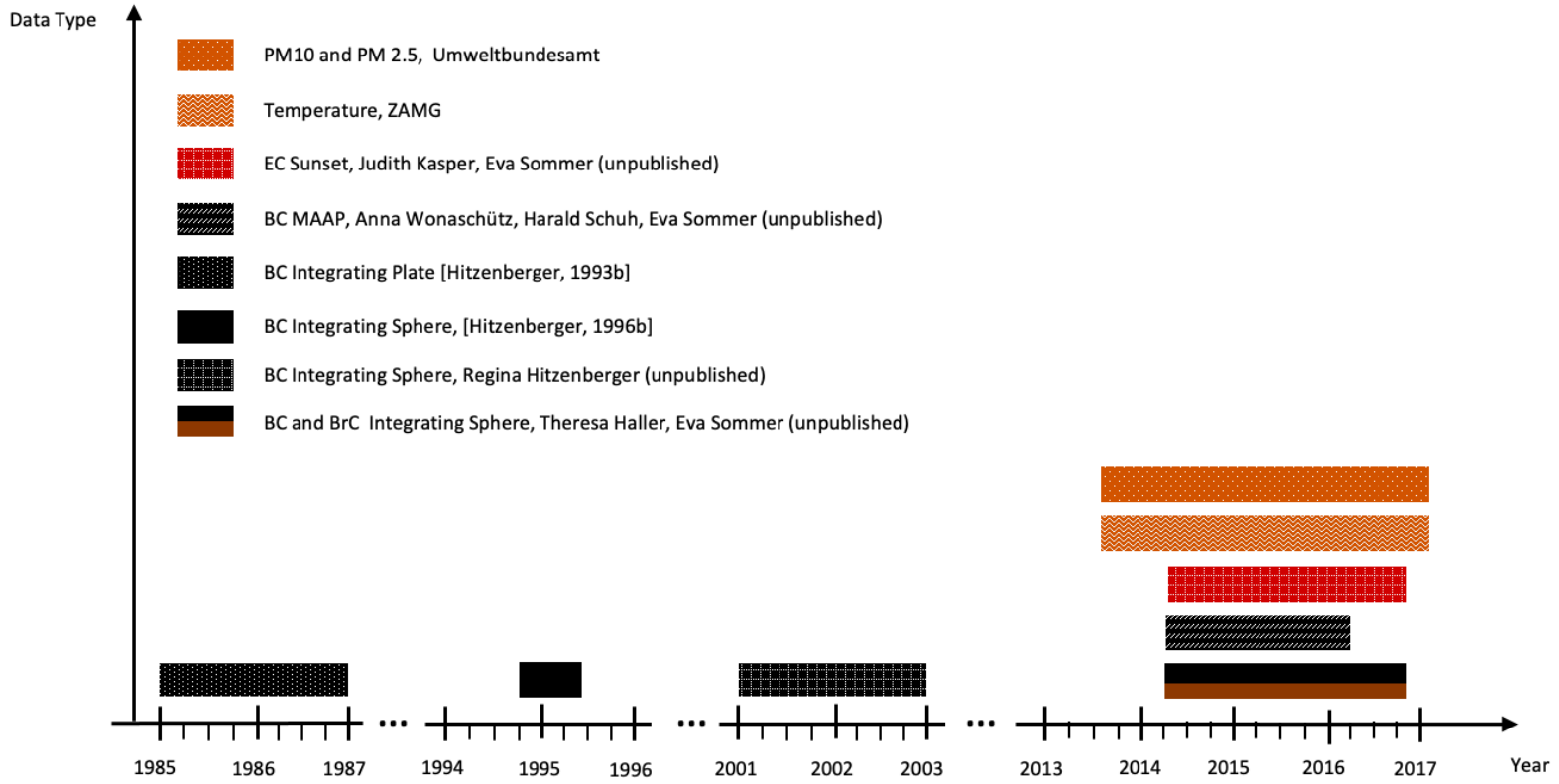

Figure 27: Timeline of the various data types used to determine seasonal variations and long term trends of BC and BrC mass concentrations in the urban aerosol of Vienna.

3.4 Data Processing

The following Chapter is dedicated to the description of how the data was processed. A summary of the available data and the respective measurement methods and periods can be found in Table 2. All calculations and plots were created by the author using Python 3 and the pandas data analysis library. The filter collection efficiency for all measurements was assumed to be 1.

Time period	Measured quantity	Published by	Method	Site	Filter material	Inlet
Jan. 1985 - Dec. 1986	σ_a	(Hitzenberger, 1993b)	Integrating Plate	Roof top lab	Polycarbonate	TSP
15.10.1994 - 15.05.1995	BC	partly published by Hitzenberger et al. (1996b)	Integrating Sphere	Balcony	Polycarbonate	TSP
03.01.2001 - 26.12.2002	BC	Regina Hitzenberger unpublished	Integrating Sphere	Balcony	Polycarbonate	TSP
15.02.2014 - 02.10.2016	BC and BrC BC EC	Theresa Haller and Eva Sommer, unpublished	Integrating Sphere MAAP Sunset Analyzer	Roof top lab	Quartz fibre	PM2.5

Table 2: Available Data

3.4.1 Determining Black Carbon Concentrations from Measurements of σ_a with the Integrating Plate Method

In her study on the light absorption of the Viennese urban aerosol in the mid-1980ies, Hitzenberger (1993b) did not directly measure BC concentrations, but only the aerosol's absorption coefficient σ_a using the Integrating Plate Method (see section 3.2.1). Therefore, in the course of the present study, the corresponding BC concentrations were calculated from the original data provided by Regina Hitzenberger. In this section, the calculation of the BC concentrations is described.

The Integrating Plate is an instrument designed to measure an aerosol's absorption coefficient $\sigma_{a,ae}$. Another important value considering an aerosol's absorption properties is its specific absorption coefficient $B_{a,ae}$, which is the ratio of the absorption coefficient $\sigma_{a,ae}$ and the mass concentration of light absorbing particles in the aerosol $c_{m,ae}$. Therefore the mass concentration of a light absorbing aerosol can be calculated as follows (Weingartner et al., 2003):

$$c_{m,ae} = \frac{\sigma_{a,ae}}{B_{a,ae}} \tag{22}$$

The subscript ae indicates the whole aerosol as opposed to the subscript BC denoting only the fraction of black carbon (BC) (see Equation 23). $\sigma_{a,ae}$ can be calculated from Lambert-Beers's law (Equations 20 and 21 in Chapter 2.1), where the intensities I and I_0 are measured with the Integrating Plate Method. The area A of the sample filter and the sample volume V are given by the filter sampling setup. However, one of the objectives of this thesis is to determine a long term trend of BC mass concentrations in the Viennese urban aerosol. For BC Equation 22 can also be written as:

$$c_{m,BC} = \frac{\sigma_{a,BC}}{B_{a,BC}} \tag{23}$$

In order to calculate the amount of BC contained in an atmospheric aerosol with a known absorption coefficient $\sigma_{a,ae}$, one has to be able to assume that the whole light absorbing fraction contained in the aerosol can be attributed to BC ($\sigma_{a,ae} = \sigma_{a,BC}$).
If this assumption holds, combining Equations 22 and 23 yields:

$$c_{m,BC} = c_{m,ae}\,\frac{B_{a,ae}}{B_{a,BC}} \tag{24}$$

In the calculations described above, the specific absorption coefficient of BC $B_{a,BC}$

has to be taken from literature. However, the specific absorption coefficient of black carbon is not a well known factor. It varies with the size distribution and the complex index of refraction of BC, which in turn depend on specific BC sources, and therefore can be quite different depending on the measurement site. Hitzenberger (1993b) used a specific absorption coefficient of $B_{a,BC} = 8\ \mathrm{m}^2/\mathrm{g}$ for their calculations of BC mass concentrations. Later, this value was found to underestimate BC concentrations and a value of $B_{a,BC} = 6\mathrm{m}^2/\mathrm{g}$ for the Viennese urban aerosol has been suggested (Hitzenberger et al., 1996b). In the calculations for the filter samples analysed with the Integrating Plate $B_{a,BC} = 6\ \mathrm{m}^2/\mathrm{g}$ was used in the present thesis. The BC mass concentrations were calculated following Equation 24. However, since the BC mass concentrations were not directly measured with this method, the calculated BC mass concentration values can only be treated as estimates (Hitzenberger et al., 1996b). Furthermore, these calculations are based on the assumption that BC is the only light absorbing component in the atmosphere, which is known to be untrue, since BrC is also slightly light absorbing. The BC concentrations calculated in this manner can therefore only be treated as an upper estimate.

3.4.2 Calculating EC, BC and BrC concentrations from filter punches

Using a calibration curve and the iterative method, the amount of BC and BrC on the filter punches is determined as described in Section 3.2.2. Likewise, the Sunset Analyser detects carbonaceous gases evolved from the sample at certain temperatures to determine the amount of OC and EC on the filter punches (see Section 3.2.3). The following section describes how the concentrations of EC, BC and BrC in the ambient air are calculated from the mass on the filter punch, the known areas of both the filter punch and the loaded part of the filter, the flow rate and the sampling time.
First, the mass of EC, BC or BrC on the filter is calculated:

$$M(Filter) = \frac{M(Punch)}{A(Punch)} A(Filter) \tag{25}$$

where $M(Filter)$ and $M(Punch)$ are the masses of EC, BC or BrC on the whole filter and the punch respectively. $A(Filter)$ and $A(Punch)$ denote the respective surface areas. The quartz fibre filters used in the present thesis had a sampling surface of $A(Filter) = 12.997\ \mathrm{cm}^2$ and a filter punch of $A(Punch) = 3.14\ \mathrm{cm}^2$ was analysed.
Furthermore, the total air volume V in m^3, which passed through the filter, is determined using the sampling time t in hours (h) and the flow rate Q in m^3/h.

$$V = Q * t \tag{26}$$

The concentration of EC, BC or BrC in µg/m^3 is therefore:

$$C = \frac{M(Filter)}{V} \tag{27}$$

The Integrating Sphere has certain detection limits due to its calibration. The detection limit for BC is 1 µg and for BrC it is 10 µg per filter punch, which, for filter punches with a diameter of 10 mm, corresponds to concentrations of approximately 0.33 µg/m^3 and 3.3 µg/m^3 respectively. Since the filter punches used for analysis in the present thesis are rather small, many values, especially for BrC, were below the detection limit. Therefore, the calibration had to be extrapolated to lower values, assuming linearity. This assumption seems reasonable, since the calibration curves became non-linear at high concentrations, but there is no reason to suspect non-linearity at concentrations lower than the lower limit of the calibration curve.

3.4.3 Calculating Mean Values of Temperature, PM and BC Concentrations

In the mid-2010s, a Leckel Filter Sampler (see Section 3.1.1) was used and the time of filter change was around noon (varying between 11:00 am and 01:00 pm).
Each filter was assigned a consecutive number corresponding to the day on which the sampling time ended. Therefore, a filter sample 'taken on' November 2nd, actually contains the aerosol from November 1st at 12:00 noon to November 2nd 11:00 am. For purposes of comparability, the hourly values of temperature and particulate matter (PM) obtained from the Austrian Central Agency of Meteorology (Zentralanstalt für Meteorologie, ZAMG) and the Austrian Environmental Agency (Umweltbundesamt, UAB), were averaged over the same time period. Additionally, the BC values obtained every 6 minutes by the MAAP were also averaged over this period. Therefore, a temperature or BC value for November 2nd denotes an average temperature or BC value from November 1st 12:00 noon to November 2nd 11:00 am. All additional data (PM2.5 and temperature) presented in Chapter 4 are averaged over 24 hours from noon to noon.
In order to investigate long term trends of BC concentrations in the Viennese air, seasonal mean values were calculated. For that purpose, two distinct seasons were defined: Winter season is taken to be the months December, January and February and summer is defined to last from June to August. Furthermore, monthly mean values were calculated for all the investigated timeframes.

4 Results

4.1 Method Comparison

The following section is dedicated to the comparison of the results from different instruments and analysis techniques that were used in the present thesis.
An extensive study on comparing measurement methods for BC and EC was conducted in the course of a diploma thesis in 2007 based on measurements conducted in February and March 2006 (Reisinger, 2007). The underlying data of this thesis were kindly provided to be used in the present work for comparison purposes.

4.1.1 Integrating Sphere and MAAP

BC was monitored with a MAAP from February 15$^{\text{th}}$ 2014 to February 11$^{\text{th}}$ 2016 in parallel with the filter samples obtained with the Leckel Filter Sampler. In the following section a comparison of the BC concentrations obtained with the MAAP and those obtained with the Integrating Sphere from filter samples is presented.

Figure 28 shows BC values measured with the Integrating Sphere Method and the MAAP respectively, over the whole time frame from 2014 to 2016. At a first glance, the two instruments seem to agree rather well, with only rare occasions where the MAAP detects severely higher concentrations.
In Figures 29b to 29e, scatterplots with daily average BC values from the Integrating Sphere analysis on the x-axis and MAAP values on the y-axis are displayed for different concentrations and seasons. The orange line represents a line with x = y. In green, the respective calculated linear regression is displayed. Functions of the calculated regressions for all seasons and concentrations can be found in Table 3.

Overall, the MAAP detects higher concentrations than the Integrating Sphere Method, which can be clearly seen in Figure 29a. The general overestimation of the MAAP is well in accordance with the findings of Reisinger et al. (2008). However, Reisinger (2007) found a linear regression line of $y = 0.480\,x + 0.584$ with a correlation coefficient of $R^2 = 0.767$, which is quite different from the one found in the present study ($y = 1.106\,x + 0.189, R^2 = 0.566$).

As can be observed in Figure 29a, the discrepancy between the two instruments becomes

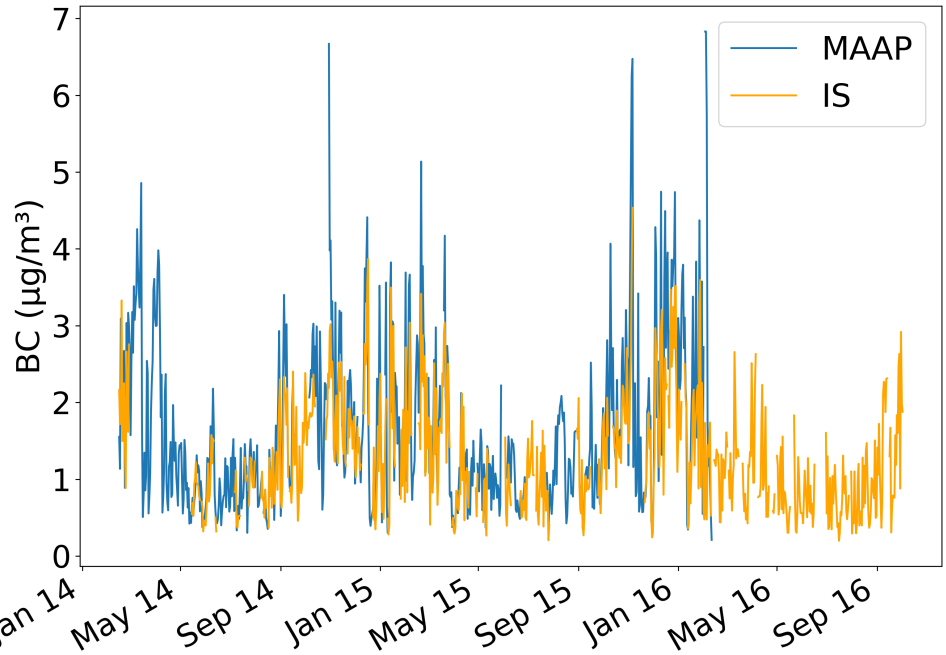

Figure 28: Daily averages of BC concentrations measured with the MAAP and the Integrating Sphere (IS)

more pronounced for higher concentrations. It becomes apparent that the regressions vary quite strongly when calculated for higher and lower concentrations respectively. It is evident that the correlation is quite weak for low concentrations (see Figure 29b) but even worse at higher concentrations (see Figure 29c). The general overestimation of BC concentrations of the MAAP might also be due to artifacts originating from incorrect dark counts in the photodetector (Hyvärinen et al., 2013). Corrections for these artifacts, which usually occur when the ambient BC concentrations exceed $\sim$3 µg/m^3, have been proposed by Hyvärinen et al. (2013), but they have not yet been applied to the instrument used in the present thesis.

Another potential factor that was investigated is seasonality. Since lower BC concentrations are usually to be found during the summer months, different regressions for the winter and summer months of both years were calculated. Figures 29d and 29e show scatterplots and regression lines for values obtained in winter (November to Frebruary) and summer (June to September) respectively. It becomes apparent that the two in-

	Regression line	R^2
All concentrations	y = 1.106 x + 0.189	0.566
BC > 2 µg/m^3	y = 0.999 x + 0.514	0.229
BC < 2 µg/m^3	y = 1.054 x + 0.234	0.349
Winter	y = 0.983 x + 0.519	0.403
Summer	y = 1.065 x + 0.124	0.732

Table 3: Regression parameters of BC values measured with the Integrating Sphere Method vs MAAP data

struments are in best agreement during the summer months (where BC concentrations are low). Part of this is most likely due to the fact that, as will be shown in Section 4.2, the fraction of BrC in PM2.5 is lowest in summer: the MAAP measures only at one wavelength and therefore does not correct its BC values for brown carbon (Liu et al., 2013; Reisinger, 2007). Therefore, it is likely to overestimate BC concentrations in time periods with a higher contribution of BrC. These time periods are more frequent in winter. While there are days with rather low BC concentrations in summer as in winter, BrC basically was detected solely during the colder seasons (see Section 4.2). This is most likely the reason for the correlations to work better for summer values (sorted by seasonality) than for low values (sorted by magnitude).

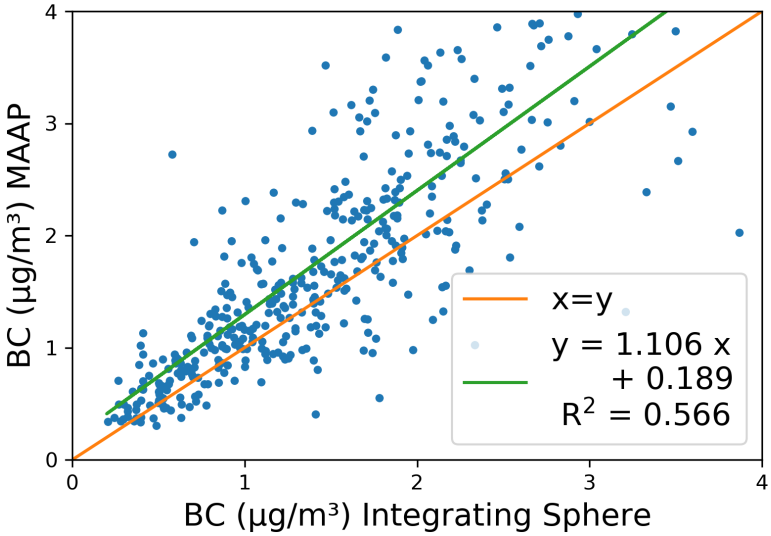

a) Comparison Integrating Sphere - MAAP: all data

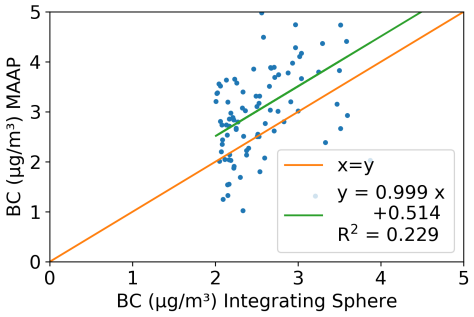

b) Comparison Integrating Sphere - MAAP for BC values above $2\mu g/m^3$

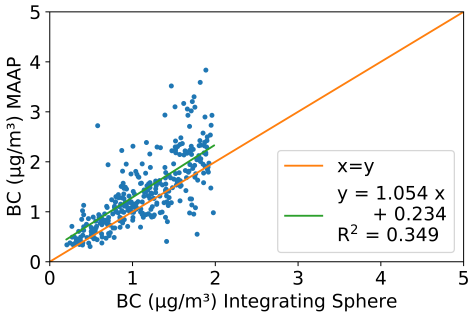

c) Comparison Integrating Sphere - MAAP for BC values below $2\mu g/m^3$

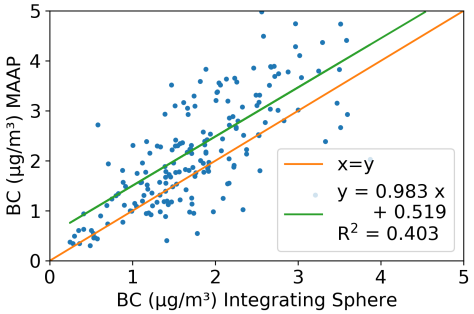

d) Comparison Integrating Sphere - MAAP from November to February

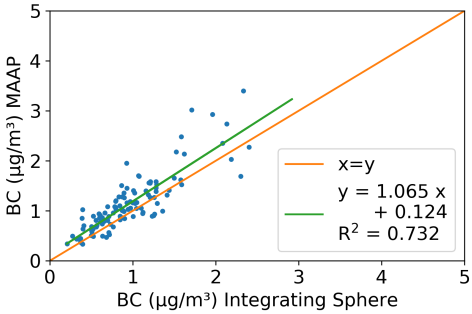

e) Comparison Integrating Sphere - MAAP from June to September

Figure 29: Comparison of BC values determined with the Integrating Sphere and the MAAP

4.1.2 Integrating Sphere and OC/EC Analysis

In addition to the Integrating Sphere measurements, the filters collected in the time period from 2014 to 2016 were simultaneously analyzed for EC with a Sunset Analyzer (see Section 3.2.3). The following chapter is dedicated to comparing results obtained with the Integrating Sphere to those obtained with the Sunset Analyzer.

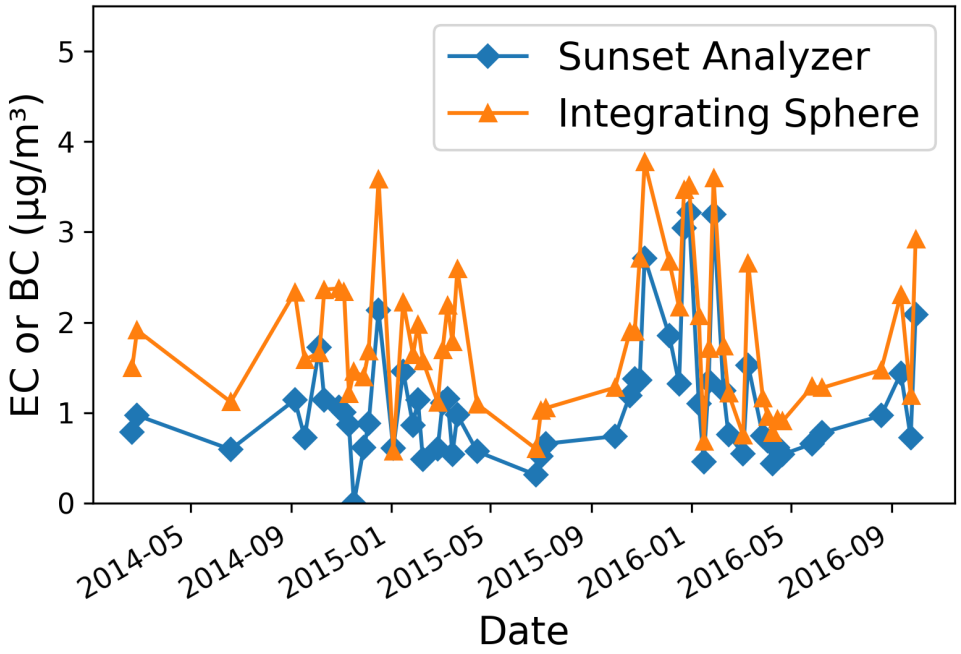

Figure 30: Timeline of daily mean BC concentrations measured with a Sunset Analyzer and the Integrating Sphere Method

Figure 30 shows the results of both BC, measured with the Integrating Sphere Method and EC, measured with a Sunset Analyzer. The two instruments seem to be in relatively good agreement. It can be clearly seen in Figures 30 and 31a that in general, less EC than BC was detected. Considering the definitions in Section 1.4 and Appendix A, this is not surprising, since, as it is was described in Chapter 1.4, there might be numerous light absorbing aerosol components that might not have the thermo-chemical properties by which the Sunset Analyzer selects for.
Furthermore, the results obtained in the present study are in good agreement with previous publications on this issue (Hitzenberger et al., 2006a; Husain et al., 2007).

In his study, Reisinger (2007) found a regression line between BC measured with the Integrating Sphere Method and EC measured following the NIOSH protocol of $EC = 0.740BC - 0.386$. This is in extraordinarily good agreement with the correlation found in the present study $EC = 0.745BC - 0.250$ (see also Figure 31a).
Furthermore, the correlation of the BC and EC measurements has been investigated for different seasons. Figures 31b and 31c show BC vs. EC concentrations measured in winter and summer months respectively. These plots show that the two instruments are in much better agreement during winter time, however, the seasonal difference is not as pronounced as it is for the correlations with the MAAP (see Section 4.1.1).

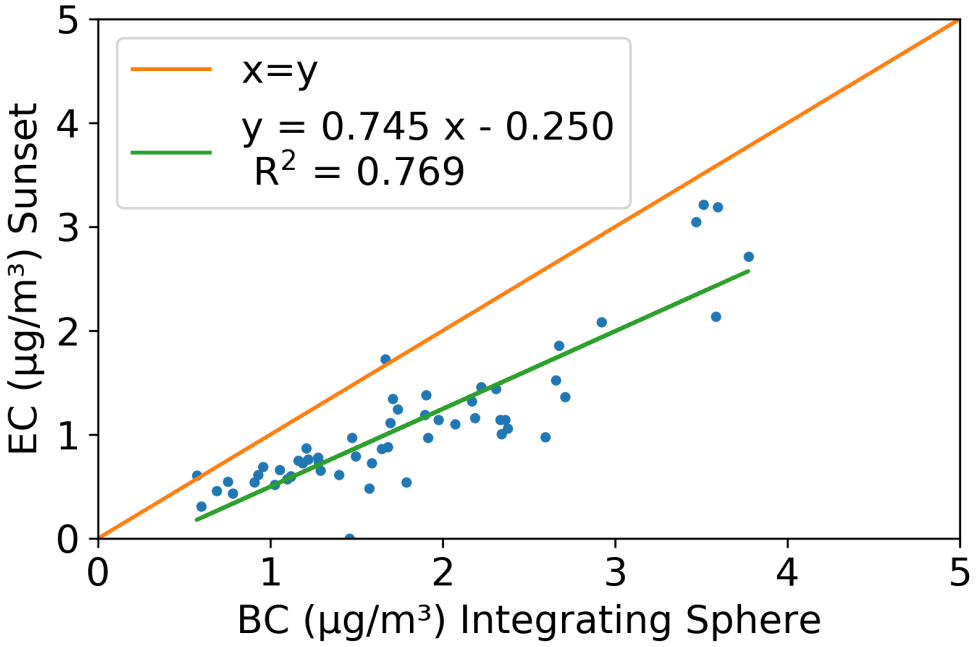

a) Comparison Integrating Sphere BC - Sunset EC

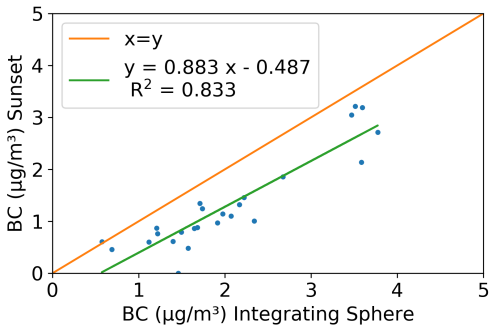

b) Comparison of Integrating Sphere and Sunset from November to February

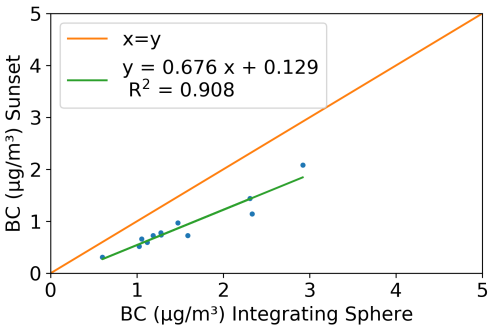

c) Comparison of Integrating Sphere and Sunset from June to September

Figure 31: Correlation of BC measured with the Integrating Sphere and EC measured with a Sunset Analyzer

4.2 Seasonal Variations 2014-2016

From February 2nd 2014 to October 10th 2016, almost daily filter samples were taken and analysed with the Integrating Sphere Method for BC and BrC concentrations. A seasonal variation in BC concentrations is expected due to the different meteorological conditions in colder and warmer months of the year and due to the presence of different sources. Temperature inversions, which prohibit the vertical mixing of air masses and thereby accumulate pollutants, are more likely to occur during the winter months and are quite common in the Viennese basin (Hiebl and Schöner, 2018). Additionally, domestic space heating is naturally more prevalent during the colder times of the year. Depending on the heating method, space heating can be an important source of either BC or BrC. Since the usage of coal and gas for space heating in private households, which is an important source for BC in urban areas, has declined steadily throughout the last decades (Statistik Austria, 2018) (see also Figure 1 in Chapter 1), the seasonal variations of BrC are expected to be more pronounced than those of BC.
This section is dedicated to examining these hypotheses by analysing the daily BC and BrC concentration values in comparison with temperature and PM2.5 data.

Fig 32 shows the absolute values of BC and BrC plotted vs time.
The absolute BC concentrations (shown in Figure 32a), vary between about 0.1 and 4 µg/m^3, which is in good agreement with Kutzner et al. (2018), who report BC concentrations varying between 0.5 and 7 µg/m^3 at seven urban background stations in Germany in the year 2009. BrC concentrations were found to reach values up to almost 5 µg/m^3 (Figure 32b) in winter, but remain very low during warmer months.

Overall, analysis of the daily filter samples with the Integrating Sphere Method from 2014 to 2016 revealed a significant seasonal variation of BC and an even stronger one for BrC.

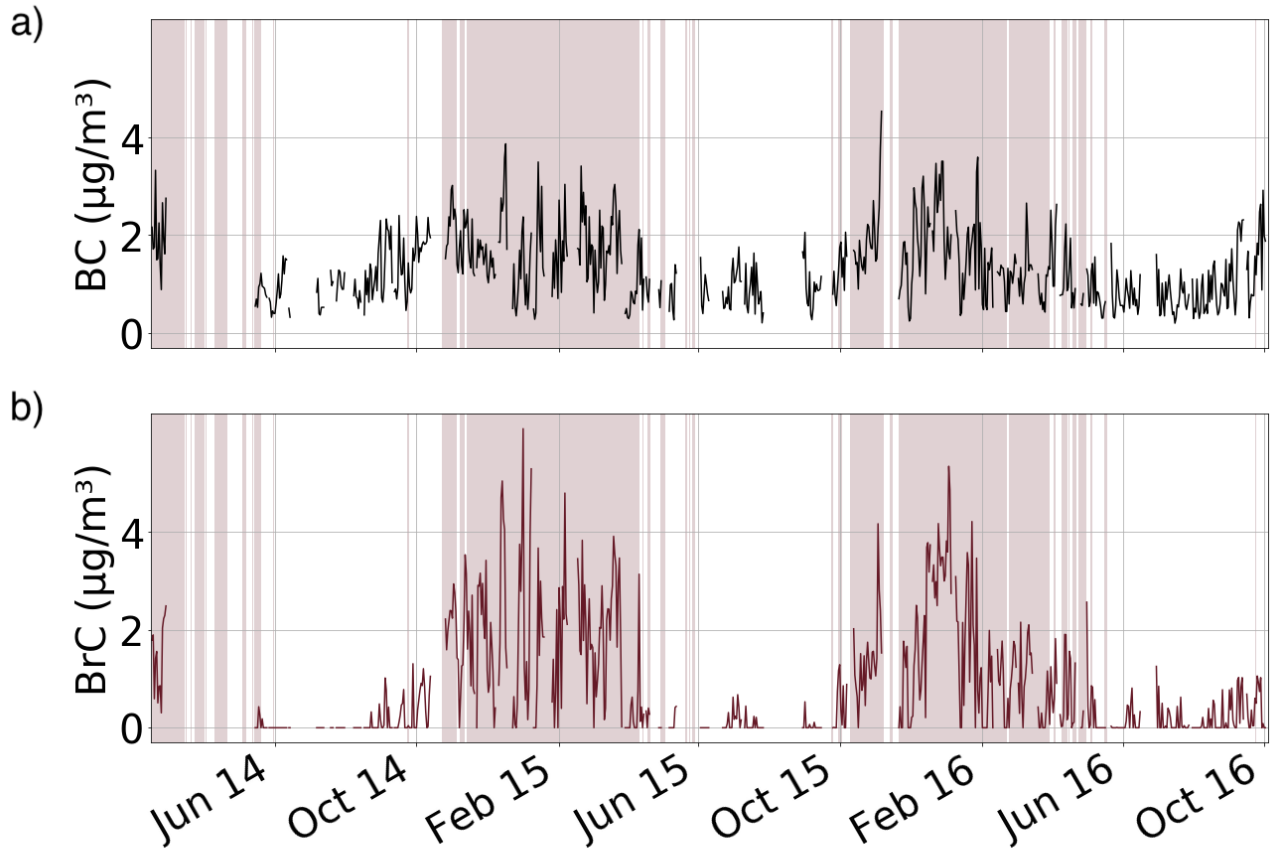

Figure 32: Timeline of BC and BrC concentrations from Feb. 2014 to Oct. 2016 measured with the Integrating Sphere Method. Days on which the average temperature was below 12 °C are indicated by the shaded background.

In order to further investigate changes of BC and BrC concentrations with different seasons (and therefore with temperature), those results were interpreted with respect to temperature values obtained by the Austrian Central Agency of Meteorology (Zentralanstalt für Meteorologie, ZAMG). In Figures 32 and following, the shaded background indicates heating periods (i.e. days on which the daily average temperature is below 12°C, following the Austrian standard ÖNORM B 8110-5 (Austrian Standards Institute, 2007)).
Figure 33 displays the daily average concentration of PM2.5 in the Viennese air over the investigated timeframe, with heating days indicated by the shaded background. It is important to keep in mind that the daily averages are calculated from noon to noon, in order to match the filter sampling time. Figure 33 shows an obvious seasonal dependence of PM2.5 values, which is in good agreement with other long-term studies conducted in European cities (e.g. Bressi et al., 2013). PM2.5 concentrations clearly increase during heating periods and reach daily mean values above 40 µg/m^3. This seasonal variation can most likely be explained by temperature inversion and the presence of space heating as an additional aerosol source, which is only present during the colder months.
The seasonal variability of BC concentrations is also likely caused by temperature inversion. It was shown that these can significantly influence concentrations of BC as well as concentrations of PM2.5 and all other aerosol fractions (Gramsch et al., 2014).

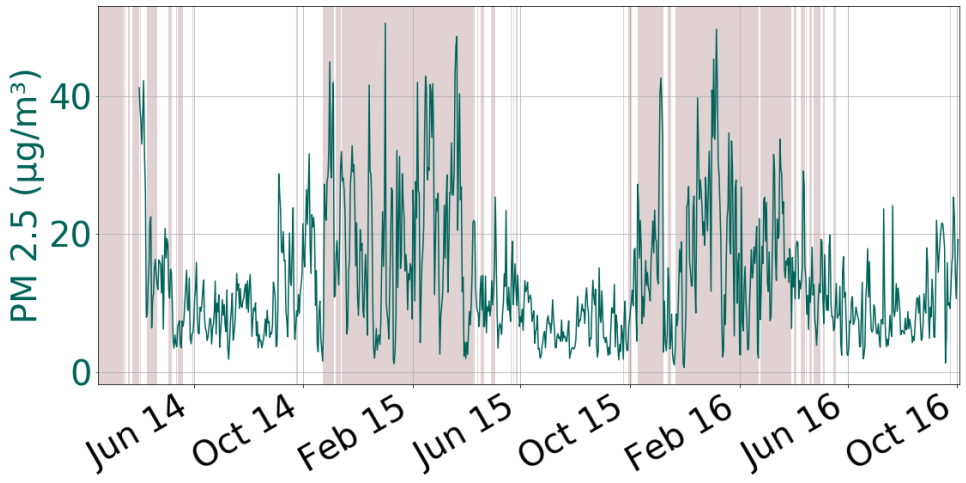

Figure 33: Daily average concentrations of PM2.5. Heating days are indicated by the shaded background.

The monthly mean values of BC and BrC concentrations are displayed in Figures 34 and 35. The monthly mean concentrations of PM2.5 are also displayed in Figure 34. Each data point is set to be on the 15th of each month. In this diagram, the strong seasonal dependence of BrC and PM2.5 becomes clearly visible. Also, the less prevalent seasonal variation of BC concentrations is observable. In Figure 35, the standard deviation of the monthly mean values is indicated by the black and red bars. BrC concentrations are scattered more broadly than BC concentrations but are still visibly higher in colder than in warmer months.

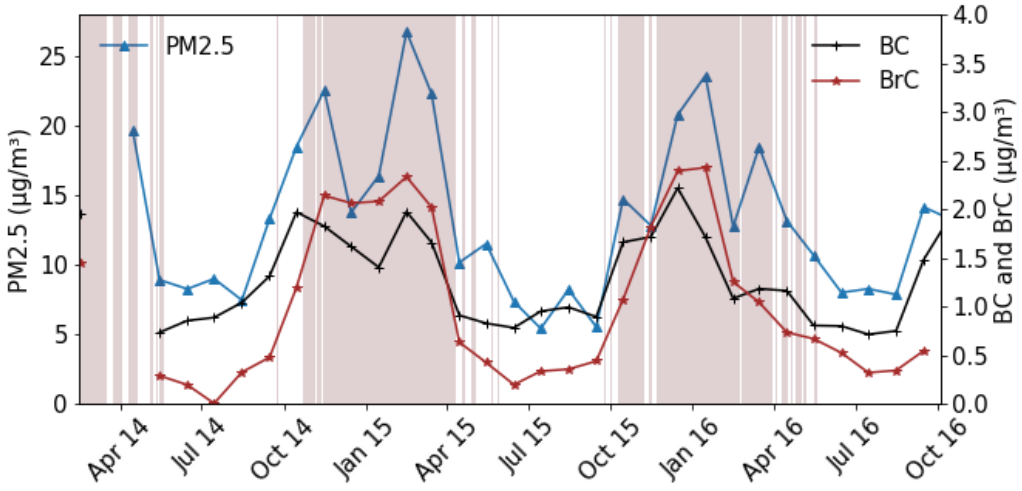

Figure 34: Monthly mean values of PM2.5, BC, BrC and temperature. Heating days are indicated by the shaded background.

Over the whole time period, BrC concentrations clearly increase during heating periods, while being barely detectable otherwise. Figure 36 shows the ratio of BrC to BC measured with the Integrating Sphere Method and the daily average temperature throughout the same time period. Over the whole period an inverse relationship of BrC/BC and temperature is clearly visible. Mean values of BC and BrC concentrations as well as the fraction of BrC in BC are displayed in Table 4 for all heating and all non-heating days (as defined above).

Observing the fractions of BC or BrC in PM2.5 allows for the exclusion of scenarios where the BC or BrC concentrations increase simply because the total concentration of particulate matter increases (e.g. due to temperature inversion).

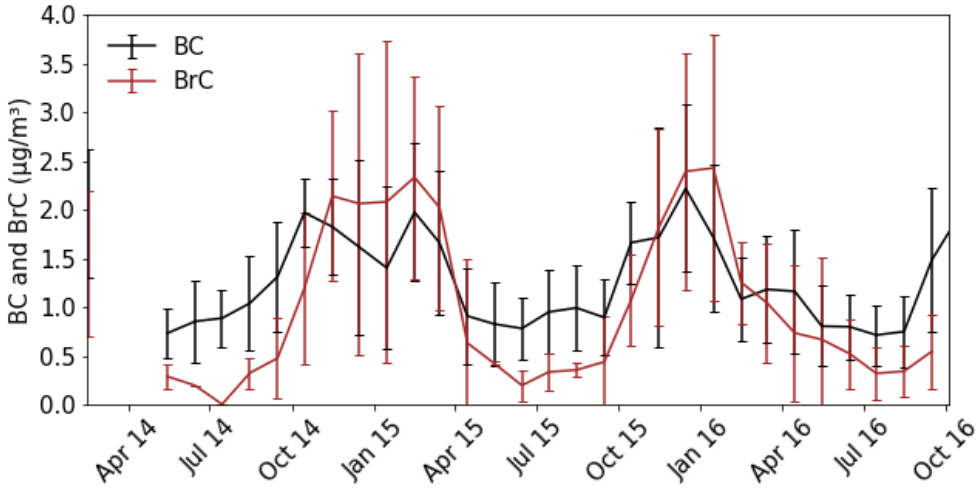

Figure 35: Monthly mean values of BC and BrC concentrations. Standard deviations of the monthly mean values are indicated by the black and red bars.

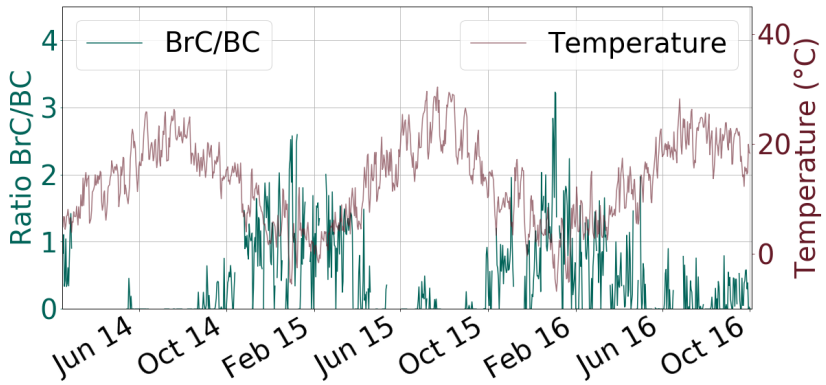

Figure 36: The blue line depicts the ratio BrC/BC from Feb. 2014 to Oct. 2016, the red line shows the average temperature on each day

In Figure 37 the fractions of BC and BrC in PM2.5 are displayed. Considering the Figures 32 and 34, it seems that the contribution of light absorbing carbon tends to be higher on days when space heating is necessary (see also Table 4). However, the fraction of BC in PM2.5 does not show substantial variations with the heating seasons. In fact, it is even slightly lower on average for days on which space heating is necessary (see Table

	T <12 °C	T >12 °C
BC (µg/m^3)	1.567	1.03
BrC (µg/m^3)	1.49	0.21
BrC/BC	0.83	0.14
BC/PM2.5	0.10	0.12
BrC/PM2.5	0.07	0.02

Table 4: Mean values for BC and BrC concentrations as well as fractions of BC and BrC in PM2.5 for both heating days and non heating days.

4). The fraction of BrC in PM2.5, on the other hand, shows a significant variation over time, clearly peaking in the coldest weeks of winter (see Figure 37). Overall, there is a strong correlation of BrC concentrations and heating periods.
The main reason for the strong seasonal dependance of BrC as well as the fraction of BrC in PM2.5 and the relatively constant fraction of BC in PM2.5 likely lies in their inherently different sources. BC is mainly produced by fossil fuel combustion, which remains relatively constant in Vienna throughout the year. BrC originates primarily from biomass burning which occurs in Vienna and its surroundings mostly in winter due to space heating (see Figure 1 in Section 1.3.3). A similar connection between the seasonality of BrC and domestic space heating has been made by Mbengue et al. (2020). They found considerably higher concentrations of BrC in a rural area in the Czech Republic during winter than during summer and were able to identify the source of this aerosol component to be biomass burning from domestic heating devices (Mbengue et al., 2020). Furthermore, in a study conducted recently in the urban area of Dublin, Ireland, it was shown that the main contributor to carbonaceous aerosol in wintertime was local emissions from residential heating (Lin et al., 2019).

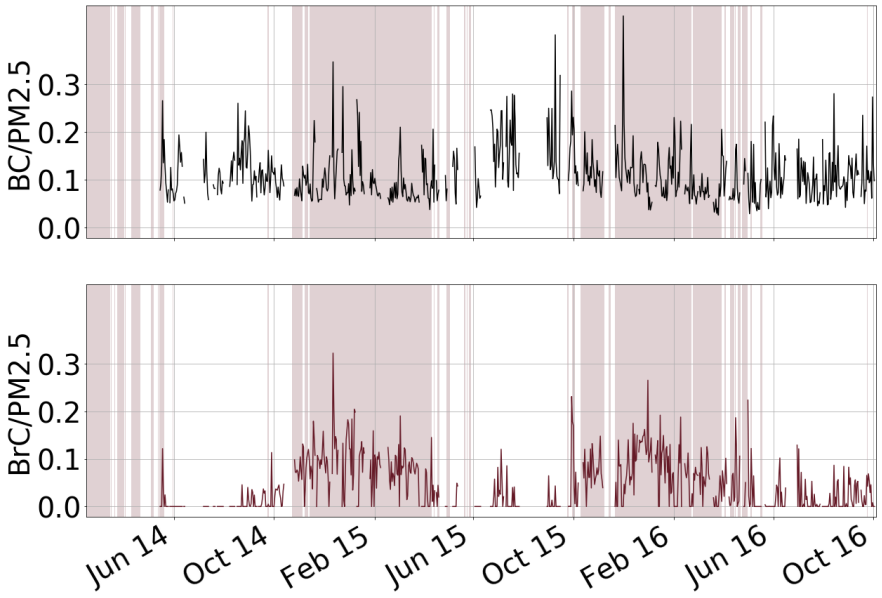

Figure 37: Fractions of BC and BrC in PM 2.5 from Feb. 2014 to Oct. 2016, heating days are indicated by the shaded background.

4.3 Long Term Trends of BC Concentrations in the Urban Aerosol of Vienna

As described in Section 3.3, in the past decades, several long term studies have been conducted in which filter samples were analysed for BC concentrations (Hitzenberger et al., 1996b; Hitzenberger, 1993b). In order to determine possible long term trends, in the following section the results obtained in the present study are compared to those from these previous studies.

From 1985 to 1986 the absorption coefficient of the Viennese urban aerosol was measured by Hitzenberger (1993b) and the corresponding BC mass concentrations were calculated by the author of this thesis (see Section 3.4.1). The monthly mean values of BC mass concentrations found in this study are given in Table 5. Only monthly averages are reported by Hitzenberger (1993b), so no standard deviations of the mean BC concentrations are available. Figure 38a shows a plot of the monthly mean values of BC mass concentrations estimated from the measured B_a of the ambient aerosol as reported by

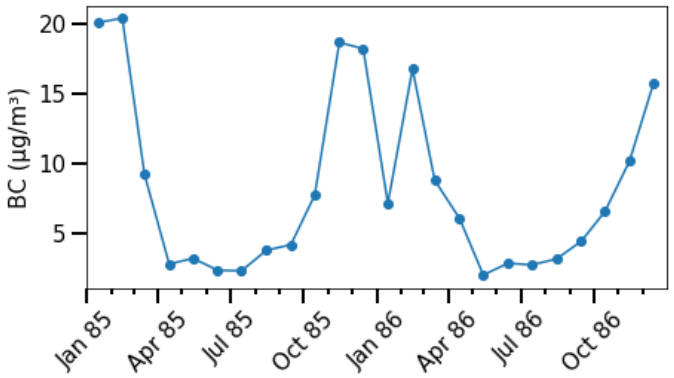

a) Monthly mean values of BC estimated from B_a from Hitzenberger (1993b) following Equation 24 with $B_a(BC) = 6\ m^2/g$

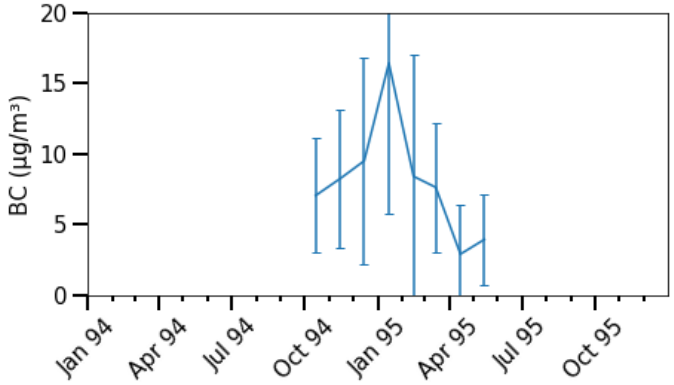

b) Monthly BC values in 1994 and 1995. Parts of the data were previously published by Hitzenberger et al. (1996b).

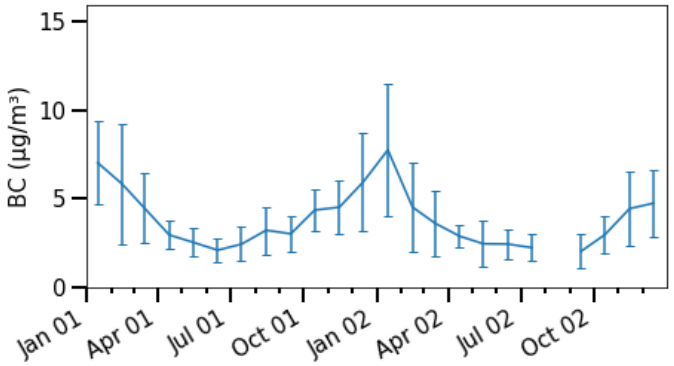

c) Monthly BC values January 2001 to December 2002 obtained by Regina Hitzenberger (unpublished).

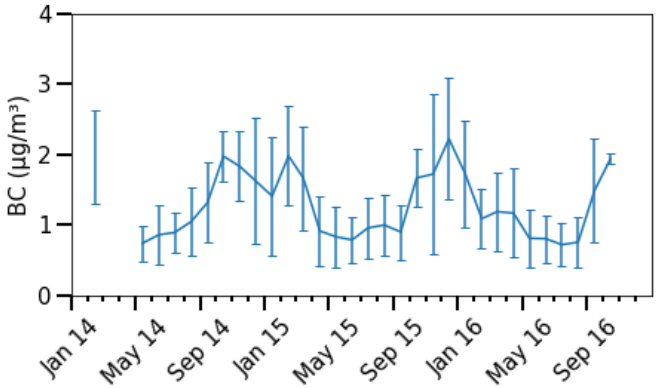

d) Monthly mean values of BC concentrations from 2014 to 2016.

Figure 38: Timelines of BC values from all investigated timeframes

BC (µg/m^3)									
	1985	**1986**	**1994**	**1995**	**2001**	**2002**	**2014**	**2015**	**2016**
January	20.04	7.15		17.97	7.03	7.76		1.40	1.72
February	20.35	16.75		12.36	5.81	4.52	1.96	1.98	1.08
March	9.21	8.79		8.13	4.46	3.61		1.66	1.18
April	2.84	6.10		5.77	2.94	2.87		0.91	1.16
May	2.23	2.05		5.34	2.52	2.44	0.73	0.83	0.81
June	2.39	2.89			2.08	2.42	0.95	0.78	0.80
July	2.35	2.77			2.42	2.22	0.89	0.95	0.71
August	3.80	3.19			3.21		1.04	1.59	0.75
September	4.21	4.44			3.00	2.02	1.31	0.90	1.48
Oktober	7.74	6.58	7.04		4.35	2.96	1.97	1.66	1.93
November	18.63	10.19	8.24		4.51	4.43	1.83	1.72	
December	18.17	15.71	9.49		5.94	4.73	1.62	2.22	

Table 5: Monthly mean values of BC concentrations in the urban aerosol of Vienna calculated from data acquired by Hitzenberger (1993b), Hitzenberger et al. (1996b), Regina Hitzenberger (unpublished) and the author of this thesis.

Hitzenberger (1993b) and Hitzenberger et al. (1996b). A clear seasonal pattern is visible, showing increased concentrations in colder months. A significant drop in BC concentrations can be seen in January 1986. However, Hitzenberger (1993b) argue, that this can be explained by the unusual weather conditions that occurred at the time. Strong winds and an exceptionally long period of foehn wind caused elevated temperatures and good aerosol mixing conditions (Hitzenberger, 1993b).

Table 5 also shows the monthly mean values for BC from October 1994 to May 1995 measured with the original version of the Integrated Sphere method (see Section 3.2.2). In Figure 38b, variations of the monthly BC values are visible; the standard deviation is indicated by the blue bars. The daily BC concentrations show a rather high variability and the number of months for which BC data was available in this time period is limited. However, it is still apparent that the highest BC concentrations are found in winter.

In the measurement period between 2001 and 2002, as in the case of the 1994 and 1995 data, the integrating sphere method was not yet extended and was therefore only able to detect BC. The data was never published but it was made available by Regina Hitzenberger to be used in this thesis.
Table 5 shows the monthly mean BC concentrations for this time period. A plot of the

monthly BC values and the respective standard deviations is shown in Figure 38c. The strong seasonal variation of BC concentrations is clearly visible. Like in all investigated time periods, BC concentrations are much higher in colder months and decline significantly during warmer seasons.

Looking at all four plots in Figure 38 in succession, it becomes apparent that the seasonal cycles of BC concentrations become flatter over these four time periods. Indeed, as it can also be seen in Figure 39, even though mean BC concentrations show a rather strong variation, the differences in summer and winter concentrations become less prevalent as time goes on. As it was argued in Section 1.7 this is most likely caused by a change in space heating sources. Additionally, a strong overall decline of BC concentrations has been observed since the 1980s.

In order to investigate long term trends of BC concentrations in the Viennese air, seasonal mean values were calculated, where the winter season is taken to be the months December, January and February and summer is defined to last from June to August. The mean BC value in both of these seasons is shown in Table 6 and in Figure 39 in comparison to all the investigated years.

Year	BC (µg/m^3)	Std. (µg/m^3)	Std. (%)
Winter (Dec.-Mar.)			
1985/86	12.72	5.55	(44%)
1994/95	11.82	8.18	(69%)
2001/02	5.91	3.31	(56%)
2014/15	1.66	0.81	(49%)
2015/16	1.59	0.81	(51%)
Summer (Jun.-Sep.)			
1985	3.19	0.96	(30%)
1986	3.32	0.77	(23%)
2001	2.62	1.02	(39%)
2002	2.24	0.85	(38%)
2014	1.10	0.50	(45%)
2015	0.91	0.40	(44%)
2016	0.95	0.58	(61%)

Table 6: Seasonal averages of BC concentrations and standard deviation (Std.) of all investigated timeframes.

In Table 6, seasonal averages and their standard deviations are displayed. Figure 39 shows a plot of both the mean winter and summer BC concentrations throughout the whole investigated timeframe. It is evident that the total mean BC concentrations in the Vienna urban air have decreased significantly over the course of the last decades. The most prominent change can be observed in the winter months. While the methods used for the determination of BC values have changed, they still remained comparable enough to make a first order estimate of the relative change of the BC concentrations. From 1985 to 2016 the mean BC concentrations in winter have decreased by about 88%. Summer values have decreased by about 70%. This is in good agreement with Kirchstetter et al. (2017), who showed that the reduction of BC concentrations over the past decades in several cities in the United States was more prevalent in colder than in warmer months. Additionally, it was shown in the analysis conducted in the course of the present thesis that the seasonal variations of BC concentrations have flattened over the investigated timeframe. While the difference between winter and summer averages was as high as 75% in the mid-1980s, it was 57% in the early 2000s and declined to 40% in the mid-2010s. This likely reflects a change towards cleaner methods of space heating. The usage of coal and oil, which is a major contributor to BC concentrations in urban areas,

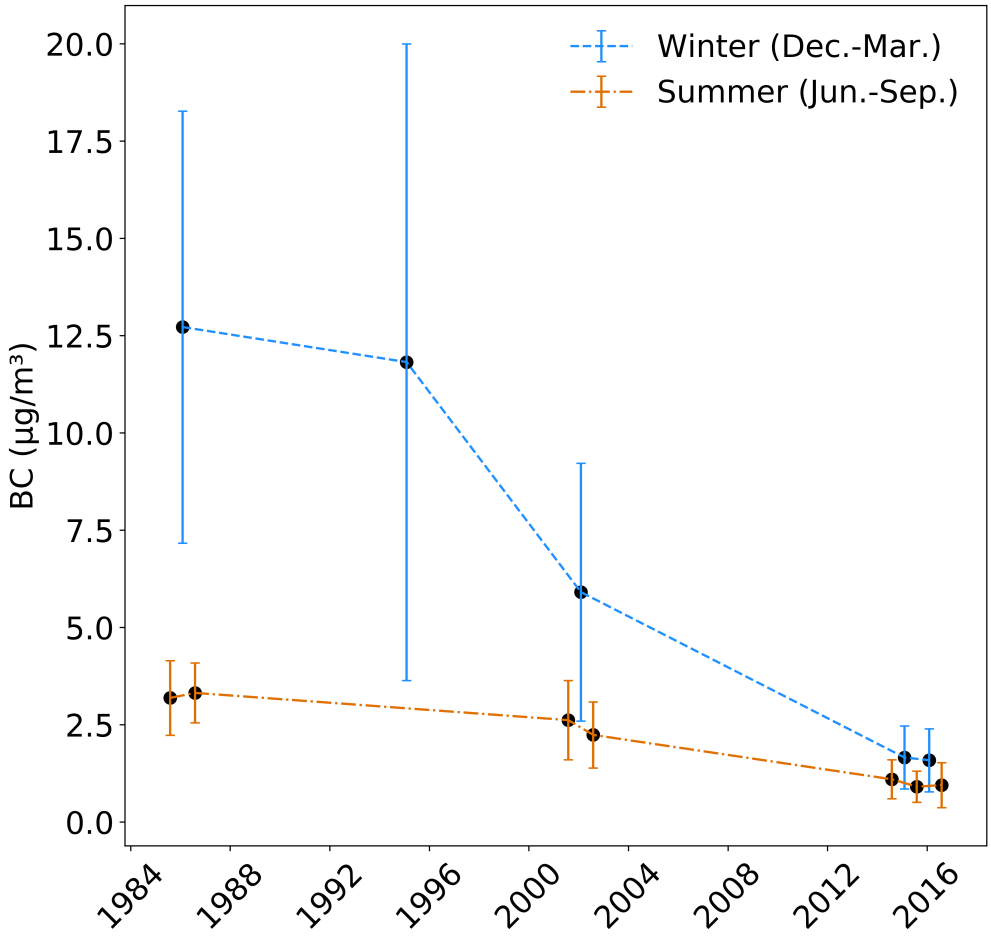

Figure 39: Seasonal mean values of BC concentrations of all investigated timeframes. The blue and orange bars indicate the standard deviation.

has strongly declined since the early 2000s, while biomass burning (emitting BrC) has increased in popularity (Statistik Austria, 2018) (see also Section 1.3.3). It also seems to be a reasonable assumption that there was a decrease in the usage of coal and oil for space heating between 1985 and the early 2000s as well. A clear flattening of the seasonal variations of BC concentrations over the past decades in connection with a change in domestic space heating sources has also been found in several cities in the United States by Kirchstetter et al. (2017) (see also Section 1.7).

Annual mean BC concentrations have decreased substantially as well. Between 2001 and 2015, a decreasing trend of -0.19 µg m^{-3} y^{-1} can be observed, which is considerably greater than what was found by Kutzner et al. (2018), who report a decreasing trend between -0.07 and -0.02 µg m^{-3} y^{-1} from 2005 to 2014 at urban background sites in Germany. The decreasing trend found in the present thesis would be much better comparable to the trend presented by Kutzner et al. (2018) for German traffic sites from 2005 to 2014 (-0.31 to -0.15 µg m^{-1} y^{-1}).
From 1985 to 2001 a decreasing trend of -0.331 µg m^{-3} y^{-1} was found. This does not imply that the actual reduction of BC concentrations is spread evenly over the decades. In fact, this process may well have happened stepwise and not steadily. However, the overall trend is in good agreement with Kirchstetter et al. (2017), who report that the annual mean BC concentrations in New Jersey have decreased from 13 to 2 µg m^{-3} from the 1960s to the year 2000, which corresponds to a trend of about -0.314 µg m^{-3} y^{-1}.

Overall, the findings of this thesis are well comparable to the existing literature, although several limitations of the data have to be kept in mind. Corrections of BC for BrC concentrations were not conducted until the most recent measurement period in the mid-2010s. Furthermore, there was a change in measurement methods over the investigated decades, limiting especially the mid-1980s data to be only treated as an upper estimate. In order to quantify possible overestimations, a systematic assessment of the comparability of BC values obtained with the Integrating Plate and the Integrating Sphere Method could be the topic of future work. Despite these limitations, the hypothesis underlying this thesis (see Section 1.7) could be confirmed in a first order estimate.

4.4 Conclusions

In the course of this study, two main observations are made: 1) total BC mass concentrations in Vienna have decreased appreciably over the past decades and 2) while the seasonal variation of BC concentrations has somewhat 'smoothed out', a strong seasonal dependence of BrC concentrations can be observed.
Since the 1980s, many efforts have been made to improve the air quality in European cities and to minimise pollution. According to the data underlying this thesis, these measures have proven to be effective. Based on the data acquired in the course of this thesis a first estimate could be made that since 1985, mean BC concentrations have declined by 88% in winter and by 70% in summer.

Total aerosol concentrations tend to be significantly higher in winter than they are in summer. This effect is partly linked to higher aerosol emissions in winter and to temperature inversion, which also occurs when temperatures are low (Gramsch et al., 2014). To assess the seasonal variability of BC and BrC concentrations, it is more conclusive to take a look at the fractions of BC and BrC in total PM. It was found that the fraction of BC in PM2.5 was indeed quite constant during the years 2014 to 2016, while the fraction of BrC showed a great seasonal variability. Most likely, the different magnitude of seasonal cycles of BC and BrC can be linked to their different sources, as it has also been observed by Mbengue et al. (2020). While urban BC is mainly produced by fossil fuel burning in vehicles and industry, BrC largely originates from biomass burning (see Section 1.4).

It is important to note that the studies presented here use various measurement techniques and definitions for BC. Therefore, the comparability of absolute values might be limited. However, the order of magnitude of the concentration values, as well as the general trends that were found are good agreement with the results obtained by Kirchstetter et al. (2017) and Mbengue et al. (2020). While there are some discrepancies to what was found by Kutzner et al. (2018), a general trend of decreasing BC concentrations in European cities, as also reported by Font and Fuller (2016), could be confirmed.

5 References

Adler, G., Wagner, N. L., Lamb, K. D., Manfred, K. M., Schwarz, J. P., Franchin, A., Middlebrook, A. M., Washenfelder, R. A., Womack, C. C., Yokelson, R. J., et al. (2019). Evidence in biomass burning smoke for a light-absorbing aerosol with properties intermediate between Brown and Black Carbon. *Aerosol Science and Technology*, 53(9):976–989.

Albrecht, B. A. (1989). Aerosols, cloud microphysics, and fractional cloudiness. *Science*, 245(4923):1227–1230.

Amann, M., Klimont, Z., and Wagner, F. (2013). Regional and global emissions of air pollutants: recent trends and future scenarios. *Annual Review of Environment and Resources*, 38:31–55.

Andreae, M. O. and Gelencsér, A. (2006). Black carbon or brown carbon? The nature of light-absorbing carbonaceous aerosols. *Atmospheric Chemistry and Physics*, 6(10):3131–3148.

Austrian Standards Institute (2007). ÖNORM-B 8110-5. *Wärmeschutz im Hochbau*, Teil 5:8110–5.

Bell, M. L. and Davis, D. L. (2001). Reassessment of the lethal London fog of 1952: novel indicators of acute and chronic consequences of acute exposure to air pollution. *Environmental Health Perspectives*, 109(suppl 3):389–394.

Beresnev, S. and Vasiljeva, M. (2018). Black carbon aerosol in stratosphere. In *24th International Symposium on Atmospheric and Ocean Optics: Atmospheric Physics*, volume 10833, page 108339D. International Society for Optics and Photonics.

Berner, A. and Luerzer, C. (1980). Mass size distributions of traffic aerosols at Vienna. *The Journal of Physical Chemistry*, 84(16):2079–2083.

Bond, T. C., Doherty, S. J., Fahey, D. W., Forster, P. M., Berntsen, T., DeAngelo, B. J., Flanner, M. G., Ghan, S., Kärcher, B., Koch, D., et al. (2013). Bounding the role of black carbon in the climate system: A scientific assessment. *Journal of Geophysical Research: Atmospheres*, 118(11):5380–5552.

Borsós, T., Řimnáčová, D., Ždímal, V., Smolík, J., Wagner, Z., Weidinger, T., Burkart, J., Steiner, G., Reischl, G., Hitzenberger, R., et al. (2012). Comparison of particulate

number concentrations in three Central European capital cities. *Science of the Total Environment*, 433:418–426.

Boucher, O., Randall, D., Artaxo, P., Bretherton, C., Feingold, G., Forster, P., Kerminen, V.-M., Kondo, Y., Liao, H., Lohmann, U., Rasch, P., Satheesh, S., Sherwood, S., Stevens, B., and X.Y., Z. (2013). *Climate Change 2013: The Physical Science Basis. Contribution of Working Group I to the Fifth Assessment Report of the Intergovernmental Panel on Climate Change*, chapter "Clouds and Aerosols". Cambridge University Press.

Bressi, M., Sciare, J., Ghersi, V., Bonnaire, N., Nicolas, J., Petit, J.-E., Moukhtar, S., Rosso, A., Mihalopoulos, N., and Féron, A. (2013). A one-year comprehensive chemical characterisation of fine aerosol (PM 2.5) at urban, suburban and rural background sites in the region of Paris (France). *Atmospheric Chemistry and Physics*, 13(15):7825–7844.

Burnett, R., Chen, H., Szyszkowicz, M., Fann, N., Hubbell, B., Pope, C. A., Apte, J. S., Brauer, M., Cohen, A., Weichenthal, S., et al. (2018). Global estimates of mortality associated with long-term exposure to outdoor fine particulate matter. *Proceedings of the National Academy of Sciences*, 115(38):9592–9597.

Cavalli, F., Viana, M., Yttri, K. E., Genberg, J., and Putaud, J.-P. (2010). Toward a standardised thermal-optical protocol for measuring atmospheric organic and elemental carbon: the EUSAAR protocol. *Atmospheric Measurement Techniques, 3, 79–89.*

Cavazos-Guerra, C., Lauer, A., and Rosenthal, E. (2017). Clean Air and White Ice: Governing Black Carbon Emissions Affecting the Arctic. In *Governing Arctic Change*, pages 231–256. Springer.

Chen, C., Wang, X., Lv, C., Li, W., Ma, D., Zhang, Q., and Dong, L. (2019). The effect of air pollution on hospitalization of individuals with respiratory and cardiovascular diseases in Jinan, China. *Medicine*, 98(22).

Chowdhury, S., Dey, S., Guttikunda, S., Pillarisetti, A., Smith, K. R., and Di Girolamo, L. (2019). Indian annual ambient air quality standard is achievable by completely mitigating emissions from household sources. *Proceedings of the National Academy of Sciences*, 116(22):10711–10716.

Dockery, D. W., Pope, C. A., Xu, X., Spengler, J. D., Ware, J. H., Fay, M. E., Ferris Jr,

B. G., and Speizer, F. E. (1993). An association between air pollution and mortality in six US cities. *New England Journal of Medicine*, 329(24):1753–1759.

European Commission (2019). Air quality standards https://ec.europa.eu/environment/air/quality/standards.htm. accessed: 11.12.2019.

Feng, Y., Ramanathan, V., and Kotamarthi, V. (2013). Brown carbon: a significant atmospheric absorber of solar radiation? *Atmospheric Chemistry and Physics*, 13(17):8607–8621.

Filippo, A. D. and Maricq, M. M. (2008). Diesel nucleation mode particles: semivolatile or solid? *Environmental Science & Technology*, 42(21):7957–7962.

Finlayson-Pitts, B. J. and Pitts, J. N. (1986). *Atmospheric Chemistry: Fundamentals and Experimental Techniques*. John Wiley & Sons.

Font, A. and Fuller, G. W. (2016). Did policies to abate atmospheric emissions from traffic have a positive effect in London? *Environmental Pollution*, 218:463–474.

Gauderman, W., Avol, E., Gilliland, F., Vora, H., Thomas, D., Berhane, K., McConnell, R., Kuenzli, N., Lurmann, F., Rappaport, E., Margolis, H., Bates, D., and Peters, J. (2004). The effect of air pollution on lung development from 10 to 18 years of age. *New England Journal of Medicine*, 351(11):1057–1067.

Gelencsér, A., May, B., Simpson, D., Sanchez-Ochoa, A., Kasper-Giebl, A., Puxbaum, H., Caseiro, A., Pio, C., and Legrand, M. (2007). Source apportionment of PM2.5 organic aerosol over Europe: Primary/secondary, natural/anthropogenic, and fossil/biogenic origin. *Journal of Geophysical Research: Atmospheres*, 112(D23).

Gramsch, E., Cáceres, D., Oyola, P., Reyes, F., Vásquez, Y., Rubio, M., and Sánchez, G. (2014). Influence of surface and subsidence thermal inversion on pm2. 5 and black carbon concentration. *Atmospheric Environment*, 98:290–298.

Habenreich, T. (1983). *Zur Bestimmung des Absorptionskoeffizienten des Wiener Aerosols; sein Zusammenhang mit meteorologischen und anthropogenen Parametern*. PhD thesis, University of Vienna.

Hänel, G. (1987). Radiation budget of the boundary layer. ii- simultaneous measurement of mean solar volume absorption and extinction coefficients of particles. *Beiträge zur Physik der Atmosphäre*, 60:241–254.

Hansen, A., Rosen, H., and Novakov, T. (1984). The aethalometer—an instrument for the real-time measurement of optical absorption by aerosol particles. *Science of the Total Environment*, 36:191–196.

Hansen, J., Sato, M., Ruedy, R., Lacis, A., and Oinas, V. (2000). Global warming in the twenty-first century: An alternative scenario. *Proceedings of the National Academy of Sciences*, 97(18):9875–9880.

Heintzenberg, J. (1982). Size-segregated measurements of particulate elemental carbon and aerosol light absorption at remote arctic locations. *Atmospheric Environment (1967)*, 16(10):2461–2469.

Hemeon, W., Haines Jr, G. F., and Ide, H. M. (1953). Determination of haze and smoke concentrations by filter paper samplers. *Air Repair*, 3(1):22–28.

Hickey, A. J. and Mansour, H. M. (2019). *Inhalation aerosols: physical and biological basis for therapy*, volume 1. CRC press.

Hiebl, J. and Schöner, W. (2018). Temperature inversions in Austria in a warming climate – changes in space and time. *Meteorologische Zeitschrift (Contributions to Atmospheric Sciences)*, 27(4):309–323.

Hinds, W. C. (2011). Physical and chemical processes in aerosol systems. In *Aerosol Measurement: Principles, Techniques, and Applications: Third Edition*, pages 31–40. John Wiley and Sons.

Hinds, W. C. (2012). *Aerosol Technology: properties, behavior and measurement of airborne particles*. John Wiley & Sons.

Hitzenberger, R. (1993a). Absorption measurements with an integrating plate photometer calibration and error analysis. *Aerosol Science and Technology*, 18(1):70–84.

Hitzenberger, R., Dusek, U., and Berner, A. (1996a). Black carbon measurements using an Integrating Sphere. *Journal of Geophysical Research: Atmospheres*, 101(D14):19601–19606.

Hitzenberger, R., Fohler-Norek, C., Dusek, U., Galambos, Z., and Sidla, S. (1996b). Comparison of recent (1994) black carbon data with those obtained in 1985 and 1986 in the urban area of Vienna, Austria: implications for future environmental policy decisions. *Science of the Total Environment*, 189:275–280.

Hitzenberger, R., Petzold, A., Bauer, H., Ctyroky, P., Pouresmaeil, P., Laskus, L., and Puxbaum, H. (2006a). Intercomparison of thermal and optical measurement methods for elemental carbon and black carbon at an urban location. *Environmental Science & Technology*, 40(20):6377–6383.

Hitzenberger, R. and Tohno, S. (2001). Comparison of black carbon (BC) aerosols in two urban areas–concentrations and size distributions. *Atmospheric Environment*, 35(12):2153–2167.

Hitzenberger, R., Tursic, J., Grgic, I., Berner, A., Ctyroky, P., and Podkrajsek, B. (2006b). Particle size distribution of carbon in aerosols collected in Vienna and Ljubljana. *Chemosphere*, 65:2106–2113.

Hitzenberger, R. M. (1993b). Absorption coefficients and mass concentrations of the urban aerosol of Vienna, Austria, during the years 1985 and 1986. *Water, Air, and Soil Pollution*, 71(1-2):131–153.

Huang, J. and Jaeglé, L. (2017). Wintertime enhancements of sea salt aerosol in polar regions consistent with a sea ice source from blowing snow. *Atmospheric Chemistry and Physics*, 17(5):3699.

Husain, L., Dutkiewicz, V. A., Khan, A., and Ghauri, B. M. (2007). Characterization of carbonaceous aerosols in urban air. *Atmospheric Environment*, 41(32):6872–6883.

Hyvärinen, A.-P., Laakso, L., Beukes, J., Van Zyl, P., Josipovic, M., and Garland, R. (2013). Correction for a measurement artifact of the Multi-Angle Absorption Photometer (MAAP) at high black carbon mass concentration levels. *Atmospheric Measurement Techniques*.

IARC Working Group on the Evaluation of Carcinogenic Risks to Humans (2014). *IARC Monographs: Diesel and Gasoline Engine Exhausts and some Nitroarenes*. International Agency for Research on Cancer Lyon, France.

Janssen, N. A., Gerlofs-Nijland, M. E., Lanki, T., Salonen, R. O., Cassee, F., Hoek, G., Fischer, P., Brunekreef, B., and Krzyzanowski, M. (2012). Health effects of black carbon https://www.euro.who.int/en/health-topics/environment-and-health/air-quality/publications/2012/health-effects-of-black-carbon-2012. accessed: 21.10.2020.

Jiang, M. Y., Li, J. Q., Wu, Y. Q., Lin, N. T., Wang, X. M., and Fu, F. F. (2011). Chemical characterization of nanometer-sized elemental carbon particles emitted from diesel vehicles. *Journal of Aerosol Science*, 42(6):365–371.

Jimenez, J., Canagaratna, M., Donahue, N., Prevot, A. S. H., Zhang, Q., Kroll, J., DeCarlo, P., Allan, J., Coe, H., Ng, N., and et al (2009). Evolution of organic aerosols in the atmosphere. *Science*, 326:1525–1529.

Kholod, N. and Evans, M. (2016). Reducing black carbon emissions from diesel vehicles in Russia: An assessment and policy recommendations. *Environmental Science & Policy*, 56:1–8.

Kirchstetter, T. W., Preble, C. V., Hadley, O. L., Bond, T. C., and Apte, J. S. (2017). Large reductions in urban black carbon concentrations in the United States between 1965 and 2000. *Atmospheric Environment*, 151:17 – 23.

Klimont, Z., Kupiainen, K., Heyes, C., Purohit, P., Cofala, J., Rafaj, P., Borken-Kleefeld, J., and Schöpp, W. (2017). Global anthropogenic emissions of particulate matter including black carbon. *Atmospheric Chemistry and Physics*, 17(14):8681–8723.

Kopp, R. E. and Mauzerall, D. L. (2010). Assessing the climatic benefits of black carbon mitigation. *Proceedings of the National Academy of Sciences*, 107(26):11703–11708.

Kreyling, W. G., Semmler-Behnke, M., and Möller, W. (2006). Ultrafine particle–lung interactions: does size matter? *Journal of Aerosol Medicine*, 19(1):74–83.

Kuklinska, K., Wolska, L., and Namiesnik, J. (2015). Air quality policy in the US and the EU–a review. *Atmospheric Pollution Research*, 6(1):129–137.

Kulmala, O., Laakso, L., Lehtinen, K., Riipinen, I., Dal Maso, M., Anttila, T., Kerminen, V.-M., Horrak, U., Vana, M., and Tammet, H. (2004). Initial steps of aerosol growth. *Atmospheric Chemistry and Physics Discussions*, 4(5):5433–5454.

Kupiainen, K. and Klimont, Z. (2007). Primary emissions of fine carbonaceous particles in Europe. *Atmospheric Environment*, 41(10):2156–2170.

Kutzner, R. D., von Schneidemesser, E., Kuik, F., Quedenau, J., Weatherhead, E. C., and Schmale, J. (2018). Long-term monitoring of black carbon across Germany. *Atmospheric Environment*, 185:41 – 52.

Laskin, A., Laskin, J., and Nizkorodov, S. A. (2015). Chemistry of atmospheric brown carbon. *Chemical Reviews*, 115(10):4335–4382.

Li, N., Georas, S., Alexis, N., Fritz, P., Xia, T., Williams, M. A., Horner, E., and Nel, A. (2016). A work group report on ultrafine particles (american academy of allergy, asthma & immunology): Why ambient ultrafine and engineered nanoparticles should receive special attention for possible adverse health outcomes in human subjects. *Journal of Allergy and Clinical Immunology*, 138(2):386–396.

Lin, C., Ceburnis, D., Huang, R.-J., Xu, W., Spohn, T., Martin, D., Buckley, P., Wenger, J., Hellebust, S., Rinaldi, M., et al. (2019). Wintertime aerosol dominated by solid-fuel-burning emissions across Ireland: insight into the spatial and chemical variation in submicron aerosol. *Atmospheric Chemistry and Physics*, 19(22):14091–14106.

Lin, C.-I., Baker, M., and Charlson, R. J. (1973). Absorption coefficient of atmospheric aerosol: A method for measurement. *Applied Optics*, 12(6):1356–1363.

Liu, J., Bergin, M., Guo, H., King, L., Kotra, N., Edgerton, E., and Weber, R. (2013). Size-resolved measurements of brown carbon in water and methanol extracts and estimates of their contribution to ambient fine-particle light absorption. *Atmospheric Chemistry and Physics*, 13(24):12389–12404.

Loeb, N. G., Wielicki, B. A., Doelling, D. R., Smith, G. L., Keyes, D. F., Kato, S., Manalo-Smith, N., and Wong, T. (2009). Toward optimal closure of the Earth's top-of-atmosphere radiation budget. *Journal of Climate*, 22(3):748–766.

Lu, Z., Zhang, Q., and Streets, D. G. (2011). Sulfur dioxide and primary carbonaceous aerosol emissions in China and India, 1996–2010. *Atmospheric Chemistry and Physics*, 11(18):9839–9864.

Martin, R. V., Brauer, M., van Donkelaar, A., Shaddick, G., Narain, U., and Dey, S. (2019). No one knows which city has the highest concentration of fine particulate matter. *Atmospheric Environment: X*, page 100040.

Massey, D., Kulshrestha, A., Masih, J., and Taneja, A. (2012). Seasonal trends of PM10, PM5. 0, PM2. 5 & PM1. 0 in indoor and outdoor environments of residential homes located in North-Central India. *Building and Environment*, 47:223–231.

Mbengue, S., Serfozo, N., Schwarz, J., Ziková, N., Šmejkalová, A. H., and Holoubek, I. (2020). Characterization of Equivalent Black Carbon at a regional background site in Central Europe: Variability and source apportionment. *Environmental Pollution*, 260:113771.

Mie, G. (1908). Beiträge zur Optik trüber Medien, speziell kolloidaler Metallösungen. *Annalen der Physik*, 330(3):377–445.

Mohr, C., Thornton, J. A., Heitto, A., Lopez-Hilfiker, F. D., Lutz, A., Riipinen, I., Hong, J., Donahue, N. M., Hallquist, M., Petäjä, T., et al. (2019). Molecular identification of organic vapors driving atmospheric nanoparticle growth. *Nature Communications*, 10(1):1–7.

Myhre, G., Aas, W., Cherian, R., Collins, W., Faluvegi, G., Flanner, M., Forster, P., Hodnebrog, O., Klimont, Z., Lund, M., et al. (2017). Multi-model simulations of aerosol and ozone radiative forcing due to anthropogenic emission changes during the period 1990-2015. *Atmospheric Chemistry and Physics*, 17(4):2709–2720.

Myhre, G., Shindell, D., Bréon, F.-M., Collins, W., Fuglestvedt, J., Huang, J., Koch, D., Lamarque, J.-F., Lee, D., Mendoza, B., Nakajima, T., Robock, A., Stephens, G., Takemura, T., and Zhang, H. (2013). *Climate Change 2013: The Physical Science Basis. Contribution of Working Group I to the Fifth Assessment Report of the Intergovernmental Panel on Climate Change*, chapter Anthropogenic and Natural Radiative Forc- ing. In: Climate Change 2013: The Physical Science Basis. Contribution of Working Group I to the Fifth Assessment Report of the Intergovernmental Panel on Climate Change. Cambridge University Press.

Nguyen, T. B., Lee, P. B., Updyke, K. M., Bones, D. L., Laskin, J., Laskin, A., and Nizkorodov, S. A. (2012). Formation of nitrogen-and sulfur-containing light-absorbing compounds accelerated by evaporation of water from secondary organic aerosols. *Journal of Geophysical Research: Atmospheres*, 117(D1).

Oberdörster, G., Oberdörster, E., and Oberdörster, J. (2005). Nanotoxicology: an emerging discipline evolving from studies of ultrafine particles. *Environmental Health Perspectives*, 113(7):823–839.

Österreichisches Umweltbundesamt (2020a). Feinstaub - PM2,5 https://www.umweltbundesamt.at/umweltthemen/luft/luftschadstoffe/staub/pm25. accessed: 21.10.2020.

Österreichisches Umweltbundesamt (2020b). Täglicher Luftgütebericht https://www.umweltbundesamt.at/umweltthemen/luft/daten-luft/tgl-bericht. accessed: 02.07.2020.

Paasonen, P., Visshedjik, A., Kupiainen, K., Klimont, Z., Denier van der Gon, H., and Kulmala, M. (2013). Aerosol particle number emissions and size distributions: implementation in the gains model and initial results. Technical report, International Institute for Applied Systems Analysis, Schlossplatz 1 A-2361 Laxenburg, Austria.

Peng, J., Hu, M., Guo, S., Du, Z., Zheng, J., Shang, D., Zamora, M. L., Zeng, L., Shao, M., Wu, Y.-S., et al. (2016). Markedly enhanced absorption and direct radiative forcing of black carbon under polluted urban environments. *Proceedings of the National Academy of Sciences*, 113(16):4266–4271.

Peng, R. D., Bell, M. L., Geyh, A. S., McDermott, A., Zeger, S. L., Samet, J. M., and Dominici, F. (2009). Emergency Admissions for Cardiovascular and Respiratory Diseases and the Chemical Composition of Fine Particle Air Pollution. *Environmental Health Perspectives*, 117(6):957–963.

Petzold, A., Ogren, J. A., Fiebig, M., Laj, P., Li, S.-M., Baltensperger, U., Holzer-Popp, T., Kinne, S., Pappalardo, G., Sugimoto, N., et al. (2013). Recommendations for reporting "black carbon" measurements. *Atmospheric Chemistry and Physics*, 13(16):8365–8379.

Petzold, A. and Schönlinner, M. (2004). Multi-angle absorption photometry—a new method for the measurement of aerosol light absorption and atmospheric black carbon. *Journal of Aerosol Science*, 35(4):421–441.

Pima County Department of Environmental Quality (2017). 2016 Air Quality Summary Report For Pima County, Arizona https://repository.asu.edu/attachments/192804/content/2016AirQualitySummary.pdf. accessed: 21.10.2020.

Pöschl, U. (2005). Atmospheric aerosols: composition, transformation, climate and health effects. *Angewandte Chemie International Edition*, 44(46):7520–7540.

Pósfai, M. and Buseck, P. R. (2010). Nature and climate effects of individual tropospheric aerosol particles. *Annual Review of Earth and Planetary Sciences*, 38.

Putaud, J.-P., Raes, F., Van Dingenen, R., Brüggemann, E., Facchini, M.-C., Decesari, S., Fuzzi, S., Gehrig, R., Hüglin, C., Laj, P., et al. (2004). A European aerosol phenomenology—2: chemical characteristics of particulate matter at kerbside, urban, rural and background sites in Europe. *Atmospheric Environment*, 38(16):2579–2595.

Raza, M., Chen, L., Leach, F., and Ding, S. (2018). A review of particulate number (PN) emissions from gasoline direct injection (GDI) engines and their control techniques. *Energies*, 11(6):1417.

Reisinger, P. (2007). Vergleich verschiedener Methoden zur Messung von Ruß im urbanen Aerosol von Wien im Winter. Master's thesis, University of Vienna.

Reisinger, P., Wonaschütz, A., Hitzenberger, R., Petzold, A., Bauer, H., Jankowski, N., Puxbaum, H., Chi, X., and Maenhaut, W. (2008). Intercomparison of measurement techniques for black or elemental carbon under urban background conditions in wintertime: Influence of biomass combustion. *Environmental Science & Technology*, 42(3):884–889. PMID: 18323117.

Riemer, N. and West, M. (2013). Quantifying aerosol mixing state with entropy and diversity measures. *Atmospheric Chemistry & Physics*, 13(22):11423–11439.

Rubow, K. L. (1982). *Submicron Aerosol Filtration Characteristics of Membrane Filters.* PhD thesis, University of Minnesota.

Schwarz, J. P., Gao, R., Spackman, J., Watts, L., Thomson, D., Fahey, D., Ryerson, T., Peischl, J., Holloway, J., Trainer, M., et al. (2008). Measurement of the mixing state, mass, and optical size of individual black carbon particles in urban and biomass burning emissions. *Geophysical Research Letters*, 35(13).

Seinfeld, J. H. and Pandis, S. N. (2006). *Atmospheric chemistry and physics: From air pollution to climate change.* John Willey & Sons Inc., New York.

Shi, Z., Xie, X., Li, X., Yang, L., Xie, X., Lei, J., Sha, Y., and Liu, X. (2019). Snow-darkening versus direct radiative effects of mineral dust aerosol on the Indian summer monsoon onset: role of temperature change over dust sources. *Atmospheric Chemistry & Physics*, 19(3).

Statistik Austria (2018). Energieeinsatz der Haushalte https://www.statistik.at/web_de/statistiken/energie_umwelt_innovation_mobilitaet/energie_und_umwelt/energie/energieeinsatz_der_haushalte/index.html. accessed: 21.10.2020.

Sven Leckel Ingenieurbüro GmbH (2008). *Bedienungsanleitung Filterwechsler SEQ47/50.* Sven Leckel Ingenieurbüro GmbH, Leberstraße 63, D-10829 Berlin/Germany, 01/08 edition.

Twomey, S. (1977). The influence of pollution on the shortwave albedo of clouds. *Journal of the Atmospheric Sciences*, 34(7):1149–1152.

United States Environmental Protection Agency (2016). National Ambient Air Quality Standards https://www.epa.gov/criteria-air-pollutants/naaqs-table. accessed: 21.10.2020.

Van Dingenen, R., Raes, F., Putaud, J.-P., Baltensperger, U., Charron, A., Facchini, M.-C., Decesari, S., Fuzzi, S., Gehrig, R., Hansson, H.-C., et al. (2004). A European aerosol phenomenology—1: physical characteristics of particulate matter at kerbside, urban, rural and background sites in Europe. *Atmospheric Environment*, 38(16):2561–2577.

Weingartner, E., Saathoff, H., Schnaiter, M., Streit, N., Bitnar, B., and Baltensperger, U. (2003). Absorption of light by soot particles: determination of the absorption coefficient by means of aethalometers. *Journal of Aerosol Science*, 34(10):1445–1463.

Wonaschütz, A., Hitzenberger, R., Bauer, H., Pouresmaeil, P., Klatzer, B., Caseiro, A., and Puxbaum, H. (2009). Application of the Integrating Sphere Method to Separate the Contributions of Brown and Black Carbon in Atmospheric Aerosols. *Environmental Science & Technology*, 43(4):1141–1146.

World Health Organization, Occupational and Environmental Health Team (2006). WHO Air quality guidelines for particulate matter, ozone, nitrogen dioxide and sulfur dioxide : global update 2005 : summary of risk assessment https://www.euro.who.int/en/health-topics/environment-and-health/air-quality/publications/pre2009/air-quality-guidelines.-global-update-2005.-particulate-matter,-ozone,-nitrogen-dioxide-and-sulfur-dioxide. accessed: 21.10.2020.

Xie, M., Chen, X., Holder, A. L., Hays, M. D., Lewandowski, M., Offenberg, J. H., Kleindienst, T. E., Jaoui, M., and Hannigan, M. P. (2019). Light absorption of organic carbon and its sources at a southeastern US location in summer. *Environmental Pollution*, 244:38–46.

Yamineva, Y. and Liu, Z. (2019). Cleaning the air, protecting the climate: Policy, legal and institutional nexus to reduce black carbon emissions in China. *Environmental Science & Policy*, 95:1–10.

6 Appendix A - Technical Terms and Abbreviations frequently used in Aerosol Science

- TSP - total suspended particulate matter (includes particulates of all sizes and chemical compositions)
- PM10 - particulate matter with particles smaller than $10\mu m$
- PM2.5 - particulate matter with particles smaller than $2.5\mu m$
- TC - 'total carbon', the total carbonaceous fraction of atmospheric aerosol
- EC - 'elemental' carbonaceous aerosol (see Section 1.4, elemental carbon)
- OC - carbonaceous particulate material of organic origin (see Sections 1.4 and 1.4.1)
- BC - carbonaceous aerosol appearing black (see Section 1.4, black carbon)
- BrC - carbonaceous aerosol appearing brown (see Section 1.4, brown carbon)
- σ_a - absorption coefficient of an aerosol (see Section 2.1)
- B_a - specific absorption coefficient of an aerosol (see Section 3.4.1)

In the present thesis, mainly the suggestions from Petzold et al. (2013) will be used and when referring to EC, BC and BrC the following definitions are adhered to:

- EC: inorganic carbonaceous aerosol that is thermally stable in an inert atmosphere up to very high temperatures (about 3 700°C) and only oxidises at temperatures above 340°C (Petzold et al., 2013). EC is measured following the EUSAAR2 protocol (Cavalli et al., 2010)
- BC: inorganic carbonaceous aerosol that absorbs light at all wavelengths in the visible spectrum
- BrC: carbonaceous aerosol particulates that absorb light depending on its wavelength. The instrument used to measure BrC was calibrated with humic-like substances (Wonaschütz et al., 2009)

7 Appendix B - Standard Operating Procedure for the Sunset Analyzer

The following document provides a standard operating procedure for the measurement of elemental (EC) and organic carbon (OC) collected on filter samples using a Sunset Analyzer. It is divided into two sections: 1) the preparation and measurement of a sucrose solution for instrument calibration and 2) day-to-day use of the Sunset Analyzer for EC/OC measurements.

Calibration with sucrose solution

Preparation of sucrose solutions

Sucrose solutions must be stored in a refrigerator and should not be used for more than 30 days after preparation.

- Clean a 100 ml volumetric flask first with tap water, then with ultrapure water.
- Dry the 100 ml volumetric flask with compressed air.
- Weigh in 1.18162 g of sucrose using a clean disposable aluminium bowl.
- Put the sucrose into the dry volumetric flask and fill it up to 100 ml with ultrapure water.
- Shake the flask vigorously for about one minute, in order to uniformly mix the solution.
- Label the solution accordingly with content, concentration, date and your name
- Store the solution in a refrigerator

The instructions above are for preparing a solution containing 5 µgC/µl. For calibration of the Sunset Analyzer (if it has not been in use for several months or after maintenance) it is advisable to prepare several solutions with different carbon concentrations. Calculate the amount of sucrose required for preparing a solution containing a specific mass of carbon as follows:

$$
\begin{aligned}
mass\,of\,carbon\,(\mathrm{g}) &= mass\,of\,sucrose\,(\mathrm{g}) * \frac{molecular\,weight\,of\,carbon}{molecular\,weight\,of\,sucrose} \\
&= mass\,of\,sucrose\,(\mathrm{g}) * \frac{12 * 12.0107\,\mathrm{g/mol}}{1 * 342.2965\,\mathrm{g/mol}} \\
&= mass\,of\,sucrose\,(\mathrm{g}) * 0.42106
\end{aligned}
\tag{28}
$$

Calibration

- Follow the instructions on how to turn on the instrument and measure sucrose standards
- Measure at least ten filters containing different amounts of carbon ranging from 5 µgC to 200 µgC

SOP for EC/OC measurement

Whenever the Sunset Analyzer has not been in use for more than a month, at least three sucrose standards should be measured.
At the beginning of each measurement day, at least one sucrose standard should be measured.

Preparation:

- Place a tweezer and a filter punch of the desired size (1 cm^2 or 1.5 cm^2 punch area) with a 50:50 mixture of isopropanol and ultrapure water in a glass container and put it in an ultrasonic bath for 10 min.
- Wash the tweezer and the punch with ultrapure water and dry them with compressed air.

Turn on the instrument:

- Switch on the hydrogen generator
- Switch on the computer and log in as "Regina" (no password required)
- Start the program OCEC828.exe

- Open the window "Flow rates"
- Adjust the flow rates according to the target values displayed (check if valves on gas cylinders are open)
- Set the hydrogen flow rate to about 90 cm^3/min and ignite the flame ionization detector using a lighter
- Check that the flame is burning by placing the lid of a plastic petri dish above the exhaust tube. When the flame was successfully ignited, a streak of condensed water should be observable on the lid, when held at the right angle. Carefully reduce the hydrogen flow to its target value
- Switch on the methanizer oven and wait until it has reached its target temperature (about $500°C$)
- Create a new .txt file in the desired folder. All raw data obtained on that day will be saved in this file.

Measure a sucrose standard:

- Put an empty filter punch into the sample oven (or use the one from the previous day):
  - Open the sample oven by removing the clamp and the lid
  - Remove the O-ring and place the quartz boat on the holder using a clean tweezer
  - Place the filter punch on the quartz boat
  - Close the sample oven using the O-ring and the clamp
- Clean the oven (by pressing "Action" and "Clean Oven")
- Take the volumetric flask containing the sucrose solution out of the fridge and shake it vigorously
- Pour a small amount of the solution into a dry sealable test tube and wait until the solution has reached room temperature
- Shake the test tube and pipette the desired amount of solution onto the empty filter punch using an Eppendorf pipette

- Name the sample as follows: "amount"-"from" "solution"
  e.g.: 10µl-from5µgC/µl
- Type in your name and choose the correct punch area of your filter punch (e.g. 1 cm^2)
- Choose the current .txt file and run the program "Trocknen"(the program does not have to be run until the end, it can be interrupted as soon as the laser transmission and reflection signals are constant)
- When the sucrose solution on the filter is dried(i.e. the laser signals are both constant), the actual measurement can be started (by running the program "EUSAAR2")

If the measured organic carbon content on the sucrose standards is within 10% of its target value, measurement of the actual filter samples can be started

Measurement of filter samples

- Open the sample oven by removing the clamp and the lid
- Remove the O-ring and place the quartz boat on the holder using a clean tweezer
- Place the filter punch on the quartz boat
- Close the sample oven using the O-ring and the clamp
- Type in the sample ID, your name and choose the correct punch area
- Run the program 'EUSAAR2'

Shutting down the instrument

The sunset analyzer is usually kept running in standby mode. However, when putting it in standby mode, the following matters need to be kept in mind:

- Gas flows are not switched off entirely. A small amount of gas should always be flowing through the system (trickle-flow). Therefore, do not apply too much pressure when closing the solenoid valves controlling the gas flows.

- The hydrogen flow must not be switched off while the methanizer oven is above 200°C! Therefore, when the last filter sample has been measured, switch off the methanizer oven (switch at the back of the Sunset Analyzer) and leave everything else (including the program OCEC828.exe) running. It takes about half an hour for the oven to cool below 200°C. Only then switch off the hydrogen generator and close the solenoid valves controlling the gas flows.
- The Sunset Analyzer is put into standby mode by selecting 'Action' and 'All Off' in the program OCEC828.exe